

University of Southampton Research Repository
ePrints Soton

Copyright © and Moral Rights for this thesis are retained by the author and/or other copyright owners. A copy can be downloaded for personal non-commercial research or study, without prior permission or charge. This thesis cannot be reproduced or quoted extensively from without first obtaining permission in writing from the copyright holder/s. The content must not be changed in any way or sold commercially in any format or medium without the formal permission of the copyright holders.

When referring to this work, full bibliographic details including the author, title, awarding institution and date of the thesis must be given e.g.

AUTHOR (year of submission) "Full thesis title", University of Southampton, name of the University School or Department, PhD Thesis, pagination

UNIVERSITY OF SOUTHAMPTON

FACULTY OF SCIENCE

DEPARTMENT OF PHYSICS

**DEVELOPMENT OF SHORT PULSE SOURCES
AT 1.5 μ m FOR NON-LINEAR PROPAGATION
STUDIES IN OPTICAL FIBRES**

by David Patrick Shepherd

Thesis submitted for the Degree of Doctor of Philosophy

May 1989

CONTENTS

Abstract	v
Acknowledgements	vi
1. INTRODUCTION	1
1.1 Aims	3
1.2 Thesis Layout	6
1.3 References	
2. LOW THRESHOLD OPERATION OF A CAPILLARY WAVEGUIDE CH₄ RAMAN LASER AT 1.54μm	8
2.1 Introduction	8
2.2 Raman Scattering	8
2.2.1 The Raman Gain	8
2.2.2 The Population Density	14
2.2.3 The Raman Linewidth	14
2.2.4 The Differential Raman Scattering Cross Section	14
2.2.5 Raman Exponential Gain At Threshold	15
2.2.6 Threshold Pump Power For Guided And Unguided Media	16
2.2.7 Capillary Waveguide Design	18
2.2.8 Transient Raman Scattering	18
2.3 The Pump Laser	18
2.3.1 Choice Of Pump Laser	18
2.3.2 Actively Stabilised Acousto-Optic Mode-locking	20
2.4 A Single Pass Waveguide Raman Laser	23
2.4.1 Introduction	23
2.4.2 Experimental Arrangement And Results	24
2.5 A Synchronously Pumped Waveguide Raman Laser	28
2.5.1 Threshold Pump Power	28
2.5.2 Experimental Arrangement And Results	31
2.6 Summary	33
2.7 References	38
3. A LONGITUDINALLY PUMPED Yb:Er PHOSPHATE GLASS LASER AT 1.536μm	40
3.1 Introduction	40

3.2 The Yb:Er System	40
3.2.1 Choice Of Pumping Scheme	40
3.2.2 Rate Equation Analysis	41
3.3 Quasi-CW Operation	48
3.3.1 The Pump Laser	50
3.3.2 Experimental Arrangement And Results	50
3.3.3 Q-Switched Operation At 5Hz	58
3.4 CW Operation	61
3.4.1 Experimental Arrangement And Results	61
3.4.2 High Repetition Rate Q-Switched Operation	65
3.5 An Yb:Er Fibre Laser	65
3.6 Summary	71
3.7 References	74
4. MODE-LOCKING OF Yb:Er GLASS LASERS AND THEIR USE FOR NON-LINEAR PULSE PROPAGATION STUDIES IN SILICA OPTICAL FIBRES	76
4.1 Introduction	76
4.2 Mode-Locking Of The Yb:Er Glass Laser	76
4.2.1 Mode-locking Of Inhomogeneously Broadened Lasers	76
4.2.2 A Quasi-CW Mode-Locked Yb:Er Glass Laser	81
4.2.2.1 Mode-Locked And Q-Switched Operation	88
4.2.3 A Mode-Locked Yb:Er Fibre Laser	91
4.2.4 A CW Mode-Locked Yb:Er Glass Laser	96
4.3 Non-Linear Pulse Propagation In Optical Fibres	101
4.3.1 Non-Linearity And Pulse Compression	101
4.3.2 The Non-Linear Schrödinger Equation	102
4.3.3 Solitons	104
4.4 Experimental Demonstration Of Soliton Pulse Compression	106
4.5 Design Considerations For An Yb:Er Glass Soliton Laser	110
4.6 Summary	119
4.7 References	120
5. CONCLUDING REMARKS	123
5.1 Summary Of Results Achieved	123

APPENDICES (relevant publications)

1. Low Threshold Operation Of A Waveguide CH_4 Raman Laser At $1.54\mu\text{m}$	127
2. A Synchronously Pumped Waveguide CH_4 Raman Laser At $1.54\mu\text{m}$	130
3. A $1.54\mu\text{m}$ Er Glass Laser Pumped By $1.064\mu\text{m}$ Nd:YAG Laser	134
4. CW Operation Of A Nd:YAG Pumped Yb:Er Phosphate Glass Laser at $1.54\mu\text{m}$	138
5. Efficient Operation Of An Yb Sensitised Er Fibre Laser At $1.56\mu\text{m}$	141
6. Active Mode-Locking And Q-Switching Of A $1.54\mu\text{m}$ Er Glass Laser Pumped By A $1.064\mu\text{m}$ Nd:YAG Laser	143
7. Active Mode-Locking Of An Yb:Er Fibre Laser	147
8. Studies Of Excited-State Absorption At $1.5\mu\text{m}$ In Er^{3+} Doped Silica Fibres	149

UNIVERSITY OF SOUTHAMPTON

ABSTRACT

FACULTY OF SCIENCE

PHYSICS

Doctor of Philosophy

DEVELOPMENT OF SHORT PULSE SOURCES AT $1.5\mu\text{m}$ FOR NON-LINEAR
PROPAGATION STUDIES IN OPTICAL FIBRES

by David Patrick Shepherd

The development of sources of short mode-locked pulses at $1.5\mu\text{m}$ is described. Pulses of sufficient power in this spectral region are of great interest for the study of non-linear pulse propagation in optical fibres, where the interplay of negative group velocity dispersion and self-phase modulation can lead to soliton formation and pulse compression.

Initial work concentrated on a Nd:YAG pumped methane Raman laser at $1.54\mu\text{m}$. The use of a high pressure cell and a capillary waveguide reduces the stimulated Raman scattering threshold to just $\sim 190\text{kW}$. The use of synchronous pumping is shown to reduce this even further, to $\sim 50\text{kW}$, which is an order of magnitude less than the peak power available from a typical cw pumped, mode-locked and Q-switched Nd:YAG laser. These threshold values are shown to be in close agreement with theoretical predictions. Peak output powers of nearly 70kW are available in bandwidth-limited, 100ps full width half maximum duration pulses.

We then describe a Nd:YAG pumped Yb:Er phosphate glass laser, showing it to be a versatile source in the $1.5\mu\text{m}$ spectral region. Pulsed, cw, mode-locked and Q-switched operation have been demonstrated in bulk and fibre forms. A simple rate equation model of this sensitised 3-level laser system is shown to be in rough agreement with experimental results, with absorbed power thresholds as low as $\sim 500\text{mW}$ and $\sim 12\text{mW}$ being found in the bulk and fibre forms respectively. Typical mode-locked pulse durations of $\sim 70\text{ps}$ are found and subsequent pulse compression via high order soliton propagation has given pulses of $\sim 400\text{fs}$.

Finally the Yb:Er laser is assessed as a candidate for enhanced mode-locking via a non-linear external cavity, as in the soliton laser.

ACKNOWLEDGEMENTS

I am grateful to my supervisor Professor D.C.Hanna for all the help and encouragement he has given me during this research. I also gratefully acknowledge the help of my industrial supervisor Dr.R.Wyatt, especially for the generous loan of very many optical components. Much of the experimental work presented here was performed in collaboration with my past and present colleagues in the laser physics group whom I would all like to thank, especially Dr.M.T.T.Pacheco and Dr.S.G.Mussett (for the Raman laser work), A.Kazer and D.Espie (for the Yb:Er laser work), and M.W.Phillips and Dr.P.J.Suni (for the fibre laser work). I would also like to acknowledge M.E.Fermann and J.E.Townsend of the Department of Electronics and Information Engineering for their work on the Yb:Er fibre laser.

This work has been supported by a SERC/JOERS grant and I have received support from both SERC and BTRL in the form of a CASE studentship.

1. Introduction

1.1 Aims

The central aim of this thesis is to investigate methods of production of short mode-locked pulses in the low loss spectral window of the negative (anomalous) group velocity dispersion region of silica optical fibres ($\sim 1.55\mu\text{m}$). It has been shown, [1], that the propagation of optical pulses in (loss-less) single mode fibres is described by the non-linear Schrödinger equation as below,

$$\left[\frac{\partial}{\partial z} + (1/v_g) \frac{\partial}{\partial t} \right] E(z, t) = (i/2) \left[\frac{d^2 \beta}{d\omega^2} \right] \left[\frac{\partial^2 E(z, t)}{\partial t^2} \right] - i\kappa |E(z, t)|^2 E(z, t) \dots (1.1)$$

= (i) - (ii)

where $E(z, t)$ is the pulse envelope, $\beta(\omega)$ is the propagation constant, $1/v_g = d\beta/d\omega$ is the inverse group velocity, and κ is a (positive) constant dependent on the single mode fibre used. This equation and its soliton solutions are discussed in more detail in chapter 4, but it is sufficient here to note that for a convex upwards pulse ($\partial^2 E / \partial t^2 < 0$ over the central portion of the pulse) the non-linear self-phase modulation term, (ii), can be brought into balance with the dispersive term, (i), as long as we have negative group velocity dispersion ($d^2 \beta / d\omega^2 < 0$). Under such circumstances the pulse propagates with an unchanging pulse shape. This, in fact, corresponds to the lowest order soliton solution of equation (1). At lower intensities the dispersion term dominates resulting in pulse broadening, while at higher intensities the pulse shape becomes periodic and will always initially undergo compression.

The first experimental demonstration of this behaviour was made by Mollenauer et al in 1980, [2], and there has since been significant interest in the possibility of high-bit rate communication systems involving non-linear

pulse propagation (for example see ref.[3-9]). This interest was enhanced by the discovery that the fibre Raman gain can be used to compensate the fibre loss and amplify the solitons with practically no change in pulse shape, [6-9]. Thus the non-linear, all optical system is seen to have many advantages to the conventional linear system with electronic repeaters, some of which are:

- 1) The elimination of dispersive pulse broadening which would otherwise eventually cause the pulses to overlap, leading to loss of information and limiting the maximum possible bit-rate.
- 2) The repeater separation is therefore governed merely by the fibre loss rather than the group velocity dispersion
- 3) Compatibility with using the fibre Raman gain (with simple cw diode laser pumps at the beginning and end of each amplification period) leading to an all optical system that avoids the use of bit-rate limiting "high-speed" electronics.
- 4) Compatibility with wavelength multiplexing, with no need to demultiplex at each repeater.

It is reasonable to suggest that, from eqn.(1.1), a linear system at the zero group velocity dispersion wavelength should also be possible. However in practice pulses of usefully large energy in this region are found to suffer significant broadening through a combination of non-linear effects and higher order dispersion, [8]. Thus the soliton system appears to be the only way forward for long distance all optical communications.

Higher order solitons are also of interest due to their initial pulse compression behaviour. This is an attractive way of obtaining short pulses as it merely involves launching light into a suitable length of fibre rather than the much more complicated diffraction grating

technique, [10,11].

Much interest, [12-19], has also been generated by the fact that non-linear processes, such as soliton formation, in an external cavity can lead to improved mode-locked performance of the "master" laser. In this way $\sim 1.5\mu\text{m}$ colour centre lasers have had their normal mode-locked performance ($\sim 10\text{ps}$) enhanced by a factor of ~ 200 leading to pulsedwidths near the limit set by the gain bandwidth ($\sim 50\text{fs}$), [20].

Thus it is clear that there is a need for convenient and versatile sources of $\sim 1.5\mu\text{m}$ mode-locked pulses with which to investigate the general field of non-linear effects in the negative dispersion region of silica optical fibres. At the present time there are few sources which can meet this requirement, which explains why the colour centre laser has dominated the experimental work undertaken to date.

Although all the work presented here is directed by this central aim it should also raise some interesting points in the general field of new laser sources, as indicated in the next section.

1.2 Thesis Layout

In chapter two we describe the low threshold operation of a capillary waveguide CH_4 Raman laser. Pumped with a mode-locked and Q-switched $1.064\mu\text{m}$ Nd:YAG laser, the Raman laser produces a train of (slightly shortened) pulses at $1.544\mu\text{m}$. The optimum conditions for low threshold operation are discussed. Theoretical and experimental results are shown to be in close agreement in both single pass and synchronously pumped configurations, with very low thresholds being achieved. The suitability of this source for soliton experiments is considered, although this technique through variation of the pump laser and Raman medium should be of general interest as a method of frequency conversion of short pulses.

In chapters three and four we describe a

longitudinally pumped Yb:Er phosphate glass laser at $1.536\mu\text{m}$. Er³⁺ doped glass has a well known 3-level laser transition in the $1.5\mu\text{m}$ spectral region, [21]. Due to the scarcity and weakness of suitable absorption bands in Er³⁺ it is often co-doped with various sensitizer ions. Here we use Yb³⁺ which is known to allow pumping by Nd:glass lasers at $1.054\mu\text{m}$, [22], and we demonstrate, for the first time, that pumping via the widely available $1.064\mu\text{m}$ Nd:YAG laser is also possible.

In chapter three we describe this laser's basic operation, pulsed or cw, in bulk or fibre forms and we also identify some of its advantages compared to the colour centre laser. A very simple rate equation analysis of this co-doped, 3 level laser system is shown to give reasonable agreement with the observed thresholds.

In the first part of chapter four we describe the actively mode-locked behaviour of the Yb:Er laser in all its forms, using the techniques of amplitude and phase modulation, typically obtaining a stable bandwidth limited output. Thus this source which is capable of running pulsed or cw, Q-switched and/or mode-locked, in either bulk or fibre form is seen as a very versatile source with which to carry out investigations of soliton behavior. Besides this application it also raises some points of general interest such as,

- 1) Low threshold cw operation of a bulk 3-level laser through the use of longitudinal pumping and a short active medium length, i.e. "mini-laser" techniques.
- 2) An interesting example of the use of co-doping, especially in the fibre laser case where slope efficiencies were the largest found to date for such a laser.
- 3) An interesting example of mode-locking in a fibre laser, where all the necessary ingredients for soliton formation (i.e. negative group velocity dispersion and a

large non-linearity) are present within the active medium.

In the second part of chapter four we discuss the non-linear Schrödinger equation and the properties of solitons more fully, and as an example we describe the soliton pulse compression of the mode-locked Yb:Er laser in a length of single mode optical fibre. A very large single stage pulse compression is obtained with the corresponding frequency spectrum showing the onset of soliton self frequency shift effects, [23-26]. Finally we consider the possibility of constructing a "soliton laser" based on the various forms of Yb:Er laser we have described.

Some concluding remarks on this work are given in chapter five, while appendices one to eight contain the relevant published literature. The references are listed in numerical order at the end of each chapter for the convenience of the reader.

1.3 References

- [1] A.Hasegawa and F.Tappert, *Appl. Phys. Lett.* 23 (1973) 142
- [2] L.F.Mollenauer, R.H.Stolen and J.P.Gordon, *Phys. Rev. Lett.* 45 (1980) 1095
- [3] A.Hasegawa and Y.Kodoma, *Proc. IEEE* 69 (1981) 1145
- [4] K.J.Blow and N.J.Doran, *Opt. Comm.* 42 (1982) 403
- [5] N.J.Doran and K.J.Blow, *IEEE J. Quantum Electron.* QE-19 (1983) 1883
- [6] A.Hasegawa, *Opt. Lett.* 8 (1983) 650
- [7] L.F.Mollenauer, R.H.Stolen and M.N.Islam, *Opt. Lett.* 10 (1985) 229
- [8] L.F.Mollenauer, J.P.Gordon and M.N.Islam, *IEEE J. Quantum Electron.* QE-22 (1986) 157
- [9] L.F.Mollenauer and K.Smith, *Opt. Lett.* 13 (1988) 675
- [10] E.B.Treacy, *Phys. Lett.* 28A (1968) 34
- [11] B.Nikolaus and D.Grischkowsky, *Appl. Phys. Lett.* 42 (1983) 1
- [12] L.F.Mollenauer and R.H.Stolen, *Opt. Lett.* 9 (1984) 13
- [13] H.A.Haus and M.N.Islam, *IEEE J. Quantum Electron.* QE-21 (1985) 1172
- [14] K.J.Blow and D.Wood, *IEEE J. Quantum Electron.* QE-22 (1986) 1109
- [15] F.M.Mitschke and L.F.Mollenauer, *IEEE J. Quantum Electron.* QE-22 (1986) 2242
- [16] J.F.Pinto, C.P.Yakymyshyn and C.R.Pollock, *Opt. Lett.* 13 (1988) 383
- [17] P.A.Belanger, *J. Opt. Soc. Am. B* 5 (1988) 793
- [18] K.J.Blow and D.Wood, *J. Opt. Soc. Am. B* 5 (1988) 629
- [19] P.N.Kean, X.Zhu, D.W.Crust, R.S.Grant, N.Langford and W.Sibbett, *Opt. Lett.* 14 (1989) 39
- [20] F.M.Mitschke and L.F.Mollenauer, *Opt. Lett.* 12 (1987)

[21] E.Snitzer and R.Woodcock, *Appl. Phys. Lett.* 6 (1965) 45

[22] V.P.Gapontsev, M.E.Zhabotinskii, A.A.Izyneev,
V.B.Kravchenko and Yu.P.Rudnitskii, *JETP Lett.* 18 (1973)
251

[23] E.M.Dianov, A.Ya.Karasik, P.V.Mamyshev, A.M.Prokhorov,
V.N.Serkin, M.F.Stel'makh and A.A.Fomichev, *JETP Lett.*
41 (1985) 295

[24] F.M.Mitschke and L.F.Mollenauer, *Opt. Lett.* 11 (1986)
659

[25] J.P.Gordon, *Opt. Lett.* 11 (1986) 662

[26] P.Baud, W.Hodel, B.Zysset and H.P.Weber, *IEEE J.*
Quantum Electron. QE-23 (1987) 1938

2. LOW THRESHOLD OPERATION OF A CAPILLARY WAVEGUIDE CH₄ RAMAN LASER AT 1.54μm

2.1 Introduction

The aim of the work described in this chapter is to investigate the possibility of achieving a convenient source of short pulses at 1.54μm, via the low threshold frequency conversion of short pump pulses at 1.064μm, by stimulated Raman scattering (SRS) in CH₄ gas. We will first give a brief discussion of the theory of Raman scattering in order to obtain the equations necessary to calculate the expected pump power thresholds.

2.2 Raman Scattering

2.2.1 The Raman Gain

For a medium which has zero charge density and where the only current is given by the displacement current, the fields obey Maxwell's equations as below,

$$\nabla \wedge \underline{E} = - \frac{\partial \underline{B}}{\partial t} \quad (2.1)$$

$$\nabla \wedge \underline{H} = \frac{\partial \underline{D}}{\partial t} \quad (2.2)$$

$$\nabla \cdot \underline{E} = 0 \quad (2.3)$$

$$\nabla \cdot \underline{B} = 0 \quad (2.4)$$

Where the magnetic field intensity is $\underline{H} = \underline{B}/\mu_0$. For an applied electric \underline{E} the resultant electric polarisation can be described as,

$$\underline{P} = \epsilon_0 \chi \underline{E} + \epsilon_0 K^{(2)} \chi^{(2)} \underline{E}^2 + \epsilon_0 K^{(3)} \chi^{(3)} \underline{E}^3 \dots \quad (2.5)$$

where $K^{(n)}$ is a numerical factor dependent on the nonlinear process being considered. Thus the electric displacement is,

$$\begin{aligned} \underline{D} &= \epsilon_0 \underline{E} + \underline{P} = \epsilon_0 \underline{E} + \underline{P}^L + \underline{P}^{NL} \\ &= \epsilon \underline{E} + \underline{P}^{NL} \end{aligned} \quad (2.6)$$

where \underline{P}^L is the familiar linear polarisation of the medium and \underline{P}^{NL} is the nonlinear polarisation given by,

$$\underline{P}^{NL} = \epsilon_0 K^{(2)} \chi^{(2)} \underline{E}^2 + \epsilon_0 K^{(3)} \chi^{(3)} \underline{E}^3 \dots \quad (2.7)$$

Effects due to the nonlinear term become significant with the relatively large optical field strengths available from lasers. By applying the ∇^\wedge operator to eqn.(2.1) and using the identity $\nabla^\wedge \nabla^\wedge \underline{E} = \nabla(\nabla \cdot \underline{E}) - \nabla^2 \underline{E}$ we obtain,

$$-\nabla^2 \underline{E} = -(\partial^2 / \partial t^2) \mu_0 [\epsilon \underline{E} + \underline{P}^{NL}] \quad (2.8)$$

This can be re-arranged to give the wave equation as below where the phase velocity is $c = (\epsilon \mu_0)^{-1/2}$,

$$\nabla^2 \underline{E} - (1/c^2) (\partial^2 \underline{E} / \partial t^2) = (1/\epsilon c^2) (\partial^2 \underline{P}^{NL} / \partial t^2) \quad (2.9)$$

By confining ourselves to plane waves traveling in the z direction eqn.(2.9) reduces to,

$$\partial^2 \underline{E} / \partial z^2 - (1/c^2) (\partial^2 \underline{E} / \partial t^2) = (1/\epsilon c^2) (\partial^2 \underline{P}^{NL} / \partial t^2) \quad (2.9a)$$

The electric field amplitude at frequency ω_j can be written as,

$$E_{\omega_j}(z, t) = (1/2) \{E_j(z) \exp[i(\omega_j t - k_j z)] + c.c.\} \quad (2.10)$$

and similarly the nonlinear polarisation is,

$$P_{\omega_j}^{NL}(z, t) = (1/2) \{P_j^{NL}(z) \exp[i(\omega_j t - k_j z)] + c.c.\} \quad (2.11)$$

Where we have assumed a zero phase mismatch between E_{ω_j} and P_{ω_j} , as is the case for non-parametric processes such as stimulated Raman scattering, [1]. Equations (2.10) and (2.11) can be substituted into eqn.(2.9a), which must hold separately for each frequency ω_j . This is simplified by

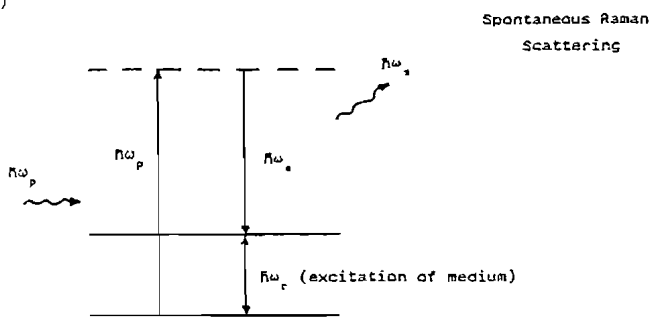
applying the "slow" variation approximation, which is that the envelope changes by only a small fraction in a distance of the order of one wavelength (thus we can drop the $\partial^2 E_j / \partial z^2$ term). We then obtain,

$$2(\partial E_j / \partial z) = -i(\omega / n_j \epsilon_0 c_0) P_j^{NL} \quad (2.12)$$

where we have used $k_j = n_j \omega_j / c_0$ and $\epsilon_j = n_j^2 \epsilon_0$ (c_0 being the velocity of light in a vacuum and n_j the refractive index at ω_j). It should be noted that we have also assumed a wave travelling in the positive z direction.

Having arrived at the general equation given above we will now concentrate specifically on the description of Raman scattering. Spontaneous Raman scattering was first discovered by Raman in 1928 [2]. It is a weak scattering process in which an incident pump photon of frequency ω_p is annihilated and a scattered photon of lower frequency ω_s is created. The energy difference $\hbar\omega_r = \hbar(\omega_p - \omega_s)$ causes an excitation of the scattering medium (e.g. in the case of CH_4 gas there is a vibrational excitation of the molecule giving a Raman shift of 2917cm^{-1}). Fig.2.1(a) summarises the effect with the scattered photon being emitted in any direction, as in spontaneous emission.

Fig 2.1(a)



(b)

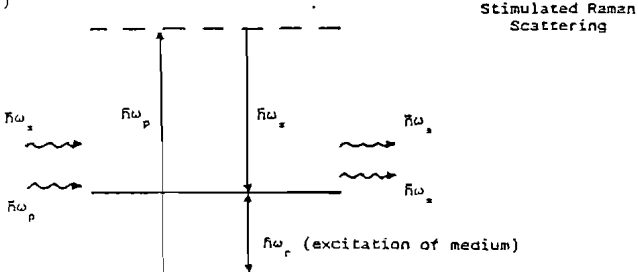
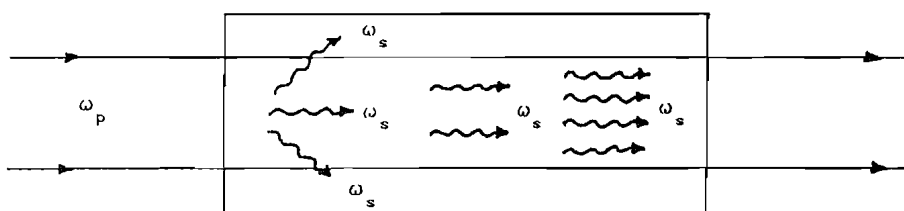
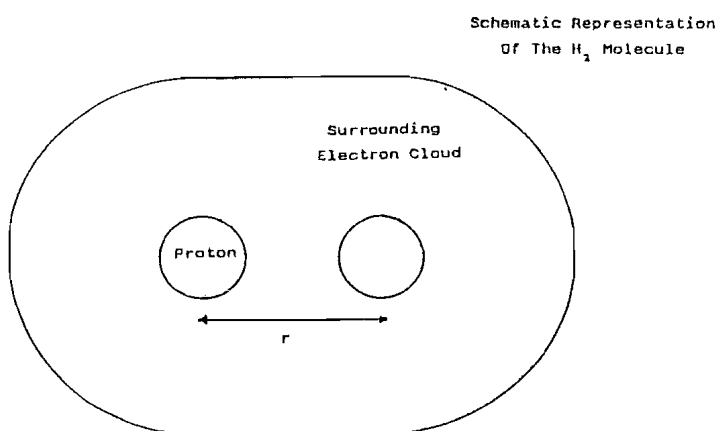


Fig.2.1(b) summarises the effect known as stimulated Raman scattering (SRS) where a molecule is subject to two incident photons, one at ω_p and one at ω_s , and the scattered photon produced as a result of annihilation of ω_p is identical to the incident photon ω_s . Thus the scattered photon is stimulated by the incident photon and, as in an ordinary laser, this provides a mechanism for amplification. Fig.2.2 shows schematically how, as a pump beam passes through a medium, stimulated emission can produce a rapid growth in the scattered wave. Spontaneous scattering can provide the noise to initiate the whole process.

Fig 2.2



SRS can also be usefully described in terms of fields and nonlinear susceptibilities rather than the photon model just described. Taking the hydrogen molecule as a simple example, if we apply an electric field E_{ω_p} we will produce an oscillating dipole moment p at the frequency ω_p such that $p=\alpha E_{\omega_p}$, where α is the polarisability.



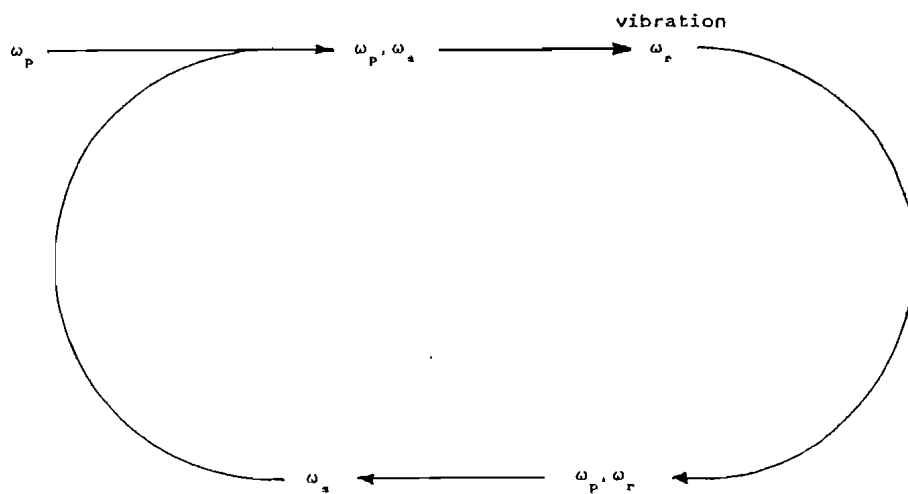
This will radiate at ω_p and is the origin of the familiar linear optical properties. However the polarisability is dependant on the separation r and if the molecule is vibrating at ω_r then α will also oscillate as below,

$$\alpha = \alpha_0 + (\partial\alpha / \partial r) (r-r_0) \cos\omega_r t \quad (2.13)$$

Thus for $E=E_0 \cos\omega_p t$ we have a dipole moment given by,

$$p = [\alpha_0 + (\partial\alpha / \partial r) (r-r_0) \cos\omega_r t] E_0 \cos\omega_p t \quad (2.14)$$

and this will have oscillation components at $(\omega_p - \omega_r)$ and $(\omega_p + \omega_r)$ which are the Stokes (ω_s) and anti-Stokes (ω_{as}) frequencies respectively. An applied electric field stretches the electron cloud and the nuclei will take up a new equilibrium separation. If this field has two components ω_p and ω_s , then the separation is modulated at a frequency $\omega_p - \omega_s$. If $\omega_p - \omega_s = \omega_r$, the natural resonance frequency, then the vibration amplitude is comparatively large. Thus by applying electric fields at ω_p and ω_s we can drive the molecular vibration ω_r , while this vibration and the field at ω_p will produce a field at ω_s . This is schematically represented below and again noise at ω_s is needed to start the process,



The amplitude of the molecular vibration is proportional to E_p and E_s and so the dipole moment and hence the polarisation has a term dependent on $|E_p|^2 E_s$. So the appropriate nonlinear polarisation is, from eqn.(2.7),

$$P^{NL} = \epsilon_0 K^{(3)} \chi_r |E_p|^2 E_s \quad (2.15)$$

Where χ_r is the Raman susceptibility, $\chi_r = \chi^{(3)}(-\omega_s; \omega_p - \omega_p, \omega_s)$. For SRS $K^{(3)}$ is $(3/2)$, see ref.[1]. At resonance only the imaginary part of the Raman susceptibility remains ($\chi_r = \chi'_r + i\chi''_r$), [3], thus equations (2.15) and (2.12) give,

$$(\partial E_s(z) / \partial z) = (3\omega_s / 4c_0 n_s) \chi'_r |E_p(z)|^2 E_s(z) \quad (2.16)$$

For the small signal case of negligible pump depletion we can put $E_p(z) = E_p(0) = E_{p0}$ and so eqn.(2.16) can be integrated to give,

$$E_s(z) = E_s(0) \exp[(3\omega_s / 4c_0 n_s) \chi'_r |E_{p0}|^2 z] \quad (2.17)$$

The time averaged intensity for a field E_ω is given by $I_\omega = (1/2) \epsilon_0 c_0 n_\omega |E_\omega|^2$, thus the Stokes intensity is,

$$I_s(z) = I_s(0) \exp[G_r] = I_s(0) \exp[g_r I_{p0} z] \quad (2.18)$$

where the Raman exponential gain G_r is given by,

$$G_r = (3\omega_s / \epsilon_0 c_0^2 n_s n_p) \chi'_r I_{p0} z \quad (2.19)$$

and g_r is the Raman gain coefficient. The imaginary part of the Raman susceptibility is given by, [4],

$$\chi'_r = \frac{16\pi^2 n_p c_0^4 \epsilon_0 \Delta N}{3n_s \omega_s^4 \hbar \Delta \omega_r} \left(\frac{d\sigma}{d\Omega} \right) \quad (2.20)$$

where ΔN is the population density, $\Delta \omega_r$ is the full width at half maximum Raman linewidth, and $(d\sigma/d\Omega)$ is the Raman differential cross section defined in terms of intensities. The Raman gain coefficient is therefore,

$$g_r = \frac{G_r}{I_{p0} z} = \frac{4\lambda_s^2 \Delta N}{\hbar \omega_s n_s^2 \Delta \omega_r} \left(\frac{d\sigma}{d\Omega} \right) \quad (2.21)$$

2.2.2 The Population Density

The population density is related to the pressure ρ and the temperature T by the simple relation,

$$\begin{aligned}\Delta N &= \vartheta \rho / kT \\ &= 7.32 \times 10^{27} \rho (\text{atm}) \vartheta / T (\text{K})\end{aligned}$$

where ϑ is the fraction of the total population density in the initial level of the Raman transition. For CH_4 gas $\vartheta=1$, [5], and so,

$$\Delta N = 7.32 \times 10^{27} \rho / T \quad (2.22)$$

2.2.3 The Raman Linewidth

The Raman linewidth for CH_4 was found to be a linear function of pressure in the 1-50atm region by Taira et al, [6]. They give the result as,

$$\Delta\omega_r = \pi c (64 + 2.4\rho) \quad (2.23)$$

where ρ is again given in atmospheres. By inspection of equations (2.21), (2.22) and (2.23) we see that the Raman gain coefficient has a pressure dependance given by,

$$g_r \propto \rho / (\rho + 26.7) \quad (2.24)$$

2.2.4 The Differential Raman Scattering Cross Section

Most of the data on the differential Raman scattering cross section given in the literature is for N_2 at some particular exciting frequency ν_n . In order to find $d\sigma/d\Omega$ at ν_n for CH_4 we use the expression given by Schrötter and Klöckner, [7].

$$(d\sigma/d\Omega)_{CH_4, \nu_n} = (d\sigma/d\Omega)_{N_2, \nu_n} (\Sigma_j) - \frac{[\nu_n - \nu_r]}{[\nu_n - 2331]}^4 \quad (2.25)$$

where ν_r is the Raman shift for CH_4 expressed in cm^{-1} and Σ_j is the "relative normalised differential Raman scattering cross section" defined and tabulated in ref.[7]. To find $(d\sigma/d\Omega)_{CH_4}$ at the pump frequency ν_p used we can apply the following transformation, [8],

$$\left[\frac{d\sigma}{d\Omega} \right]_{CH_4, \nu_p} = \left[\frac{d\sigma}{d\Omega} \right]_{CH_4, \nu_n} \frac{\left[\frac{1}{\Omega_{ig} - \nu_p} + \frac{1}{\Omega_{ig} + \nu_s} \right]^2}{\left[\frac{1}{\Omega_{ig} - \nu_n} + \frac{1}{\Omega_{ig} + \nu_s} \right]^2} \left[\frac{\nu_s}{\nu'_s} \right]^4 \quad (2.26)$$

where $\nu_s = \nu_p - \nu_r$, $\nu'_s = \nu_n - \nu_r$, and Ω_{ig} is the frequency of the transition from the initial Raman level to the dominant intermediate level i in the Raman process ($\Omega_{ig} = 7 \times 10^4 cm^{-1}$ for CH_4). Combining equations (2.25) and (2.26), and substituting in $\Sigma_j = 9$ and $(d\sigma/d\Omega)_{N_2, \nu_n} = 43.2 \times 10^{-36} m^2/Sr$ at $\nu_n = 19436.4 cm^{-1}$ (as given by Schrötter and Klöckner), we obtain,

$$(d\sigma/d\Omega)_{CH_4, \nu_p} = 4.63 \times 10^{-42} \left[\frac{1}{7 \times 10^4 - \nu_p} + \frac{1}{7 \times 10^4 + \nu_s} \right]^2 \nu_s^4 \quad (2.27)$$

2.2.5 Raman Exponential Gain At Threshold

As previously stated, the process of stimulated Raman scattering is initiated by the weak noise intensity $I_s(0)$ at the Stokes frequency produced by spontaneous Raman scattering. In the small-signal region the generated Stokes intensity will show a rapid dependence on the incident pump intensity I_{p0} due to the exponential gain factor, eqn.(2.18). Thus SRS appears to have a threshold behaviour, in that below a certain incident pump intensity there is no

observable Stokes intensity or pump depletion. This definition of threshold is arbitrary in that, for instance, it depends on the sensitivity of the detector used to observe the Stokes output, but it is however a useful guide to calculating the required pump intensity.

Calculation of the required Raman exponential gain to reach threshold G_{th} (e.g. [1],[9]) shows that there is little difference in whether one defines threshold as when there is total conversion of the pump to the Stokes frequency, or as when one first achieves an observable Stokes output. In practice the required value typically lies between 20 and 30. Thus we will take $G_{th}=25$ and use the easiest practical measure of threshold as the point at which depletion of the pump is first detected.

2.2.6 Threshold Pump Power For Guided And Unguided Media

The on-axis Raman exponential gain for an unguided medium can be written as,

$$G_r = g_r \int_{-1/2}^{+1/2} \left[2P / \pi W^2(z) \right] dz \quad (2.28)$$

where l is the length of the medium, P is the peak pump power, and $W(z)$ is the pump beam spot size. Kogelnik and Li, [10], give,

$$W^2(z) = W_0^2 [1 + (2z / b)^2] \quad (2.29)$$

where b is the confocal parameter $(2\pi W_0^2 / \lambda_p)$ and W_0 is the pump beam waist spot size formed at the centre of the medium. Substituting eqn.(2.29) into eqn.(2.28) we obtain,

$$G_r = g_r (4P / \lambda) \tan^{-1}(l / b) \quad (2.30)$$

where we have used $\int dx / (x^2 + a^2) = (1/a) \tan^{-1}(x/a)$. However, eqn.(2.28) does not generally hold for Gaussian beams, where

the Stokes radiation will experience an average gain that includes the off-axis intensity. Consequently the overall Raman gain is smaller than that given in eqn.(2.30). Cotter et al, [11], give the corrected gain as,

$$G_r = [(\lambda_s/\lambda_p) \tan^{-1}(1/b)] [(4Pg_r/\lambda_s)^{1/2} - 2] (4Pg_r/\lambda_s)^{1/2} \quad (2.31)$$

The Raman exponential gain for a guided medium is given by,

$$G_r = g_r \int_0^1 \left[\frac{P \exp(-\alpha_p z)}{\pi W_0^2} - \alpha_s \right] dz \quad (2.32)$$

where α_p and α_s are the waveguide attenuation coefficients at the pump and Stokes wavelengths. For a capillary of bore radius a , Marcatili and Schmeltzer, [12], give $\alpha = 0.43\lambda^3/a^3$ for propagation of the EH_{11} mode. Efficient coupling ($\approx 98\%$) from a TEM_{00} mode pump into the EH_{11} mode may be made by satisfying the launch condition $3W_0 = 2a$, [13], where, as in eqn.(2.32), W_0 is the pump beam spot size at the capillary entrance.

It should be noted that in eqn.(2.32) we have used an effective area of πW_0^2 . This takes into account the transverse variation of the pump and Stokes beams via an overlap integral, [14]. Solving eqn.(2.32) leads to,

$$G_r = (P / \pi W_0^2) g_r l_{eff} \alpha_s^{-1} \quad (2.33)$$

where l_{eff} is the effective length of the capillary related to the actual length by,

$$l_{eff} = (1 - \exp[-\alpha_p l]) / \alpha_p \quad (2.34)$$

The guiding behaviour of the capillary reduces the beam diffraction by reflecting it back into the Raman medium. Thus a high intensity-length product, and therefore a high Raman gain, can be achieved. Re-arranging eqn.(2.33) we obtain an expression for the pump power required to achieve SRS

threshold in a capillary waveguide,

$$P_{th} = (G_{th} + \alpha_s l) \pi W_0^2 / g_r l_{eff} \quad (2.35)$$

2.2.7 Capillary Waveguide Design

Expressing eqn.(2.35) in terms of the capillary radius we find,

$$P_{th} \propto \frac{2.45 \times 10^{13}}{(1 - \exp [-0.43 \lambda_p^2 / a^3])a} + \frac{1}{(1 - \exp [-0.43 \lambda_p^2 / a^3])a^4}$$

where we have taken $l=1m$ (limited by the length of the Raman cell), and $\lambda_s = 1.544\mu m$. Thus, for $\lambda_p = 1.064\mu m$, we find the results shown in fig.2.3 which give an optimum capillary bore radius of $a \approx 70\mu m$.

2.2.8 Transient Raman Scattering

The results obtained up to this point apply to a steady state solution. However, if we use pump pulses that are temporally short compared to the dephasing time T_2 of the Raman medium (transient Raman scattering), the gain will be lower because the molecular vibrations do not have enough time to build up to their steady state value, [15]. In fact a significant degree of transience applies for pump pulse durations T_p of up to twenty times T_2 . Defining the dephasing time as $T_2 = 2/\Delta\omega_r$ we can apply a correcting factor F , as given in ref.[8], to eqn(2.35). Thus the pump power required for SRS threshold under transient conditions in a capillary waveguide is given by,

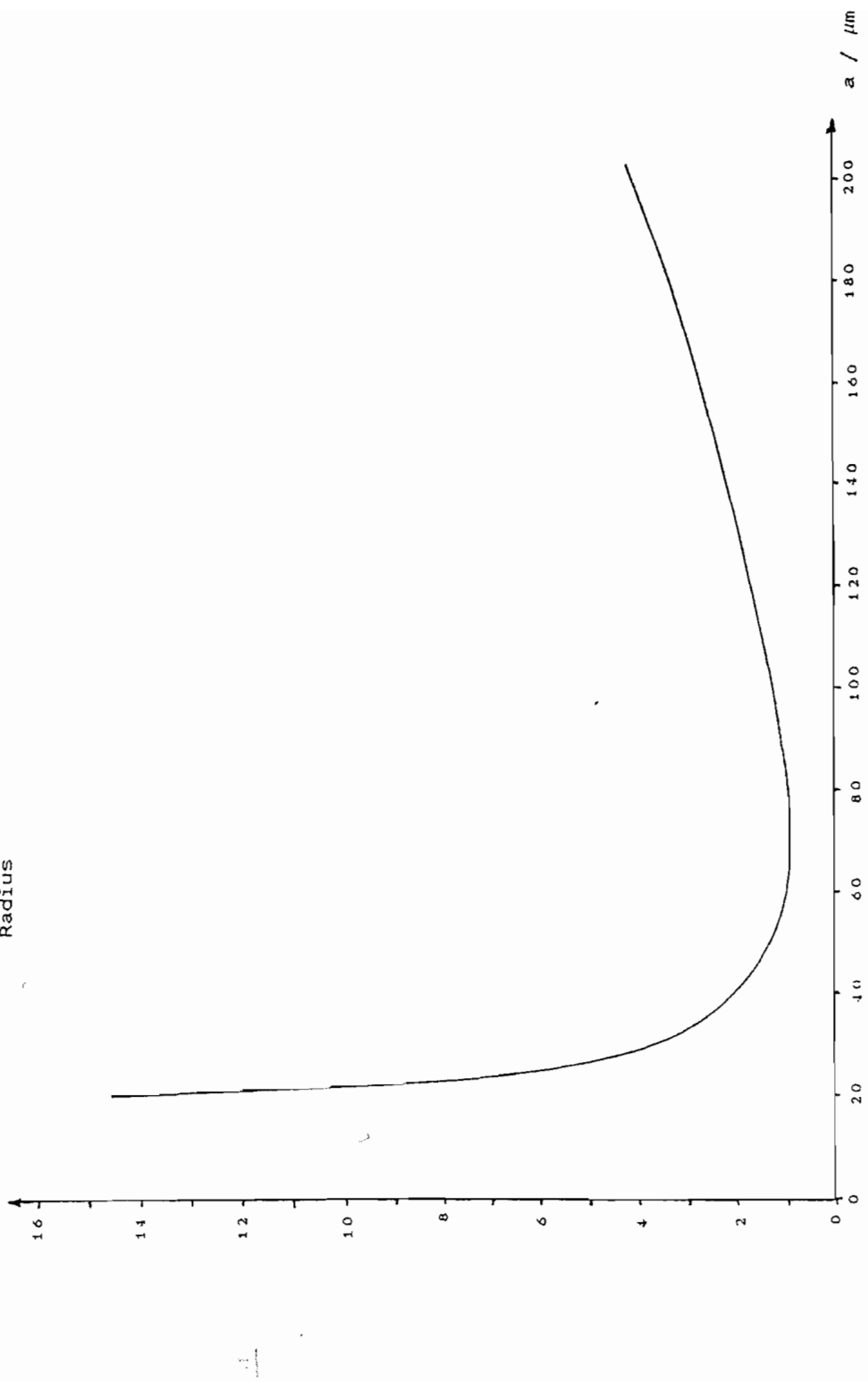
$$P_{th} = F(G_{th} + \alpha_s l) \pi W_0^2 / g_r l_{eff} \quad (2.36)$$

2.3 The Pump Laser

2.3.1 Choice Of Pump Laser

Radiation in the $1.5\mu m$ region can readily be obtained via stimulated Raman scattering of a $1.064\mu m$ Nd:YAG

Fig 2.3 Graph Of Normalised Threshold Power Against Capillary Radius



pump in CH_4 , [17]. Our aim was to obtain a convenient source of short pulses at $1.54\mu\text{m}$ suitable for use as a research tool in optical communications laboratories. With this in mind we decided to use a cw pumped, mode-locked and Q-switched, Nd:YAG laser (Spectra Physics 3000) as the pump source. This type of laser is widely available, and is capable of high Q-switch repetition rates ($\sim 1\text{kHz}$).

In practice we found the pump laser provided an output of up to $\sim 1.6\text{mJ}$ in a $\sim 200\text{ns}$ Q-switched envelope of mode-locked pulses. The mode-locked pulses had a repetition rate of $\sim 82\text{MHz}$ and a full width half maximum (FWHM) duration $T_p = 120\text{ps}$. Thus peak powers of up to $\sim 0.7\text{MW}$ were available. The output was in a clean TEM_{00} mode, which is essential for good coupling into a capillary waveguide. Fig.2.4 shows a typical train of output pulses.

2.3.2 Actively Stabilised Acousto-Optic Mode-locking

To obtain mode-locked performance with the acousto-optic modulator used in the pump laser cavity, it is necessary to match the RF drive frequency and the cavity length to one of its resonances. We would like to apply RF powers of up to 1W in order to obtain good diffraction efficiency, but the dissipation of this amount of acoustic energy gives rise to temperature changes large enough to shift the modulator resonances. Thus it was necessary to employ an active feedback stabilisation scheme, [18], to lock the acoustic resonance to the RF drive frequency. A schematic diagram of the system used is shown in fig.2.5. It relies on the observation that the phase difference between the incident and reflected RF signals passes through zero at a resonance. The directional coupler provides signals proportional to the incident and reflected RF. The phase detector then compares the two signals and gives a dc output proportional to their phase difference. This signal, after amplification, is used to control the incident RF power level via a voltage controlled attenuator. Thus a slight shift in the resonance causes a phase difference to be detected and the RF power to be altered, such that the resonance returns to its original frequency.

Fig 2.4 Pump Laser Output Train

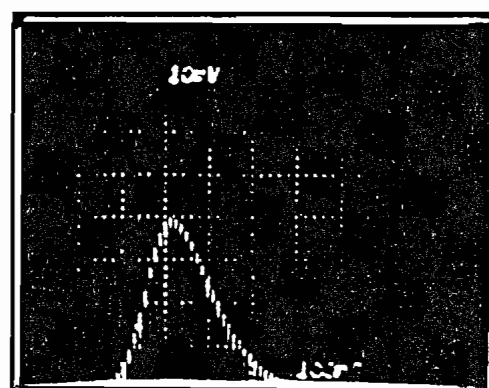
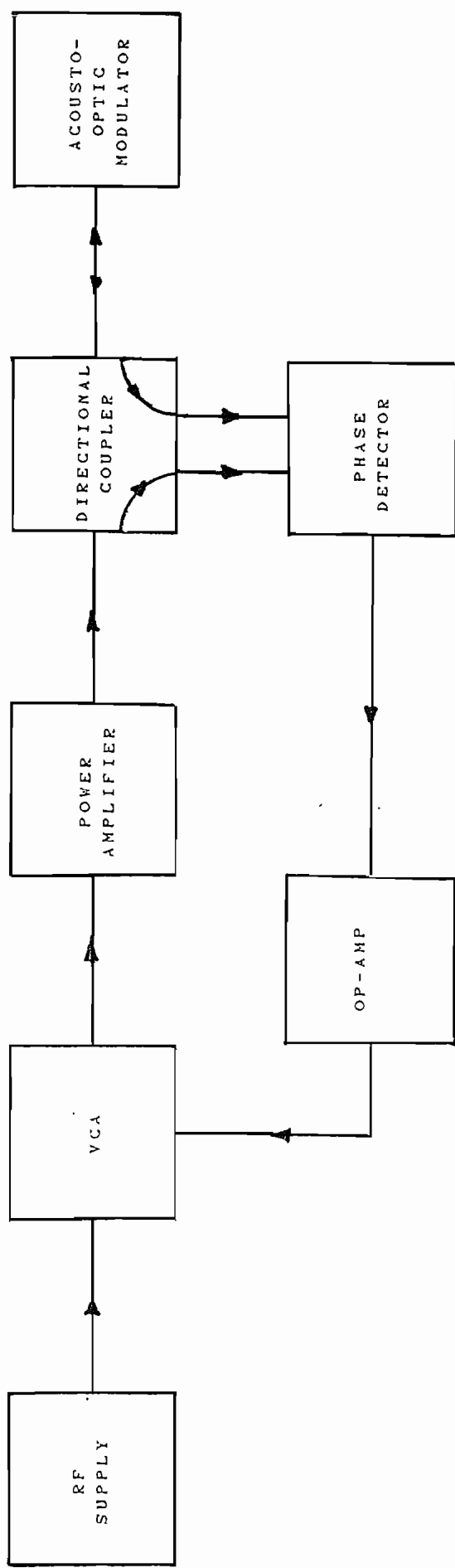


Fig 2.5 The Active Feedback Stabilisation Scheme



The use of this scheme has the added advantage that it also allows the tuning of the RF over a significant frequency range without unlocking the system, because the modulator resonance is forced to follow the RF frequency. This allows fine tuning of the frequency to the cavity length, which can have a comparatively coarse adjustment.

A temperature controlled oven is used to keep the average temperature stable so that changes in room temperature do not affect the long term stability of the locked system.

2.4 A Single Pass Waveguide Raman Laser (see appendix 1)

2.4.1 Introduction

From the equations developed in section 2.1 we are now able to calculate the Raman gain coefficient and hence the predicted power thresholds for SRS under guided or unguided conditions.

The experimental conditions are,

Pump Pulse Durations (FWHM)	$T_p = 120\text{ps}$
CH_4 Gas Pressure	$\rho = 70\text{atm.}$
Pump Wavelength	$\lambda_p = 1.064\mu\text{m}$
1st Stokes Wavelength	$\lambda_s = 1.544\mu\text{m}$

Thus we can evaluate eqns.(2.22),(2.23) and (2.27) with the results shown below,

Population Density	$\Delta N = 1.77 \times 10^{27} \text{m}^{-3}$
Raman Linewidth (FWHM)	$\Delta \omega_r = 2.19 \times 10^{11} \text{Hz}$
Differential Raman Scattering	Cross Section($d\sigma/d\Omega$) $= 7.20 \times 10^{-36} \text{m}^2 \text{Sr}^{-1}$

Substituting these values into eqn.(2.21) give a steady state Raman gain coefficient of,

$$g_r = 4.27 \times 10^{-12} \text{ m.W}^{-1}$$

If we now consider the unguided case, we can re-arrange eqn.(2.31) to obtain the SRS power threshold,

$$P_{th} = (F\lambda_s / 4g_r) \left[1 + \left[1 + \frac{G_{th} \lambda_p}{\lambda_s \tan^{-1}(1/b)} \right]^{1/2} \right]^2 \quad (2.37)$$

where we have again included a factor F to account for the transient conditions (section 2.1.8). The dephasing time is $T_2 = 2/\Delta\omega_r = 9.13\text{ps}$, and for $T_p = 120\text{ps}$ this leads to a value for F of 1.36. Thus for optimum focussing ($\tan^{-1}(1/b) = \pi/2$), we would predict an unguided SRS threshold of $\sim 2.5\text{MW}$. As stated in section 2.2.1, the peak power available from cw pumped Nd:YAG lasers is typically $\sim 0.5\text{MW}$. Therefore the need for a waveguide to reduce the SRS threshold is apparent.

In this calculation we have used the highest CH_4 pressure allowed by our Raman cell. This is because a high pressure reduces the SRS threshold in two ways :

- (1) the steady state Raman gain coefficient is increased as shown by eqn.(24)
- (2) the degree of transience is reduced because there is an increase in the Raman linewidth and a corresponding decrease in the dephasing time.

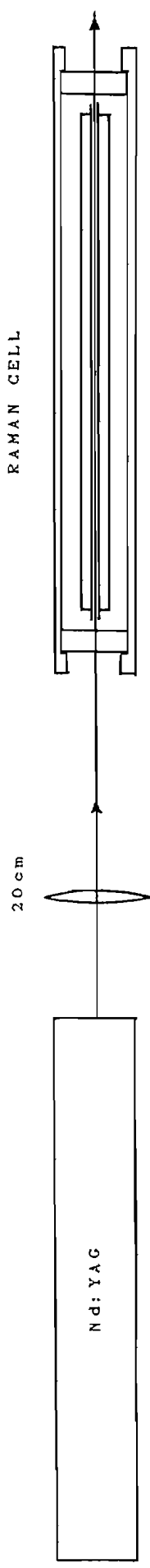
2.4.2 Experimental Arrangement And Results

Having decided upon a cw pumped Nd:YAG laser as the pump laser, we have shown that there is a requirement for a waveguide and a high CH_4 pressure in order to reach SRS threshold. With this in mind we used the experimental apparatus shown schematically in fig.2.6.

The use of a capillary waveguide Raman laser was first demonstrated by Rabinowitz et al, [19], and a number of authors (for example - [8],[20],[21]) have since shown that low SRS thresholds can be obtained with such devices.

Our Raman cell consists of a narrow bore fused

Fig 2.6 The Single Pass Capillary Waveguide Raman Laser



silica capillary waveguide supported and held straight inside another capillary of large outer diameter (~6mm). This lies in a high pressure container (up to ~70atm) which has 12mm thick fused silica windows. The waveguide is 74.6cm long and has a bore radius $a=100\mu\text{m}$, which is near to the optimum value ($\sim 70\mu\text{m}$) given in section 2.1.7. The capillary ends were cleaved and inspected to make sure they were flat and square to the bore.

The pump beam was focussed down to a $\sim 67\mu\text{m}$ waist W_0 at the capillary entrance satisfying the launch condition $3W_0=2a$. A capillary transmission of $T=57\%$ was readily obtained, compared to a theoretical value of 70%. The discrepancy between the figures is probably due to slight bending of the waveguide. The transmitted beam was in the form of a clean circular spot of diffraction limited divergence. The experimental pump attenuation coefficient is,

$$\alpha_p = -\ln(T) / l = 0.75\text{m}^{-1} \quad (2.38)$$

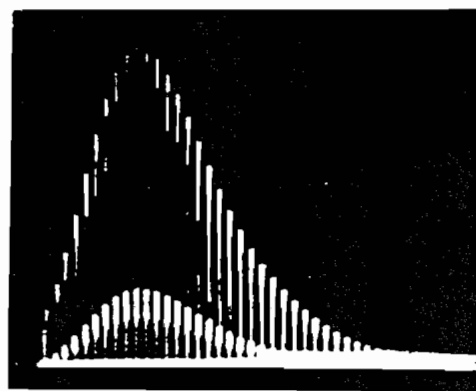
Substituting this value into eqn.(34) we get an effective length of 57.1cm. The theoretical signal attenuation coefficient is given by,

$$\alpha_s = \alpha_p (\lambda_s / \lambda_p)^2 = 1.58\text{m}^{-1} \quad (2.39)$$

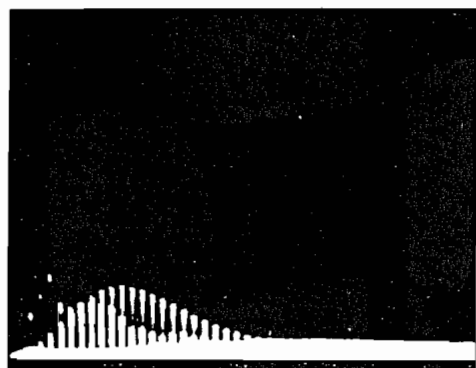
Using eqn.(36) we can now predict a SRS pump power threshold of $\sim 200\text{kW}$. This is an order of magnitude improvement on what we would expect for the unguided case. In practice we found we were able to obtain SRS at a threshold of $\sim 190\text{kW}$. A typical pump depletion and Stokes output at $1.54\mu\text{m}$ is shown in fig.2.7. Comparing figs.2.7(a) and (b) shows the strong depletion that can be caused with the full pump power incident on the capillary. The smaller interleaved pulses are due to light travelling along the capillary walls and hence are delayed with respect to the main pulses by $\sim 1\text{ns}$. When aligning the capillary for maximum pump transmission we noted that there was a corresponding minimum in the size of the interleaved pulses. This was found to be a useful practical aid to the alignment procedure. Fig.2.7(c) shows the train

Fig 2.7 Pump Depletion And Stokes Output

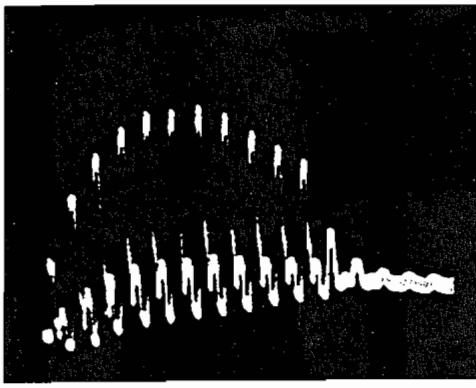
a)



b)



c)



of $1.54\mu\text{m}$ output pulses which had an amplitude stability equal to that of the pump pulses. The rising dc level on the picture is due to the response of the Ge detector used.

The pulsedwidths of the pump and output mode-locked pulses were measured using a background-free second harmonic autocorrelator, see fig.2.8. Using a KD³P crystal and Si photodiode for the pump, and a LiIO₃ crystal and extended S20 photomultiplier for the output, we obtained the results shown in fig.2.9. The mode-locked performance of the pump laser was disappointing, being typically $\sim 120\text{ps}$. However it has been observed, [22], that this type of laser shows optimum pulse amplitude stability for such pulse durations, and we have always fine tuned the mode-locking frequency to produce the most stable pump depletion. As has been found by other authors (e.g. [15],[16]) some degree of pulse shortening can occur for transient Raman scattering and we measured typical output FWHM pulsedwidths of $\sim 100\text{ps}$.

Using a pyroelectric energy meter to measure the energy in the train of output pulses, we were able to calculate that the largest individual mode-locked pulses had an energy of $\sim 7\mu\text{J}$. Thus peak output powers of $\sim 66\text{kW}$ were available.

2.5 A Synchronously Pumped Waveguide Raman Laser (see appendix 2)

We have shown that waveguide techniques can bring the threshold for a $1.544\mu\text{m}$ CH₄ Raman laser within reach of a commercial cw Q-switched and mode-locked Nd:YAG laser. We now attempted to reduce the threshold even further by combining the waveguide with a ring resonator to provide synchronous pumping. Thus Stokes output would be fed-back in synchronism with the next pump mode-locked pulse, providing a large seeding signal to the Raman scattering process.

2.5.1 Threshold Pump Power

The Stokes intensity after one pass through the waveguide is given by,

Fig 2.8 The Autocorrelator

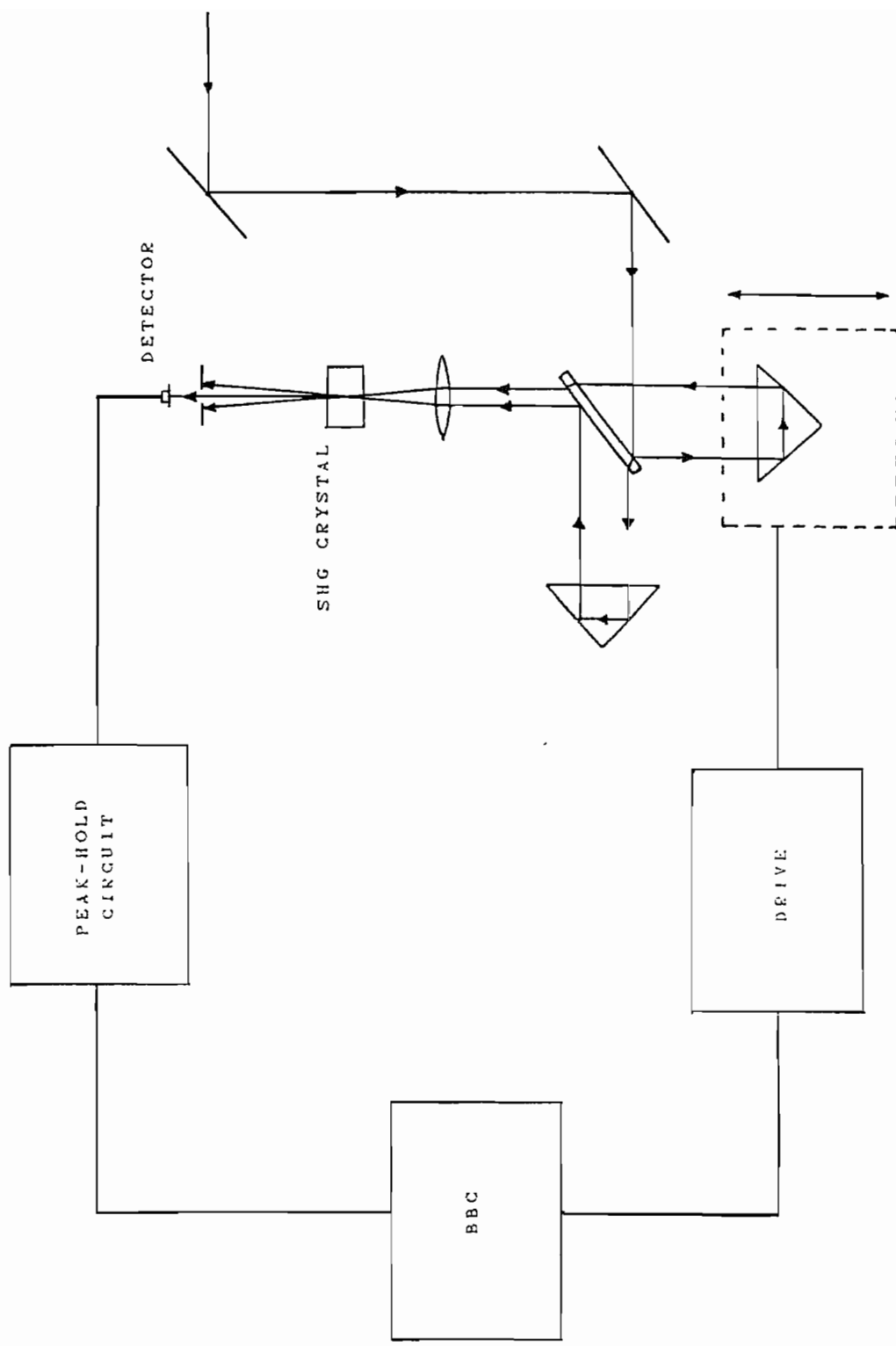
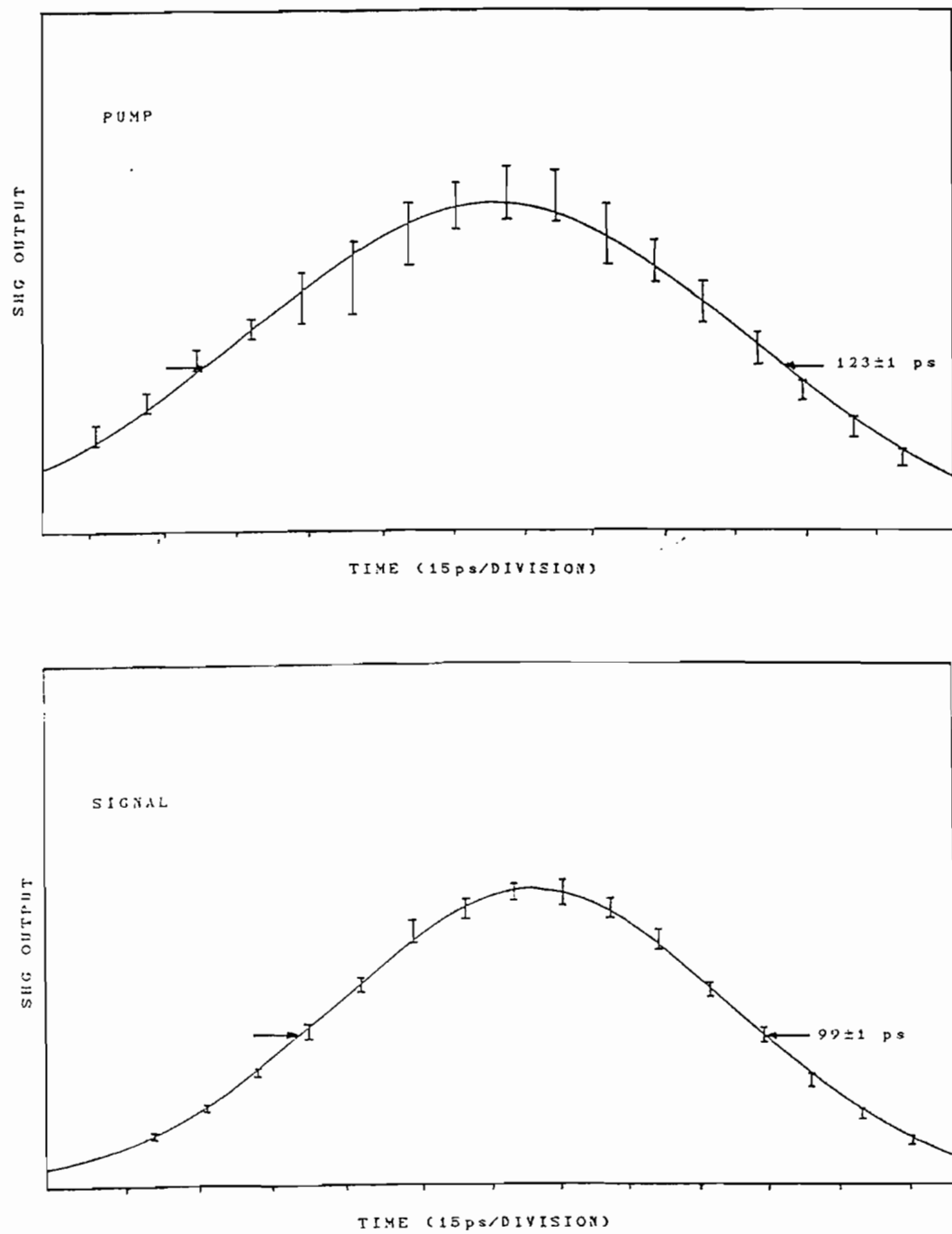


Fig 2.9 Autocorrelation Traces



$$I_{s1} = I_s(0) \exp ([g_r I_{p1} l_{eff} / F] - \alpha_s l) \quad (2.40)$$

where I_{p1} is the intensity of the corresponding pump pulse. When the second pump pulse passes through the Raman medium it amplifies the Stokes signal which is fed-back in synchronism with it. Therefore,

$$\begin{aligned} I_{s2} &= RI_{s1} \exp ([g_r I_{p2} l_{eff} / F] - \alpha_s l) \quad (2.41) \\ &= RI_s(0) \exp ([g_r l_{eff} (I_{p1} + I_{p2}) / F] - 2\alpha_s l) \end{aligned}$$

where R is the fraction of the Stokes power fed back into the capillary. Thus we obtain,

$$I_{sn} = I_s(0) R^{(n-1)} \exp \left[[g_r l_{eff} / F] \sum_{i=1}^n I_{pi} - n\alpha_s l \right] \quad (2.42)$$

In order to obtain SRS threshold we require that $G = \ln(I_{sn}/I_s(0)) = 25$, as previously stated. Therefore the threshold pump power condition is given by,

$$(n-1) \ln R + (g_r l_{eff} / \pi W_0^2 F) \sum_{i=1}^n P_{pi} - n\alpha_s l = 25 \quad (2.43)$$

2.5.2 Experimental Arrangement And Results

Fig.2.10 shows the apparatus used. The pump focussing condition is the same as for the single pass case and is provided by a 20cm focal length lens (not shown). The prisms P_1, P_2, P_3 and the beam splitter B form the ring resonator directing the Stokes wave back into the capillary. The prisms P_1, P_2 are on a common mount with a micrometer adjustment for fine tuning of the cavity length to achieve synchronism with the pump pulses. The lenses L_1 and L_2 collimate and focus the Stokes beam respectively, so that it is efficiently re-launched into the capillary, i.e. there is a waist W_0 formed at the capillary satisfying the condition $3W_0 = 2a$. The beamsplitter B has a high transmission at the pump wavelength and provides the output coupling for the Raman laser.

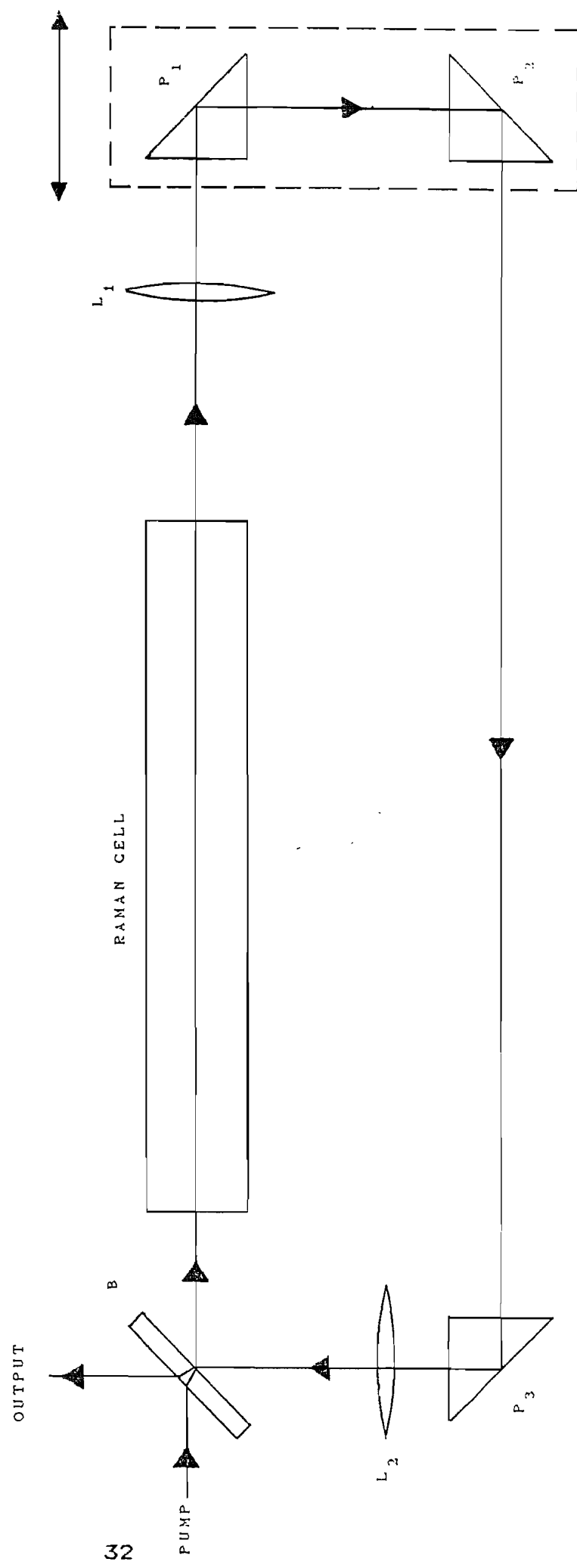


Fig 2.10 Synchronously Pumped Raman Laser

From eqn.(2.43), and using values of n and $\sum P_{pi}$ measured from a photograph of the pump pulse train, we were able to estimate a threshold of $\sim 60\text{kW}$. In practice we did slightly better than this, first observing pump depletion at peak powers of $\sim 50\text{kW}$. Fig.2.11 shows the pump pulse train at the threshold for SRS. It can clearly be seen that the first signs of depletion occur approximately 4 pulses after the peak of the Q-switched train. This is in good agreement with the results found when putting the experimental threshold powers into eqn.(2.43), which predicts that the maximum value for the exponential Raman gain would occur 4 pulses after the peak.

Fig.2.12 demonstrates the effect of synchronous feedback on the pump depletion. Fig.2.12(a) shows the transmitted pump pulse train just below the single pass threshold with the feedback arm blocked. Fig.2.12(b) shows the heavily depleted pump pulse train when the feedback is introduced, under the same pumping conditions.

Fig.2.13 shows the train of 1st Stokes output pulses for an incident pump peak power of 310kW . As before, these pulses showed excellent amplitude stability. Measurements of the energy in the output pulse train implied that individual mode-locked pulse energies of $\sim 1.3\mu\text{J}$ were available. Once again pump and signal autocorrelation measurements were made using the apparatus shown in fig.2.8. The values found for the pulse durations were similar to those seen in the single pass case. Fig.2.14 shows the autocorrelation of the Stokes output averaged over the pulse train. Thus peak output powers of $\sim 12\text{kW}$ were available. Measurements of the output bandwidth were also made but were instrument limited as we did not have the appropriate mirrors for the Fabry-Perot interferometer at that time. This measurement did at least enable us to put an upper limit on the time-bandwidth product of ~ 0.7 . This value should be compared to the value of 0.44 expected for bandwidth limited Gaussian pulses.

2.6 Summary

Fig 2.11 Threshold Pump Depletion

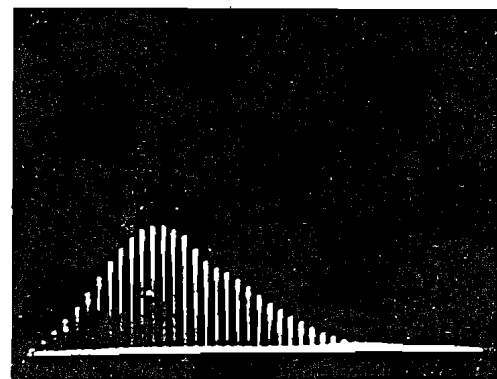


Fig 2.12 Pump Pulse Train With And Without Feedback

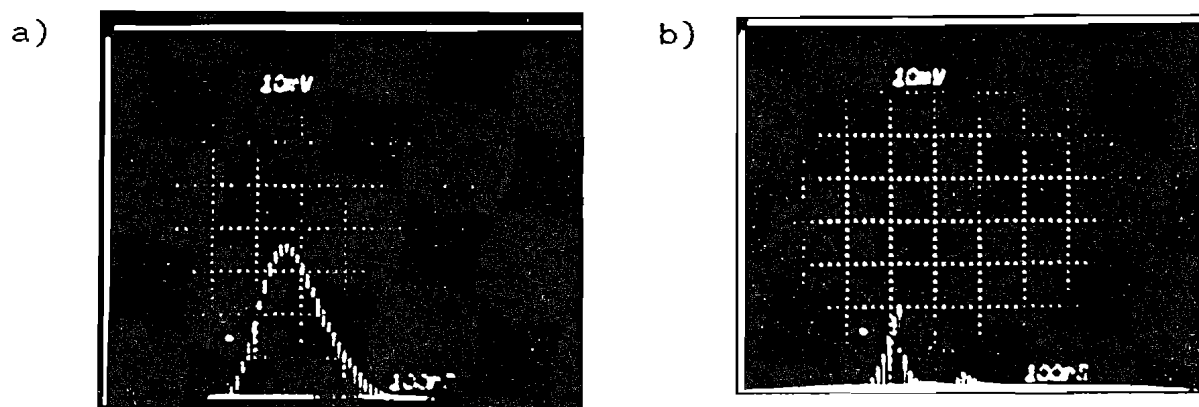


Fig 2.13 Stokes Output

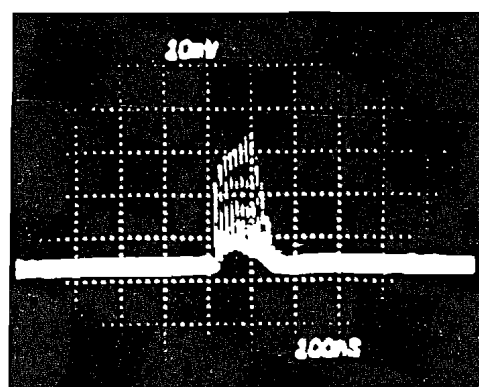
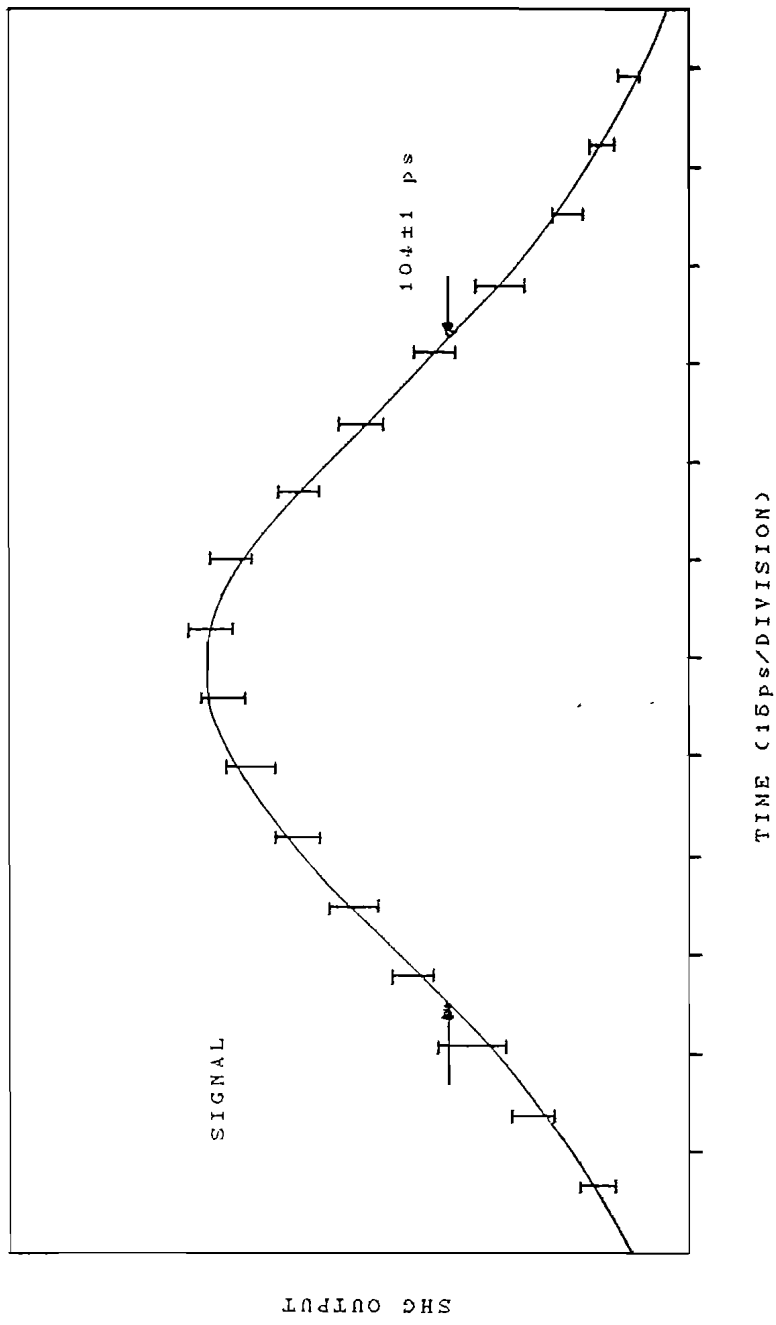


Fig 2.14 Autocorrelation Trace



We have shown that the threshold for stimulated Raman scattering in CH_4 gas can be reduced by a factor of 50, to $\sim 50\text{kW}$, by employing waveguide and synchronous pumping techniques. This allows the use of a Spectra Physics 3000 cw Nd:YAG laser as the pump, while still being $\sim 10\times$ above threshold. The train of mode-locked output pulses have FWHM durations of $\sim 100\text{ps}$ and peak powers of up to $\sim 66\text{kW}$. The output pulses are stable and are contained in a clean, circular, diffraction limited beam. Anti-Stokes radiation at 812nm was also observed for both the experimental arrangements. Second Stokes radiation at $2.8\mu\text{m}$ was not observed, despite its probably being generated in significant amounts, because of the very low transmission of the Raman cell windows at this wavelength.

It should be noted that there are two features of the pump depletion that are, as yet, unexplained. Firstly, it can be seen in fig.2.7(b) that the single pass pump depletion is not symmetric about the envelope peak. This is surprising because pump pulses of the same power on either side of the envelope peak should suffer the same degree of depletion. The second point is that despite ~ 20 or more pump pulses showing significant depletion in both experimental arrangements we typically only see ~ 10 output pulses. From simultaneous observations of the pump and output pulses it appears that the Stokes output corresponds to the initial part of the pump depletion.

Another point to be noted is that all the results discussed in this section have been taken at a Q-switch repetition rate of 5Hz, despite the fact that the pump laser can operate at repetition rates of $>1\text{kHz}$. This is because at these higher repetition rates we observed a rapid and unexpected breakdown of the CH_4 , leading to a "sooty" deposit on the inside of the cell entrance window and at the entrance of the capillary waveguide.

Thus we have successfully demonstrated the low threshold operation of a CH_4 Raman laser at $1.54\mu\text{m}$. This is of general interest as a means of frequency conversion of short pulses.

However we were specifically interested in finding a convenient source of short pulses at $1.5\mu\text{m}$ for the investigation of soliton effects and pulse compression in optical fibres. Despite it certainly being capable of such investigations, (it has enough peak power to propagate very high order solitons), this source has several practical drawbacks which led us to try and find a more attractive alternative. The main disadvantages are,

- 1) The relatively long pulselength, caused by the poor performance of the pump laser, leads to very long soliton periods (see section 4.2) requiring the use of very long lengths of fibre.
- 2) The output consists of a train of pulses of varying peak powers which would therefore all propagate different order solitons. As our autocorrelation equipment averages over the pulse train we would get a confused picture.

2.7 References

- [1] D.C.Hanna, M.A.Yuratitch and D.Cotter, "Nonlinear Optics Of Free Atoms And Molecules", Springer Series in Optical Science, Volume 17, Springer Verlag (1979)
- [2] Raman, Ind. J. Phys. 2 (1928) 387
- [3] M.Maier, Appl. Phys. 11 (1976) 209
- [4] W.R.Trutna and R.L.Byer, Appl. Opt. 19 (1980) 301
- [5] L.C.Laycock, PhD Thesis, Southampton University (1978)
- [6] Y.Taira, K.Ide and H.Takuma, Chem. Phys. Lett. 91 (1982) 299
- [7] H.W.Schrötter and H.W.Klöckner, ch.4 in "Raman Spectroscopy Of Gases And Liquids", Topics in Current Physics, Volume 11, Springer Verlag (1979)
- [8] D.C.Hanna, D.J.Pionter and D.J.Pratt, IEEE J. Quantum Electron. QE-22 (1986) 332
- [9] M.T.T.Pacheco, PhD Thesis, Southampton University (1986)
- [10] H.Kogelnik and T.Li, Appl. Opt. 5 (1966) 1550
- [11] D.Cotter, D.C.Hanna and R.Wyatt, Appl. Phys. 8 (1975) 333
- [12] E.A.J.Marcatili and R.A.Schmeltzer, Bell Syst. Tech. J. 43 (1964) 1783
- [13] R.L.Abrams, IEEE J. Quantum Electron. QE-8 (1972) 838
- [14] A.J.Berry and D.C.Hanna, Opt. Comm. 45 (1983) 357
- [15] R.L.Carmen, F.Shimizu, C.S.Wang and N.Bloembergen, Phys. Rev. A 2 (1970) 60
- [16] D.C.Hanna and D.J.Pionter, Opt. Comm. 60 (1986) 187
- [17] D.G.Bruns, H.W.Bruesselbach, H.D.Stovall and D.A.Rockwell, IEEE J. Quantum Electron. QE-18 (1982) 1246
- [18] H.Klann, J.Kuhl and D.Von Der Linde, Opt. Comm. 38 (1981) 390

- [19] P.Rabinowitz, A.Kaldor, R.Brickman and W.Schmidt, *Appl. Opt.* 15 (1976) 2005
- [20] A.J.Berry, D.C.Hanna and D.B.Hearn, *Opt. Comm.* 43 (1982) 229
- [21] W.Hartig and W.Schmidt, *Appl. Phys.* 18 (1979) 235
- [22] P.Kean, K.Smith and W.Sibbett, *Opt. Comm.* 61 (1987) 129

3. A LONGITUDINALLY PUMPED Yb:Er PHOSPHATE GLASS LASER AT 1.536 μ m

3.1 Introduction

In this chapter we describe the operation of a 1.54 μ m Yb:Er glass laser pumped by a 1.064 μ m Nd:YAG laser. This source should be capable of running pulsed or cw, Q-switched and/or mode-locked, and would thus offer a more versatile source than the Raman laser with which to carry out soliton experiments. It would also have the advantage that it should be possible to operate this laser as a soliton laser, [1].

Most of the soliton investigations reported to date have used a colour centre laser (F^{2+} centres in NaCl, [2]) as the pump source, but the Yb:Er glass laser could offer several advantages for this particular application :

- 1) Operation at room, or elevated, temperatures should be possible, whereas the colour centre laser requires cooling to liquid nitrogen temperatures for reliable operation.
- 2) The Yb:Er glass could be pulled into a fibre. Thus a mini-YAG pumped, mode-locked, Yb:Er fibre laser could be envisaged where soliton effects could be taking place within the laser medium itself.
- 3) The Yb:Er laser offers a potentially much cheaper route to obtaining mode-locked pulses in the 1.5 μ m region.

Added to these advantages is the fact that the Yb:Er laser could be efficiently Q-switched due to its long upper state lifetime (~8ms).

In this chapter we will describe the Yb:Er system and its basic operation as a laser. The mode-locking of this laser and its use for non-linear pulse propagation experiments will be described in chapter four.

3.2 The Yb:Er System

3.2.1 Choice Of Pumping Scheme

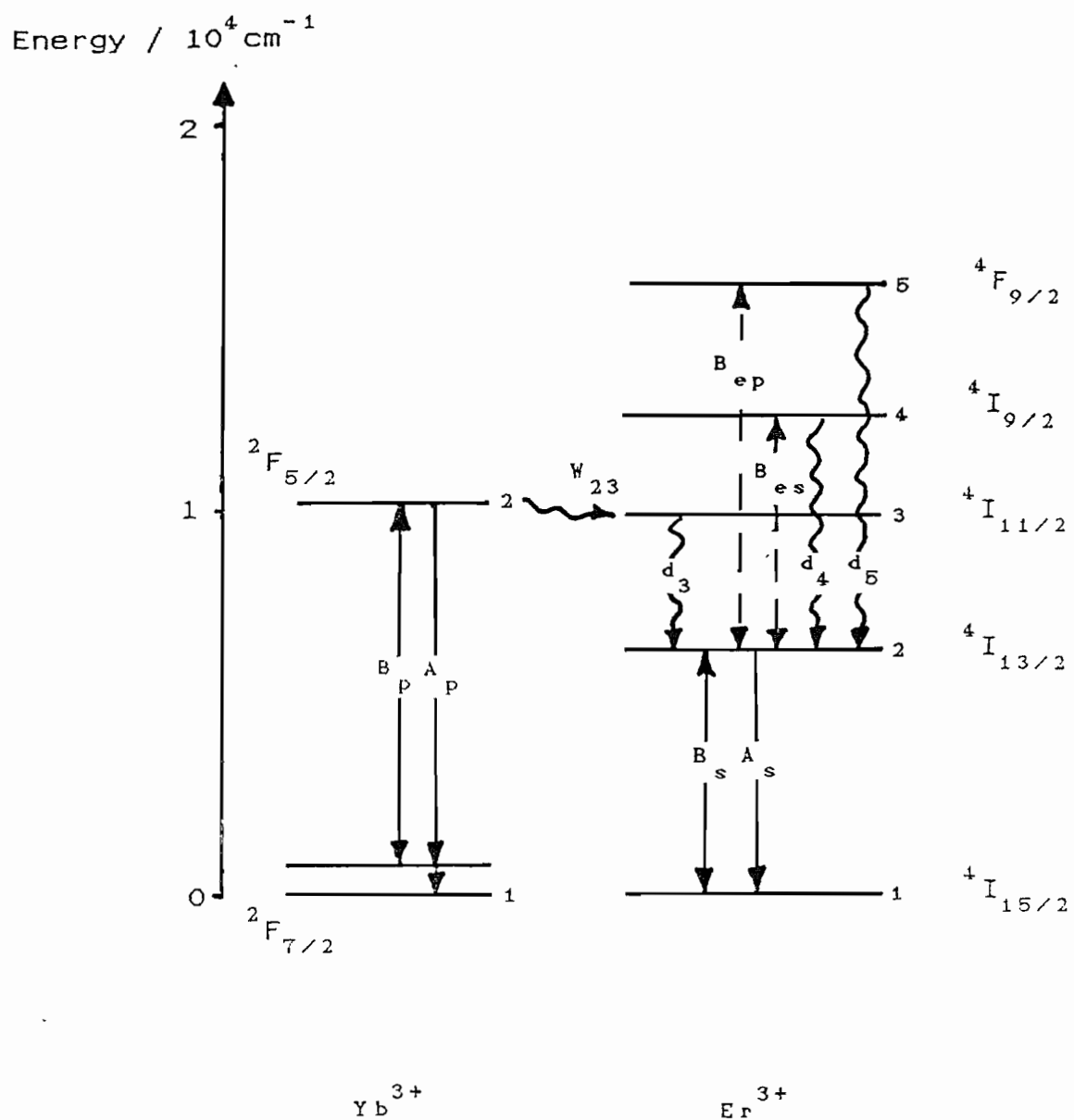
The first operation of an Yb:Er glass laser at $1.54\mu\text{m}$ was reported by Snitzer and Woodcock in 1965, [3], using a silicate glass and flash lamp pumping. Longitudinal pumping of an Yb:Er glass laser by a Nd laser was first demonstrated by Gapontsev et al in 1973, [4], using a pulsed Nd glass laser at $1.054\mu\text{m}$ as the pump. Longitudinal laser pumping allows the pump power requirements, and hence the thermal loading of the glass, to be minimised (for example see ref.[5]). As there will be significant thermal loading associated with the proposed cw operation of this three-level glass laser, we decided to use longitudinal pumping, with $1.064\mu\text{m}$ Nd:YAG lasers as the pump source. This pump source has the added advantage of wide availability in a variety of forms, i.e. as high power quasi-cw lasers, as cw lasers with output powers of 10W or more, and as miniature diode pumped lasers.

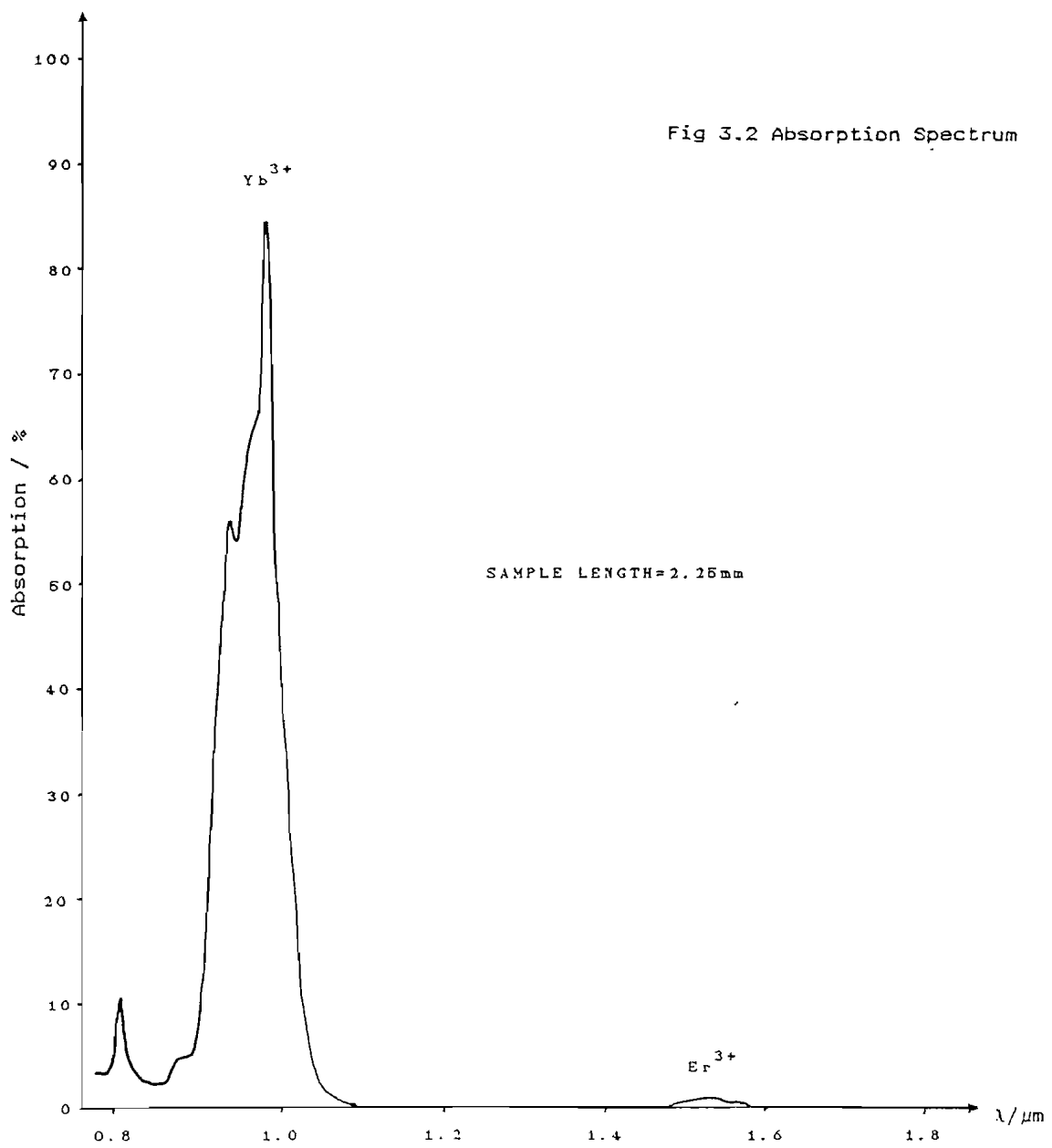
3.2.2 Rate Equation Analysis

Figs.3.1 and 3.2 show the energy level diagram and the absorption spectrum of the Yb:Er system. Pump radiation at $1.064\mu\text{m}$ is weakly absorbed by the Yb^{3+} ions causing excitation from the upper level of the $^2\text{F}_{7/2}$ multiplet. The thermal population of this level at room temperature is only $\sim 2\%$ of the total population. By heating to $\sim 100^\circ\text{C}$ it is possible to double this figure and hence double the pump absorption. The Yb^{3+} ions are excited to the $^2\text{F}_{5/2}$ level followed by non-radiative transfer of energy to the $^4\text{I}_{11/2}$ level of the Er^{3+} ions. There is then a rapid relaxation to the $^4\text{I}_{13/2}$ upper laser level. This metastable level has a lifetime of $\sim 8\text{ms}$. Lasing occurs down to the $^4\text{I}_{15/2}$ ground level at an emission wavelength of $1.536\mu\text{m}$. Thus it is clear that we have a 3 level laser system.

Also shown in fig.3.1 are the excited state absorption of both the pump and signal wavelengths from the upper laser level. Following the analysis of Galant et al, [6], we will make the simplifying assumption that these excitations relax rapidly back to the $^4\text{I}_{13/2}$ level. We can then write down the steady-state rate equations,

Fig 3.1 Energy Level Diagram For The Yb:Er System





$$\left[\frac{dn_{2p}}{dt} \right] = B_p u_p (n_{1p} - n_{2p}) - n_{2p} / \tau_{2p} - \alpha n_{1s} n_{2p} = 0 \quad (3.1)$$

$$\begin{aligned} \left[\frac{dn_{2s}}{dt} \right] &= B_s u_s (n_{1s} - n_{2s}) - n_{2s} / \tau_{2s} + d_3 n_{3s} - \\ &B_{es} u_s (n_{2s} - n_{4s}) + d_4 n_{4s} - B_{ep} u_p (n_{2s} - n_{5s}) + d_5 n_{5s} = 0 \end{aligned} \quad (3.2)$$

$$\left[\frac{dn_{3s}}{dt} \right] = \alpha n_{1s} n_{2s} - d_3 n_{3s} = 0 \quad (3.3)$$

$$\left[\frac{dn_{4s}}{dt} \right] = B_{es} u_s (n_{2s} - n_{4s}) - d_4 n_{4s} = 0 \quad (3.4)$$

$$\left[\frac{dn_{5s}}{dt} \right] = B_{ep} u_p (n_{2s} - n_{5s}) - d_5 n_{5s} = 0 \quad (3.5)$$

$$N_p = n_{1p} + n_{2p} \quad (3.6)$$

$$N_s = n_{1s} + n_{2s} + n_{3s} + n_{4s} + n_{5s} \quad (3.7)$$

Where N_s , N_p are the total population densities of the Er^{3+} and Yb^{3+} ions; n_{1s} etc. are the population densities of the various levels in the Yb:Er system; B_p , B_s , B_{ep} and B_{es} are proportional to the Einstein coefficients for the various transitions shown; τ_{2p} and τ_{2s} are the spontaneous decay times of level 2 in Yb, when there is no Er present, and of level 2 in Er; d_3 , d_4 and d_5 are the rates of decay of levels 3, 4 and 5 in Er; u_p and u_s are the densities of the pump and signal radiations; α is the quantity proportional to the rate of transfer of the excitation energy from the Yb^{3+} ions to the Er^{3+} ions.

If we assume that the rates of relaxation from levels 3, 4 and 5 of Er are high enough that $d_3 \gg \alpha n_{1s}$, $d_4 \gg B_{es} u_s$ and $d_5 \gg B_{ep} u_p$, then $n_3 = n_4 = n_5 = 0$. Using eqns. (3.1) - (3.7) we can now obtain,

$$\left[\frac{dn_{2p}}{dt} \right] = B_p u_p N_p - n_{2p} (2B_p u_p + 1/\tau_{2p}) - 0.5\alpha(N_s - \delta)n_{2p} = 0 \quad (3.8)$$

$$\left[\frac{dn_{2s}}{dt} \right] = -B_s u_s \delta - 0.5(N_s + \delta)/\tau_{2s} + 0.5\alpha n_{2p}(N_s - \delta) = 0 \quad (3.9)$$

where we have introduced the threshold inversion $\delta = n_{2s} - n_{1s}$. We can find an expression for δ by applying the threshold condition,

$$R_1 R_2 \exp(2l\delta\sigma_s - \sigma_{es}(N_s + \delta)l - 2lk_{is}) = 1 \quad (3.10)$$

where R_1, R_2 are the mirror reflectivities, k_{is} is the signal inactive absorption coefficient, σ_s is the stimulated emission cross-section, and σ_{es} is the signal excited state absorption cross-section. Re-arranging eqn.(3.8) gives,

$$n_{2p} = \frac{B_p u_p N_p}{2B_p u_p + \tau_{2p}^{-1} + 0.5\alpha(N_s - \delta)} \quad (3.11)$$

At threshold $u_s = 0$, and so from eqn.(3.9) we get,

$$n_{2p_{th}} = \frac{(N_s + \delta)}{\tau_{2s} \alpha(N_s - \delta)} \quad (3.12)$$

By inspection of eqn.(3.11) we find two conditions for efficient laser action,

$$1) B_p u_p \ll 0.5\alpha(N_s - \delta) \quad (3.13)$$

- the pump must not bleach the $1 \rightarrow 2$ excitation in Yb.

$$2) \tau_{2p}^{-1} \ll 0.5\alpha(N_s - \delta) \quad (3.14)$$

- quenching of the $^2F_{5/2}$ level in Yb should be dominated by the non-radiative transfer of energy to the $^4I_{11/2}$ level in Er.

In the ideal case, where eqns.(3.13) and (3.14) are both

satisfied and there is no excited state absorption, we obtain from eqns.(3.10),(3.11) and (3.12),

$$P_{th} = h\nu_p V (N_s + \delta) / 2\tau_2 \quad (3.15a)$$

$$\delta = \frac{2\ln k_{is} + \ln(1/R_1 R_2)}{2\sigma_s l} \quad (3.15b)$$

where V is the volume of the signal mode in the laser medium and $P_{th} = h\nu_p B_p N_p u_p V$ is the threshold absorbed pump power. This is the standard three-level laser requirement that at least half the population needs to be excited. It should also be noted that we have assumed cw operation ($\tau_{pump} \gg \tau_{2s}$).

If we now allow the condition of very high rate of transfer, eqn.(3.14), to be broken and for excited state absorption at both pump and signal wavelengths, we obtain,

$$P_{th} = h\nu_p V \frac{(N_s + \delta)}{2\tau_s} \left[1 + \frac{k_{ep} + k_{ip}}{k_p} \right] \left[1 + \frac{\tau^{-1}}{0.5\alpha(N_s - \delta)} \right] \quad (3.16a)$$

$$\delta = \frac{2\ln k_{is} + \ln(1/R_1 R_2) + \sigma_{es} N_s l}{2\sigma_s l (1 - \sigma_{es}/2\sigma_s)} \quad (3.16b)$$

Here, following [6], we have used $u_p' = u_p (1 + [k_{ep} + k_{ip}]/k_p')$, where u_p' is the total pump energy density, u_p is the "useful" pump energy density, k_{ep} is the pump excited state absorption coefficient, k_{ip} is the pump inactive absorption coefficient, and k_p' is the coefficient of the "useful" pump absorption.

The right hand term of eqn.(3.16a) can be re-expressed as,

$$\frac{\alpha n_{1s} + \tau^{-1}}{\alpha n_{1s}} = 1/\eta_t \quad (3.17)$$

where η_t is the quantum transfer efficiency.

Comparison of eqns.(3.15) and (3.16) show that due to the signal excited state absorption we now need a larger inversion to achieve threshold, and that due to pump excited state absorption and the reduced transfer efficiency it is harder for the pump to achieve this than it was before.

It has been found experimentally by several authors, [6-9], that phosphate glasses give the highest transfer efficiencies. They have two advantages in that they have a capability for fast energy migration through the donor sub-system (Yb), [10], and the relaxation rate d_3 is very fast, [8],[9], effectively removing the possibility of back transfer from the Er^{3+} to Yb^{3+} ions. It is also necessary to have relatively high ion concentrations in order to achieve high transfer efficiencies. A high Yb^{3+} concentration is obviously also favourable in terms of increasing the pump absorption. However, too high a concentration of Er^{3+} ions would inevitably raise the laser threshold, as can be seen from eqn.(3.16). In practice Yb^{3+} ion concentrations are limited to around $2 \times 10^{21} \text{ cm}^{-3}$ before crystallization begins to occur, and optimum Er^{3+} ion concentrations have been found to be of the order of 10^{19} cm^{-3} .

Table 3.1 gives the various parameters, for $1.064\mu\text{m}$ pumping of commercially available Kigre QE-7 Yb:Er phosphate glass, that are needed to calculate the expected laser threshold via eqn.(3.16). Using these parameters and assuming there are no losses ($k_{is}^{loss}=0$, $R_1 R_2=1$) we find from eqns.(3.15) and (3.16),

$$i) \quad P_{th} / V = 116 \text{ Wcm}^{-3} \quad \delta = 0 \text{ cm}^{-3}$$

$$ii) \quad P_{th}' / V = 263 \text{ Wcm}^{-3} \quad \delta' = 2.6 \times 10^{17} \text{ cm}^{-3}$$

Table 3.1

Parameter	Notes
$N_s = 1 \times 10^{19} \text{ cm}^{-3}$	From absorption spectrum.
$N_p = 2.2 \times 10^{21} \text{ cm}^{-3}$	From absorption spectrum.
$\tau_{2p} = 570 \mu\text{s}$	From ref.[6].
$\tau_{2p}' = 180 \mu\text{s}^*$	Lifetime of level 2 in Yb with Er present, (see fig.3.3)
$W_{23} = 4 \times 10^3 \text{ s}^{-1}^*$	$W_{23} = 1/\tau_{2p}' - 1/\tau_{2p}$ is the rate of transfer
$\alpha = 3.8 \times 10^{-16} \text{ cm}^3 \text{s}^{-1}$	$W_{23} = \alpha n_{1s} \approx \alpha N_s$ at low levels of excitation.
$\eta_t = 70\%^*$	The quantum transfer efficiency $\eta_t = W_{23} \tau_{2p}'$
$\sigma_s = 7 \times 10^{-21} \text{ cm}^2$	From ref.[11].
$k_p = 0.05 \text{ cm}^{-1}$	The pump absorption coefficient (@ 100°C)
$\sigma_{es} = 3.5 \times 10^{-22} \text{ cm}^2$	From ref.[12].
$\sigma_{ep} = 7.5 \times 10^{-22} \text{ cm}^2$	The pump excited state absorption coef. from ref.[6], can be used to find k_{ep} .

*These figures correspond to low excitation levels.

Analysing the contributions to the increase in threshold show that it is dominated by the fact that at threshold the transfer efficiency $\eta_t^{\text{th}} \approx 0.5$. This accounts for most of the ~2.3 times increase in absorbed energy threshold between this system (ii) and an ordinary 3-level laser (i). The effect of both pump and signal excited state absorptions are comparatively negligible. Figs.(3.4) and (3.5) show how the rate of transfer of energy W_{23} and the transfer efficiency η_t vary with the degree of excitation n_{2s}/N_s . It is interesting to note that we can put an upper limit on the expected slope efficiency of $\eta = (\nu_s/\nu_p) \eta_t^{\text{th}} = 0.35$.

Despite our final aim being to produce a cw mode-locked system, we decided, in view of the large expected threshold power requirement, to carry out our initial investigations using a quasi-cw pump source. This source (5ms pulse, 5Hz repetition rate, ~100W quasi-cw power) will give us more power in hand and will reduce the expected thermal effects compared with cw pumping.

3.3 Quasi-cw Operation (see Appendix 3)

Fig 3.3 Yb Fluorescence

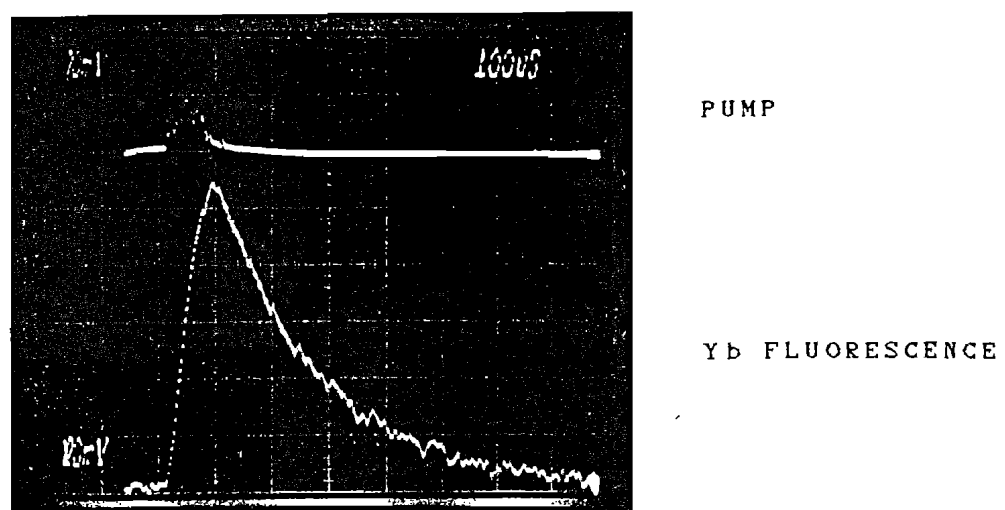


Fig 3.4 Graph Of Rate Of Transfer Against Degree Of Excitation

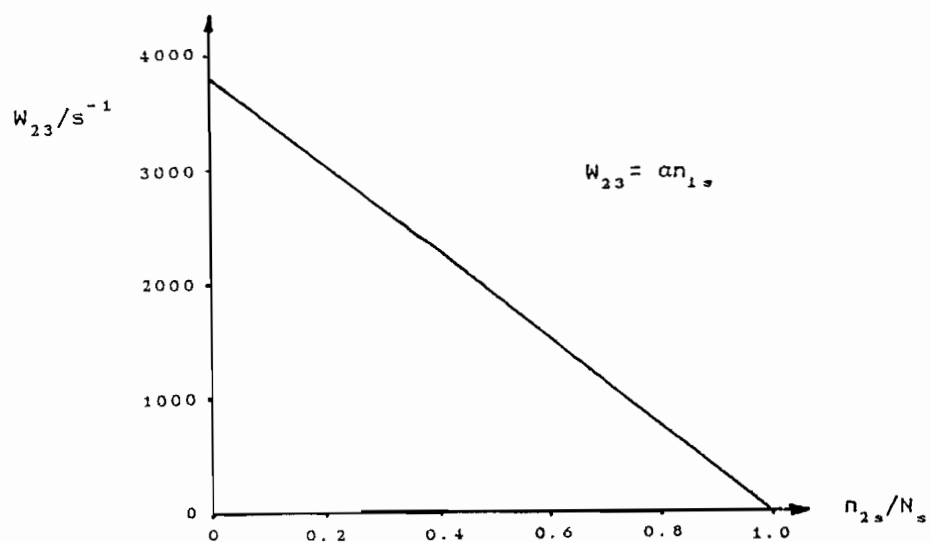
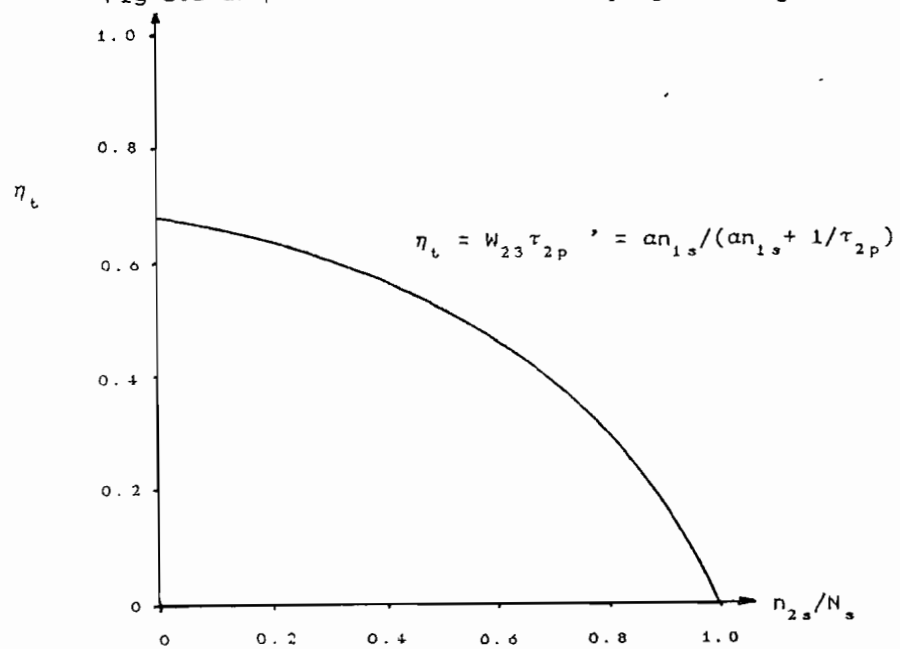


Fig 3.5 Graph Of Transfer Efficiency Against Degree Of Excitation



3.3.1 The Pump Laser

A diagram of the pump laser used for our initial investigations is shown in fig.3.6. An intra-cavity $\times 3$ telescope was used to obtain a high TEM_{00} output power. This increased the TEM_{00} mode spot size within the rod, and hence extracted more energy, [13]. Output pulses of $\sim 100W$ peak power, at a 5Hz repetition rate, were readily obtained. The pulse duration was 5ms, which is comparable to the upper state lifetime of the Yb:Er laser (8ms). Two glass plates at Brewster's angle were used to polarise the laser. This allowed the use of a polariser and quarter-wave plate to isolate the pump laser from the Yb:Er laser.

3.3.2 Experimental Arrangement And Results

Fig3.7 shows the simple semi-spherical cavity used to first obtain lasing. The plane pump input mirror had $\sim 99\%$ reflectivity at $1.54\mu m$ and $\sim 90\%$ transmission at $1.064\mu m$. Placed close to this mirror was a 7.5cm long AR coated Yb:Er phosphate glass rod. This rod was made of commercially available, Kigre QE-7 glass. The end mirror had a 20cm radius of curvature, and had $>99\%$ reflectivity at $1.54\mu m$. This cavity design allows us to vary the signal waist spot size on the input mirror, by changing the mirror separation. The pump beam was focussed to a $\sim 170\mu m$ waist spot size using a 20cm focal length lens

At room temperature lasing was seen to occur at a pump power, incident on the input mirror, of 64W. This corresponds to an absorbed pump power of 10.4W. The output is confined to a clean TEM_{00} mode by the constraints of the cavity design and pumping conditions.

As stated previously, we can significantly increase the pump absorption by heating the laser medium, thus increasing the thermal population of the absorbing level. We therefore placed the rod in a simple home-made oven and obtained the results shown in fig.3.8. This shows how the time difference between the start of the pump pulse and the signal pulse varies with temperature. Fig.3.9 shows

Fig 3.6 Pump Laser Telescopic Resonator

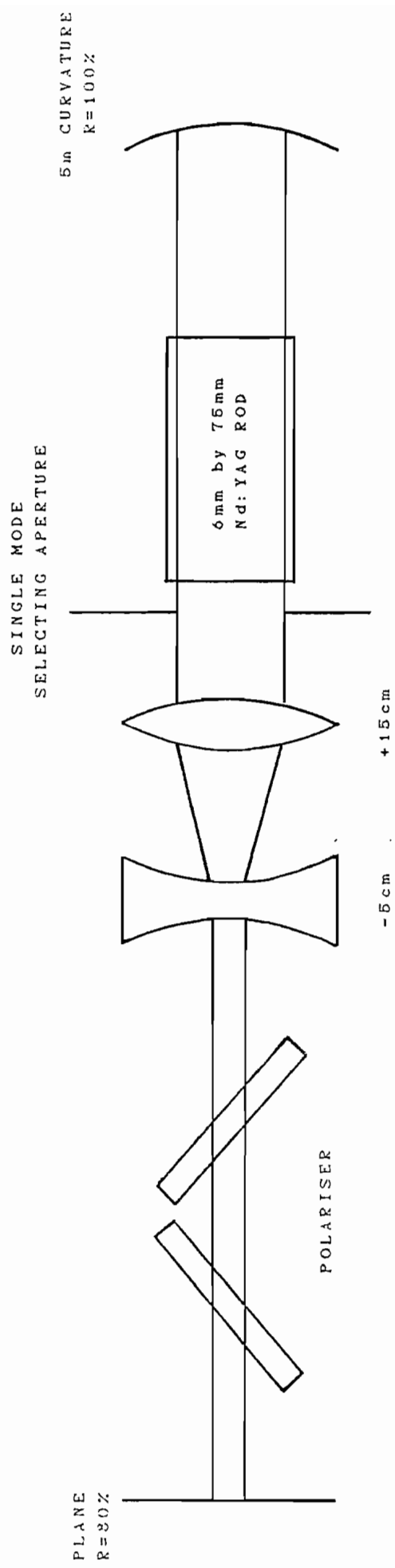


Fig 3.7 Initial Semi-Spherical Yb:Er Resonator

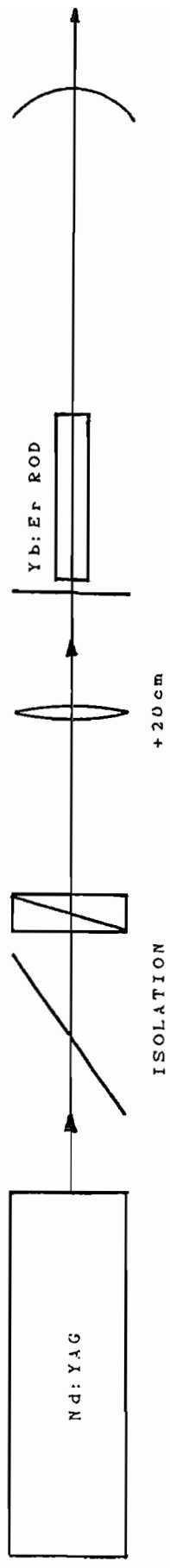


Fig 3.8 Graph Of Time Delay Between The Start Of The Pump And Signal Pulses Against Temperature

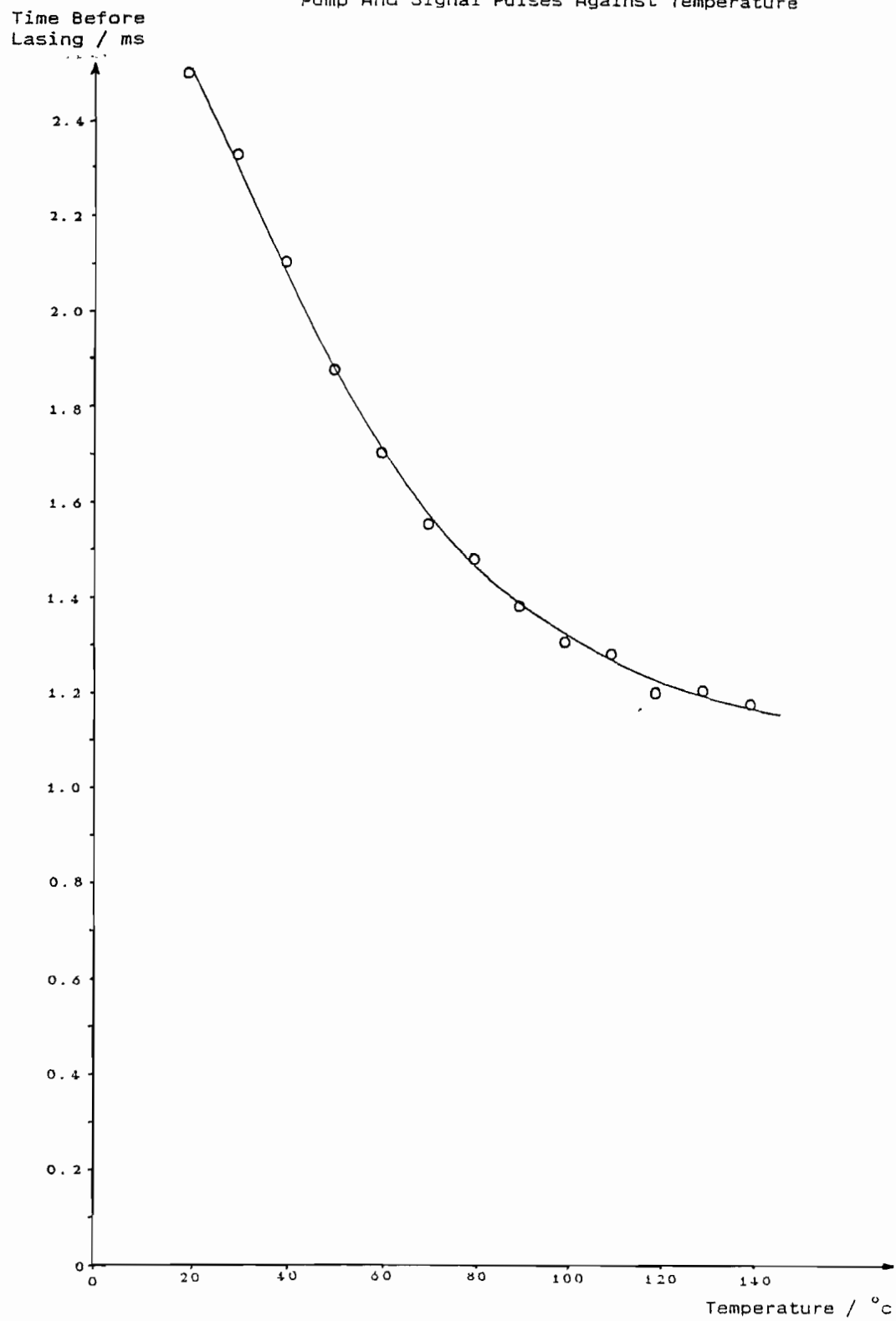
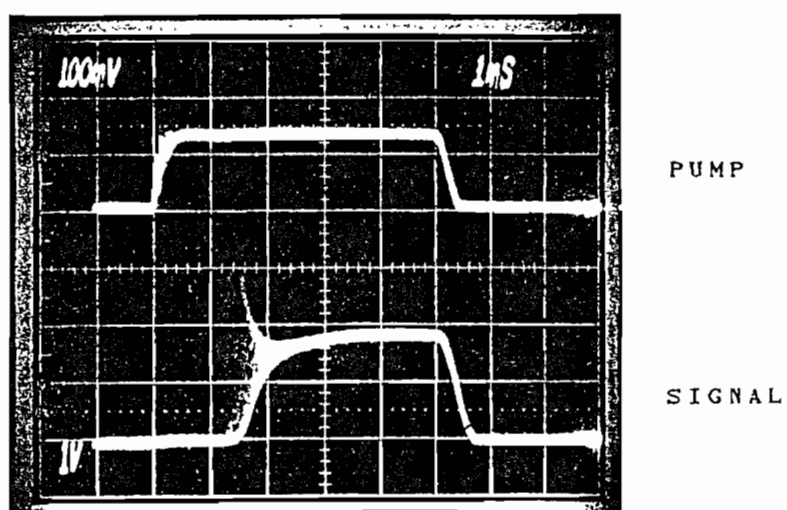


Fig 3.9 Pump And Signal Output Pulses



corresponding pump and signal pulses at an oven temperature of $\sim 100^{\circ}\text{C}$. This is the safe upper limit on the temperature for the rod AR coatings. The pump absorption at this temperature was $\sim 30\%$ and the incident pump power threshold was reduced to 32W. The absorbed pump power threshold was therefore 8.6W, in good agreement with that found at room temperature.

A glass plate was then placed in the cavity which gave a known loss with angle of tilt. The power of one of the reflections was measured and used to calculate the total output power. The results are shown in fig.3.10. Thus we found an optimum output coupling of $\sim 8\%$, for which the corresponding output power was $\sim 2.2\text{W}$ ($\sim 45\text{mW}$ average power). This was later directly confirmed using an output mirror of the appropriate reflectivity. The incident pump power threshold for this output coupling was $\sim 37\text{W}$ and so we had a slope efficiency of $\eta=13\%$.

From the expressions obtained in section 3.2.2 we can calculate an expected threshold absorbed cw power of $\sim 1.3\text{W}$, where we have assumed that the signal is focussed at the input end of the rod such that it has a confocal parameter equal to twice the length of the rod. This figure should be multiplied by a factor of $4/3$ to allow for the quasi-cw pumping conditions, see section 3.4.1, giving an expected threshold of $\sim 1.7\text{W}$. The difference between the predicted (1.7W) and experimental (8.6W) thresholds will be partly due to the fact that we have not taken into account the overlap of pump and signal radiations. This is known to be an important factor for longitudinally pumped lasers (for example see [14]), and may also explain the lower than expected slope efficiency.

In practice we have always used confocal or near confocal pumping to minimise the pumped volume. In order to allow a better pump-signal overlap, and to minimise the signal mode volume in the rod, we built the spherical cavity shown in fig.3.11. This allows us to experimentally vary the signal spot size and its location. For a $\sim 50\text{ }\mu\text{m}$ pump waist

Fig 3.10 Graph Of Output Power Against Output Coupling

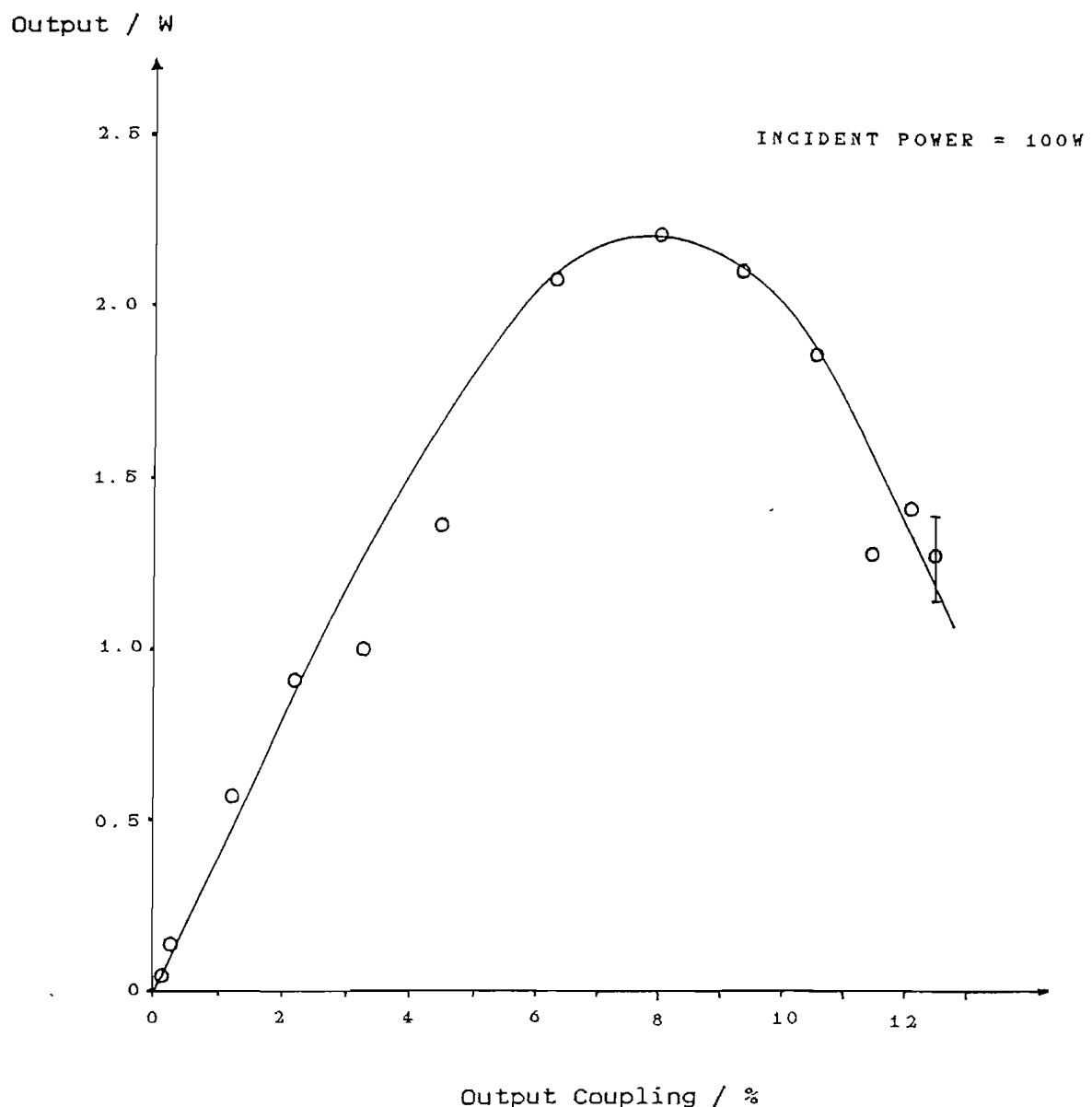
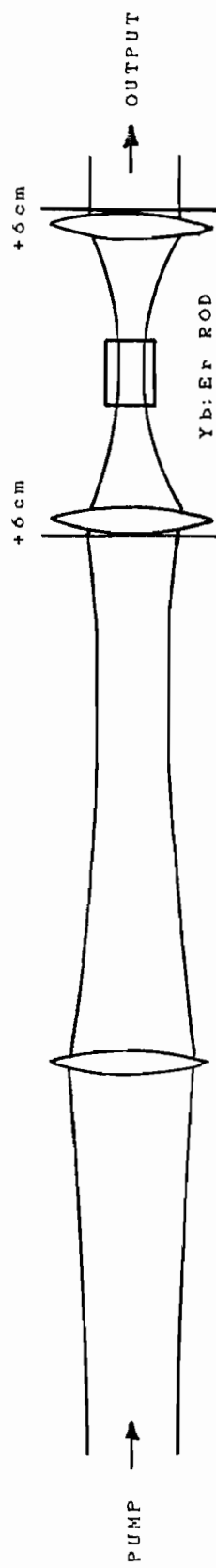


Fig 3.11 Spherical Yb:Er Laser Resonator



spot size at the centre of the rod, we now obtained an absorbed power threshold of just 4.5W, compared to the theoretical value of $\sim 0.7W$ (where we now assume the signal confocal parameter is equal to the length of the rod).

It can easily be shown that (for a zero loss cavity) the threshold absorbed power should decrease with rod length l because the minimum laser mode volume has an l^2 dependance. With this in mind we have also used a 2.5cm long rod in the same cavity as that shown in fig.3.11. However the best result we achieved was an absorbed power threshold of 2.1W. This is only a factor of two improvement on the 7.5cm rod compared to the 9 times improvement expected. This result may be due to the fact that this rod had Brewster angled faces, as later experiments with a 2cm long AR coated rod show a greatly reduced threshold, (see section 3.4.1).

3.3.3 Q-Switched Operation At 5Hz

The cavity shown in fig.3.12 was used to obtain Q-switched operation at 5Hz. We have gone back to a simple hemispherical cavity, where we now use a 50cm curvature output mirror (10% transmission at $1.54\mu m$) to give a cavity length long enough to fit in two glass plates as polarisation selecting elements, and an AR coated $LiNbO_3$ electro-optic modulation crystal. The crystal was orientated as shown in fig.3.13. Lenzo et al, [15], show that when a voltage V is applied in the x_1 direction the principal axes rotate by 45° about x_3 , and the crystal becomes optically biaxial. The voltage needed to cause a quarter wave retardation is given by,

$$V_{\pi/2} = \lambda d_1 / 4n_0^3 r_{22} l_3$$

where n_0 is the ordinary refractive index, r_{22} is the relevant electro-optic coefficient, d_1 is the thickness of the crystal in the electric field direction, and l_3 is the length of the crystal in the propagation direction. Thus when we apply a voltage $V_{\pi/2}$ ($\sim 2.6kV$) the horizontally polarised light will be returned, after a double pass through the crystal, with vertical polarisation, and will thus be

Fig 3.12 Q-Switched Yb:Er Laser Resonator

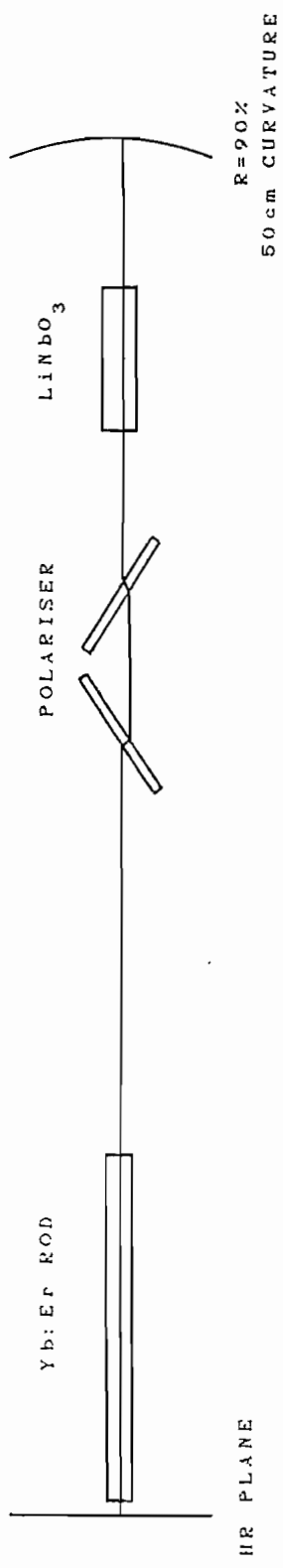


Fig 3.13 LiNbO₃ Q-Switch Crystal

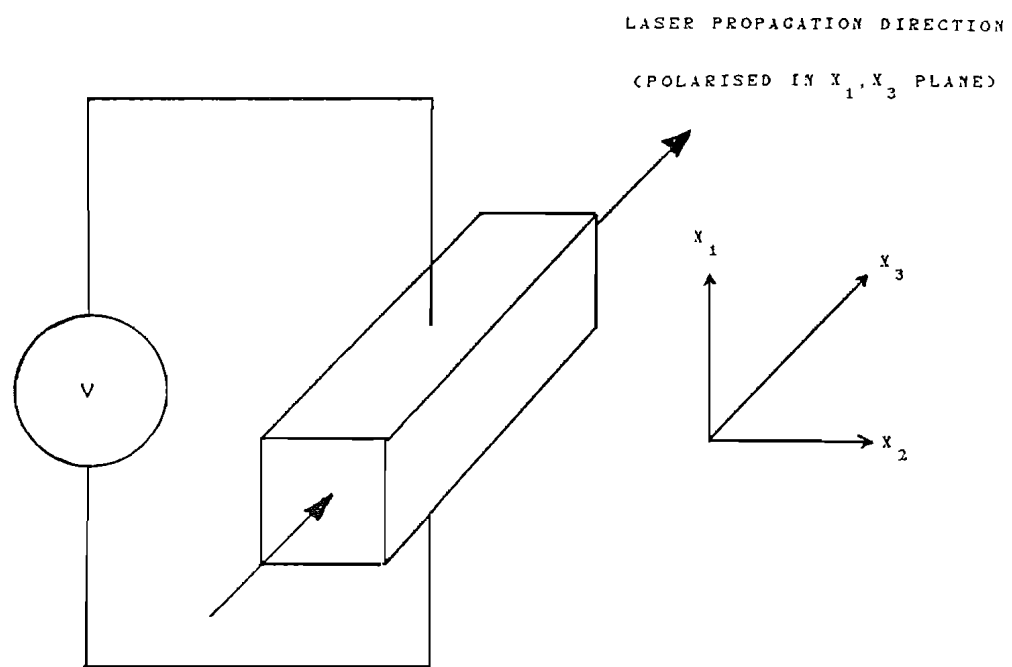
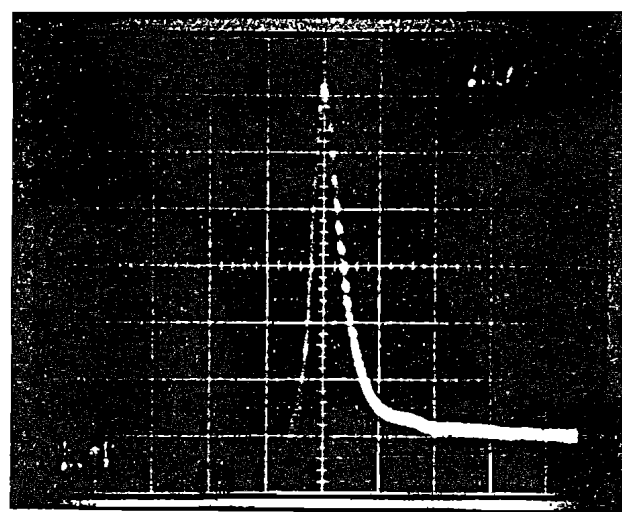


Fig 3.14 Q-Switched Output Pulse



rejected by the plate polariser. In this way we were able to hold off lasing during the pump pulse, allowing the inversion to build up. Just before the end of the pulse the voltage is turned off allowing a large Q-switched pulse to develop. The ~60ns FWHM pulse, shown in fig.3.14, had an energy of ~0.7mJ indicating a peak power of ~10kW. This corresponds to ~20% of the energy obtained in long pulse operation (~4ms) being available as Q-switched output. Observation of amplitude stability showed fluctuations of less than 5% .

3.4 CW Operation (see appendix 4)

3.4.1 Experimental Arrangement And Results

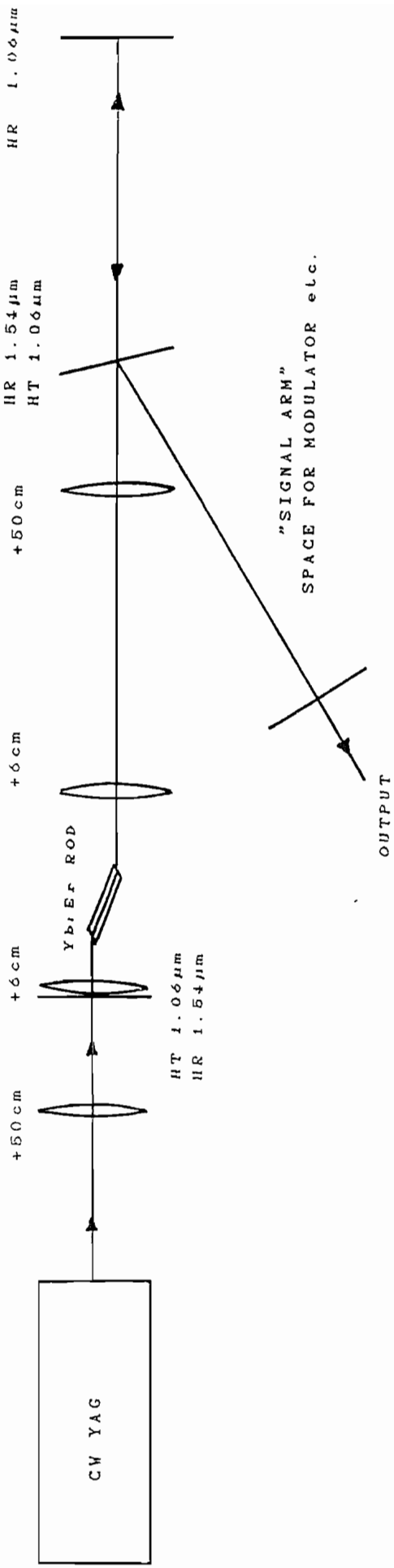
The experimental set up used is shown in fig.3.15. The pump laser is a Spectra Physics 3000 cw Nd:YAG laser giving an average output power of ~7W at $1.064\text{ }\mu\text{m}$. This is focussed to a $\sim 70\mu\text{m}$ waist spot size at the centre of the 2.5cm Yb:Er rod. The Yb:Er laser cavity is an extended version of that shown in fig.3.11, which gave the lowest thresholds for quasi-cw pumping. The two 6cm lenses allow variation of the signal spot size and location, to obtain the optimum pump and signal overlap. The 50cm focal length lens aided the extension of the cavity length to make it suitable for future mode-locking experiments. The three mirror cavity arrangement was used to allow the excess pump light to be sent back into the Yb:Er rod for further absorption. This was found to be a very easy and useful way of reducing the incident pump power requirement.

Initial investigations of cw pumping had shown that we could obtain lasing for a period of up to ~10s duration which then rapidly faded. If the pumping was continued damage centres formed within the rod. Gordon et al, [16], show that the temperature T_c at the centre of a medium pumped by a Gaussian profile beam is,

$$T_c = T_0 + P_{ht} \ln(3.562a^2 / W_0^2) / 4k\pi \quad (3.18)$$

where T_0 is the temperature at the edge of the rod (radius $a=1\text{mm}$), P_{ht} is the power absorbed per unit length that goes

Fig 3.15 CW Yb:Er Laser Cavity



into heating, k is the thermal conductivity, and W_0 is the pump spot size. Assuming that $1-(\nu_s/\nu_p)=0.31$ of the pump power goes into heating the rod we can predict typical temperature rises at the centre of the rod $\sim 20^\circ\text{C}$. The temperature of the outside of the rod is determined by how it is cooled as below, [17],

$$T_0 - T_{c1} = P_{ht} / 2\pi ah \quad (3.19)$$

where T_{c1} is the coolant temperature and h is the surface heat transfer coefficient. For air cooling $h \sim 10\text{W/m}^2\text{K}$ and thus we find $T_0 - T_{c1} \sim 600^\circ\text{C}$. Therefore the need for a good heat sink is obvious. In our initial investigations the rod lay loosely in the dural oven. To improve the removal of the heat, and essentially fix the outside temperature of the rod to the oven temperature, we wrapped the rod in copper foil and ensured the oven was in tight contact with it. With these improvements we were now able to obtain damage free cw operation at an oven (heat sink) temperature of $\sim 120^\circ\text{C}$.

Associated with the temperature distribution within the rod will be a thermal lens. The lensing effect is due to the combined effects of the change of refractive index with temperature, the change of refractive index due to thermal stress, and the thermally induced curvature of the end faces of the rod, [18]. However we should be able to compensate for the presence of such a lens through adjustment of the intra-cavity lenses.

In practice we were able to obtain cw operation at a threshold absorbed pump power of $\sim 1.6\text{W}$, compared to the best quasi-cw threshold of $\sim 2.1\text{W}$. Observation of the Er fluorescence shows that after 5ms (the length of the quasi-cw pump pulse) the fluorescence level is approximately 3/4 of its eventual cw level. Thus the reduction in threshold between the two pumping schemes is just as expected, indicating that the losses, such as thermally induced birefringence, have not significantly increased for cw pumping.

Using a 1% output coupler we found an average output power of $\sim 17\text{mW}$, for an absorbed power of 2.7W , giving a slope efficiency of $\sim 1.5\%$. Similar output powers ($\sim 22\text{mW}$) were found with a 10% output coupling, indicating that the optimum output coupling is probably somewhere between these two figures. The average power reflected off one of the Brewster surfaces of the rod was found to be $\sim 3.6\text{mW}$ when using high reflectivity cavity mirrors. Comparing this figure with that found for the 1% output coupler confirms that the loss due to depolarisation resulting from birefringence in the rod is very small.

Later results with a 2cm AR coated rod with slightly wedged ends gave a much improved performance, suggesting there may have been something wrong with the Brewster faced rod we used for the results above. The 2cm rod gave the reduction in threshold we originally expected for shorter length rods, with cw lasing now being obtained for an absorbed power of $\sim 500\text{mW}$. Predictions based on the quasi-cw pumping of the 7.5cm rod would give an expected threshold of $\sim 240\text{mW}$. The difference between these two figures may be due to the fact that the available gain will have been reduced by a factor of 3.75 making any cavity losses a more significant factor in determining the threshold.

Using a 10% output coupler we were now able to obtain an output power of $\sim 21\text{mW}$ for an absorbed power of 1.05W and a threshold of $\sim 770\text{mW}$, implying a $\sim 7.5\%$ slope efficiency. This may be improved through selection of the optimum output coupling.

These results suggest that a rod of $\sim 5\text{mm}$ length would have an absorbed power threshold of $< 100\text{mW}$. A diode pumped miniature Nd:YAG laser operating at 946nm would be very well absorbed by this length of rod, see fig.3.2, implying that it could be used to pump such a laser. Heumann et al, [19], have recently reported on the cw operation of an Er^{3+} fluoroaluminate glass at $1.6\mu\text{m}$, using the $^4\text{I}_{13/2} \rightarrow ^4\text{I}_{15/2}$ transition. In their case they have co-doped with Cr^{3+} and Yb^{3+} ions to allow pumping with a krypton laser at 647.1nm .

Although output powers of just ~2mW were obtained, it is interesting to note that they have achieved a very low absorbed power threshold (~80mW) by using a very short rod ($l=4\text{mm}$), suggesting that our above predictions are not unreasonable. An alternative way of obtaining very low lasing thresholds is to go to a fibre laser configuration, as will be discussed in section 3.5. Thus the choice of which variety of Yb:Er laser is to be used, (large Yb:Er rod [$\sim\text{few cm}$], miniature Yb:Er rod [$\sim\text{few mm}$], or fibre laser), depends on which combination of threshold and available output power meets the requirements of the particular application being considered. In our case, the results obtained for cw Nd:YAG pumping of the bulk 2cm long rod are seen as a very promising route to obtaining a mode-locked source suitable for non-linear propagation studies in optical fibres, including the possibility of a soliton laser.

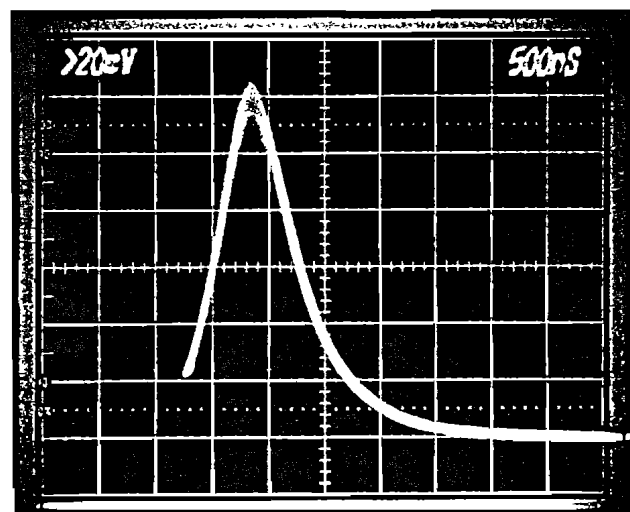
3.4.2 High Repetition Rate Q-Switched Operation

Preliminary results for the high repetition rate Q-switching of the cw pumped Yb:Er laser were found, using the Brewster faced rod and a 1% output coupler, by simply introducing a chopper in the "signal arm" of the cavity, as shown in fig.3.15. Using this part of the cavity does not interfere with the pumping conditions, as would happen anywhere else due to the blocking of the pump feedback mirror. Q-switched operation, at repetition rates up to ~125Hz, gave peak output powers of ~25W in ~750ns FWHM duration pulses. Fig 3.16 shows a time exposure of several output pulses indicating a reasonable pulse to pulse amplitude stability (<10%).

3.5 An Yb:Er Fibre Laser (see appendix 5)

It was hoped that a sample of the Kigre QE-7 glass, used in the bulk experiments, could be pulled down into the form of a fibre, so that any results obtained could be directly compared to those found for the bulk rod. Unfortunately this has proved to be a technically difficult operation and such a fibre is not, as yet, available. However recent developments in the fabrication of rare-earth doped optical fibres, [20], has made possible the production of

Fig 3.16 Time Exposure Showing Several Q-Switched Output Pulses



fibres with sufficiently high doping levels to allow good ion to ion transfer efficiencies. Thus M.E.Fermann and J.E.Townsend of the Department of Electronics and Information Engineering, Southampton University, were able to produce a silica based fibre with Yb^{3+} and Er^{3+} concentrations of ~1.7% and ~0.08% respectively. The $4.6\mu\text{m}$ core diameter (2a) fibre has a cut-off wavelength (λ_c) of $1.5\mu\text{m}$, ensuring single mode operation at the signal wavelength and good launch efficiency at the pump wavelength.

The lasing characteristics of this fibre were investigated using the cavity shown in fig.3.17. The input mirror had a 98% reflectivity at the signal wavelength and was highly transmitting at the pump wavelength. The output couplers used had reflectivities of 90% and 73% at the signal wavelength. These mirrors were butted directly onto the ends of the fibre forming a simple low loss cavity.

The laser characteristics change with the length of fibre used because of the laser's 3-level nature. Figs.3.18 and 3.19 show the results obtained with a multi-mode version of the fibre ($\lambda_c=2.6\mu\text{m}$, $2a=8.4\mu\text{m}$) which was used in initial investigations before the single mode fibre was available. Fig.3.18 shows that the absorbed power threshold increases linearly with length due to the linearly increasing number of Er^{3+} ions that need to be pumped up to achieve inversion. However the incident power threshold goes to a minimum at a length approximating to one absorption length, due to the fact that with decreasing fibre length less and less pump is actually absorbed. Fig.3.19 shows how the signal wavelength varies with fibre length. The shift, from $1.568\mu\text{m}$ at 2.8m to $1.549\mu\text{m}$ at 25cm , results from the fact that there is a small splitting of the Er^{3+} ground state. Although the gain is greater for the pure 3-level transition, at longer fibre lengths the required pump power to invert half of the Er^{3+} ions becomes very large and the laser shifts to the longer wavelength quasi-four level transition, [21].

The results obtained for the single mode fibre are summarised in table3.2.

Fig 3.17 Yb:Er Fibre Laser Resonator

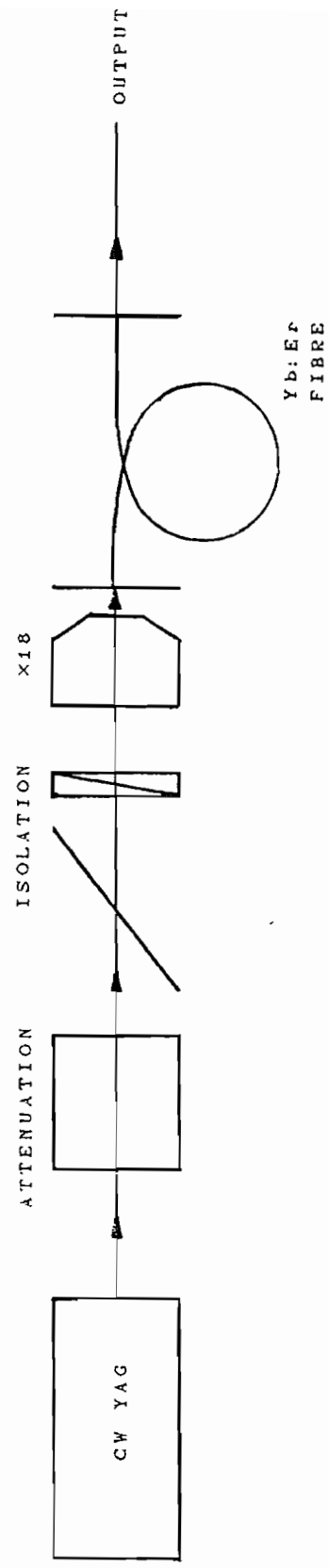


Fig 3.18 Graph Of Threshold Power Against Fibre Length

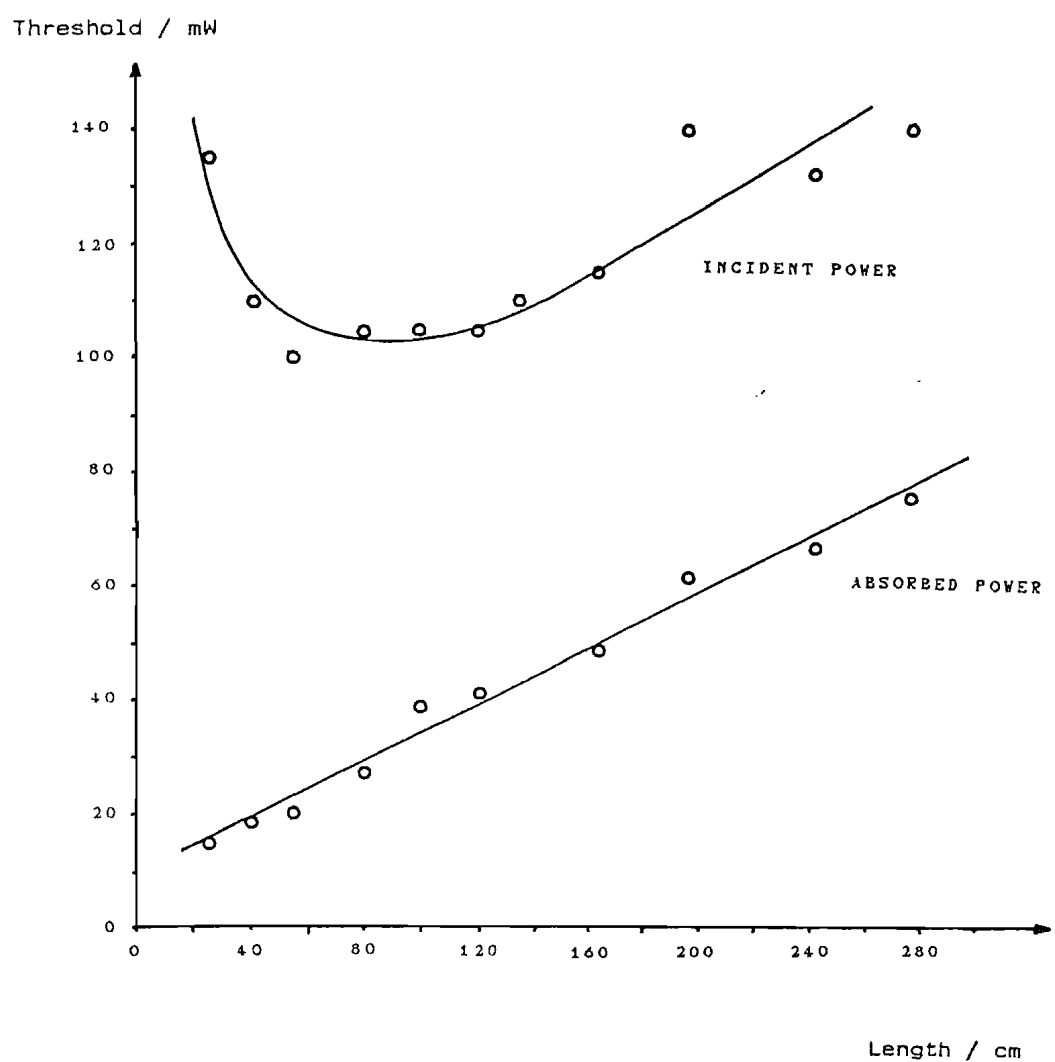


Fig 3.19 Graph Of Output Wavelength Against Fibre Length

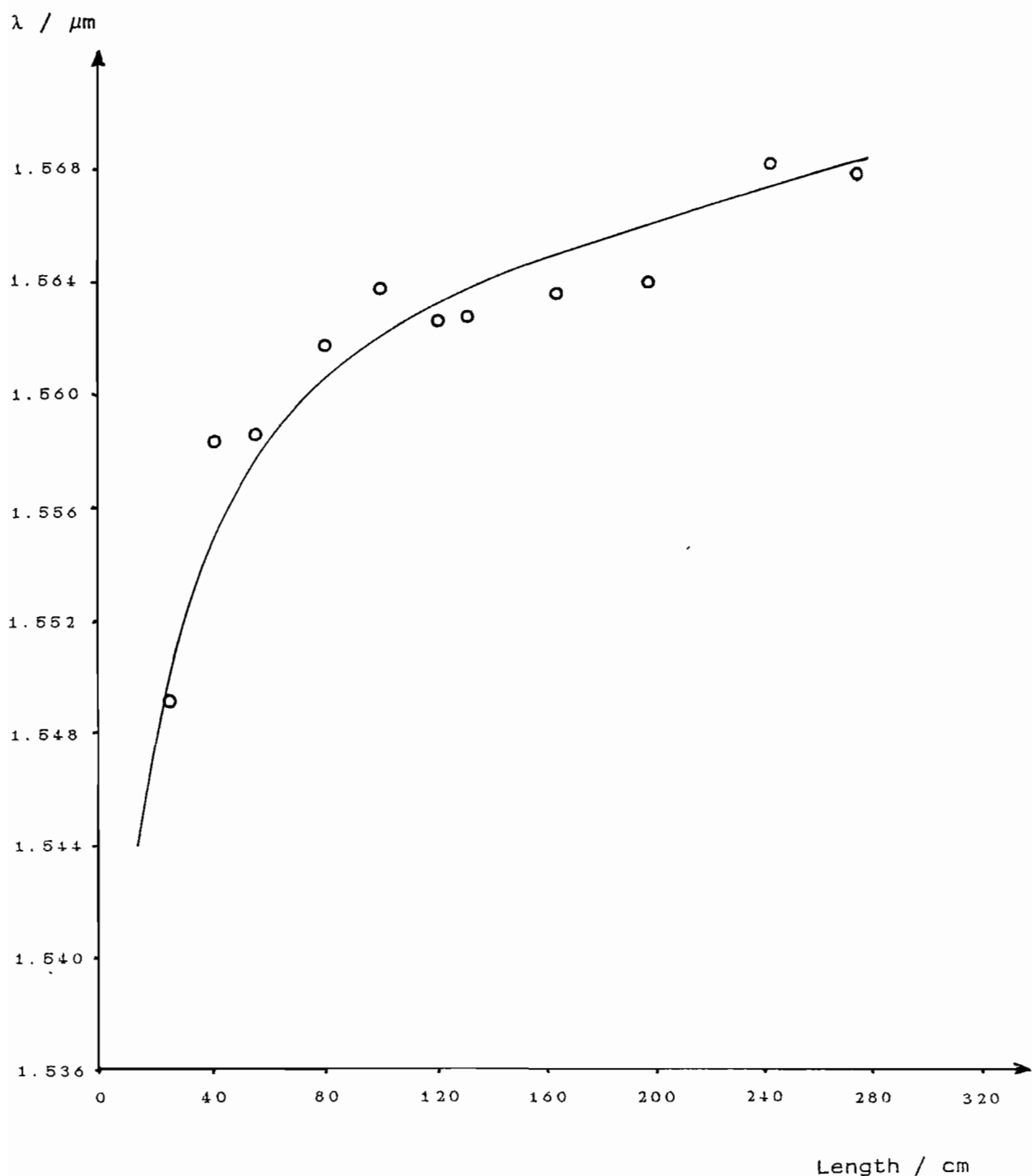


Table 3.2

	91cm length, 27% output coupler	84cm length, 10% output coupler
Threshold launched power	16mW	12mW
Threshold absorbed power	8.0mW	6.6mW
Slope efficiency (w.r.t. absorbed power)	4.2%	2.8%
Signal wavelength	1.56 μ m	1.56 μ m

These results clearly show the advantage of going to a fibre laser configuration where, due to its guiding quality, we have a very small pumped volume and a good overlap of pump and signal radiations.

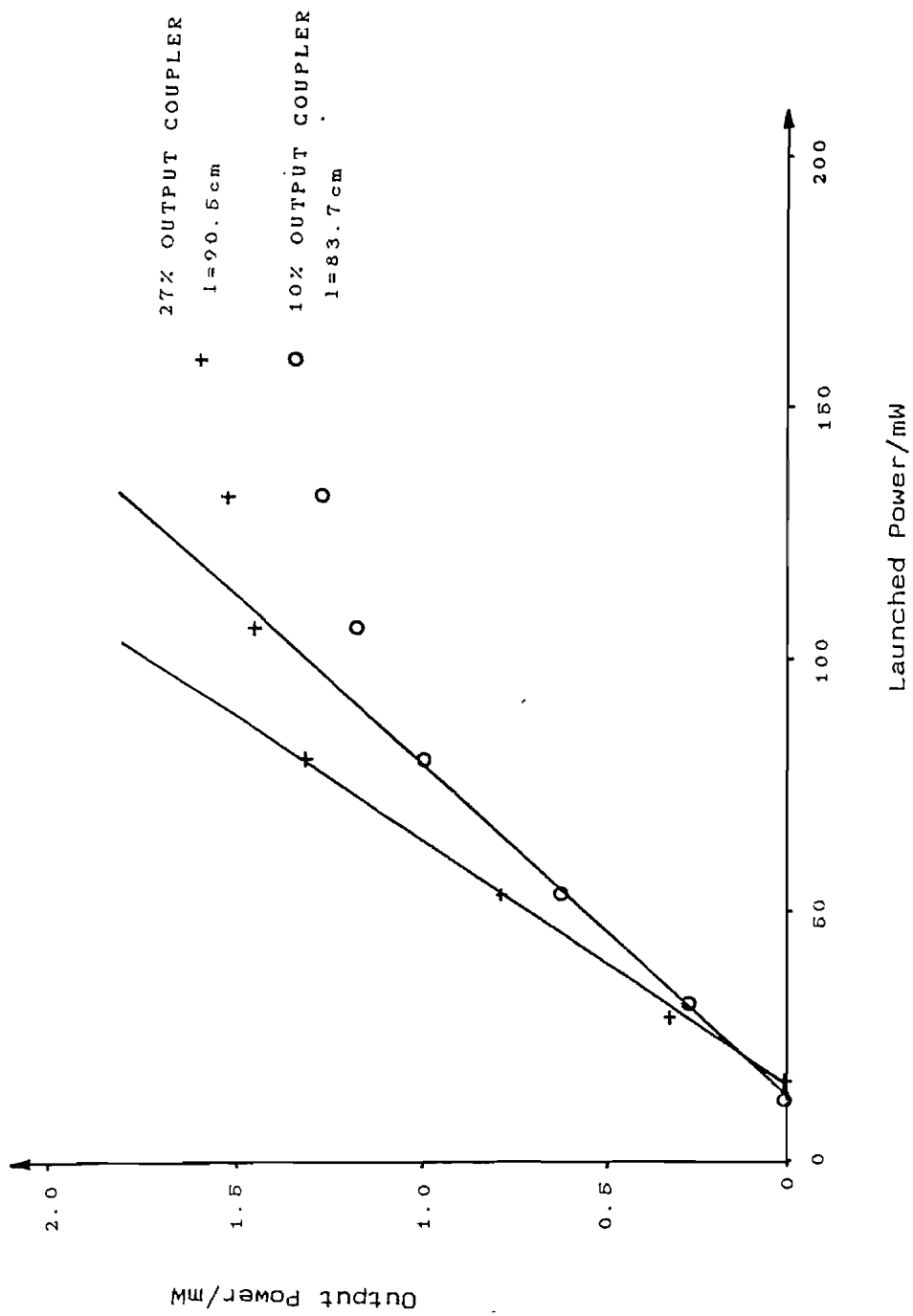
Fig.3.20 shows the output versus input characteristics of this laser. The saturation of the output at high pump powers is believed to be due to the observed saturation of the pump absorption. Thus it is clear that higher output powers are obtainable, at the expense of a higher threshold, by using longer lengths of fibre which will not saturate so quickly.

The thresholds are well within reach of diode-pumped miniature Nd lasers. Indeed such operation has subsequently been demonstrated, [22], using both miniature Nd:YAG and Nd:YLF lasers. The results that we have obtained compare favourably, especially in terms of slope efficiency, with the only previously reported Yb:Er fibre laser, [23], despite having lower doping levels. It should also be noted that pumping with a Styryl 9 dye laser at 820nm, [24], can give even better results (3.7mW threshold, 7% slope efficiency), indicating that direct diode pumping should be possible.

3.6 Summary

In summary we can say that we have shown that the Yb:Er glass laser is a versatile source of radiation at $\sim 1.5\mu\text{m}$, that can be operated in a bulk or fibre configuration. Combining this with the fact that it can be

Fig 3.20 Graph Of Output Power Against Input Power



conveniently pumped by Nd:YAG lasers, makes it a very promising source for studies of non-linear propagation in the negative dispersion region of optical fibres.

We have also shown that the simple rate equation model for the transfer system gives fair agreement with the observed results.

3.7 References

- [1] L.F.Mollenauer and R.H.Stolen, Opt. Lett. 9 (1984) 13
- [2] L.F.Mollenauer, R.H.Stolen and J.P.Gordon, Phys. Rev. Lett. 45 (1980) 1095
- [3] E.Snitzer and R.Woodcock, Appl. Phys. Lett. 6 (1965) 45
- [4] V.P.Gapontsev, M.E.Zhabotinskii, A.A.Izyneev, V.B.Kravchenko and Yu.P.Rudnitskii, JETP Lett. 18 (1973) 251
- [5] V.N.Kalinin and V.A.Fromzel, Sov. Phys. Tech. Phys. 25 (1980) 621
- [6] E.I.Galant, V.N.Kalinin, S.G.Lunter, A.A.Mak, A.K.Przhevuski, D.S.Prilezhaev, M.N.Tolstoi and V.A.Fromzel, Sov. J. Quantum Electron. 6 (1976) 1190
- [7] V.N.Kalinin, A.A.Mak, D.S.Prilezhaev and V.A.Fromzel, Sov. Phys. Tech. Phys. 19 (1974) 835
- [8] E.F.Artem'ev, A.G.Murzin, Yu.K.Fedorov and V.A.Fromzel, Sov. J. Quantum Electron. 11 (1981) 1266
- [9] E.F.Artem'ev, A.G.Murzin, Yu.K.Fedorov and V.A.Fromzel, Opt. Spectrosc. (USSR) 54 (1983) 157
- [10] V.B.Kravchenko and Yu.P.Rudnitskii, Sov. J. Quantum Electron. 9 (1979) 399
- [11] V.P.Gapontsev, S.M.Matitsin, A.A.Izineev and V.B.Kravchenko, Optics And Laser Technology Aug.(1982) 189
- [12] V.P.Gapontsev, S.M.Matitsin and A.A.Izineev, Opt. Comm. 46 (1983) 226
- [13] D.C.Hanna, C.G.Sawyers and M.A.Yuratitch, Optical And Quantum Electronics 13 (1981) 493
- [14] W.A.Clarkson and D.C.Hanna, to be published, Journal Of Modern Optics (1989)
- [15] P.V.Lenzo, E.G.Spencer and K.Nassau, J. Opt. Soc. Am. 56 (1966) 633
- [16] J.P.Gordon, R.C.Leite, R.S.Moore, S.P.S.Porto and J.R.Whinnery, J. Appl. Phys. 36 (1965) 3
- [17] W.Koechner, Appl. Opt. 9 (1970) 1429
- [18] W.Koechner, Appl. Opt. 9 (1970) 2548

- [19] E.Heumann, M.Ledig, D.Ehrt, W.Seeber, E.W.Duczynskii, H.-J.v.d.Heide and G.Huber, *Appl. Phys. Lett.* 52 (1988) 255
- [20] J.E.Townsend, S.B.Poole and D.N.Payne, *Electr. Lett.* 23 (1987) 329
- [21] L.Reekie, I.M.Jauncy, S.B.Poole and D.N.Payne, *Electr. Lett.* 23 (1987) 1076
- [22] G.T.Maker and A.I.Ferguson, *Electr.Lett.* 24 (1988) 1160

- [23] E.Snitzer, H.Po, F.Hakimi, R.Tumminelli and B.C.McCollum, OFC'88 Post-Deadline Paper New Orleans, Louisiana PD2-1 Jan.(1988)
- [24] D.C.Hanna, R.M.Percival, I.R.Perry, R.G.Smart and A.C.Tropper, *Electr.Lett.* 24 (1988) 1068

4. MODE-LOCKING OF Yb:Er GLASS LASERS AND THEIR USE FOR NON-LINEAR PULSE PROPAGATION STUDIES IN SILICA OPTICAL FIBRES

4.1 Introduction

Having described the basic operation of the $\sim 1.5\mu\text{m}$ Yb:Er glass laser in all its various forms, we will now consider the mode-locking of this laser such that it produces short pulses of light with sufficient peak power to study non-linear pulse propagation in the low loss part of the negative dispersion region of silica optical fibres.

4.2 Mode-locking Of The Yb:Er Glass Laser

We will firstly give a brief general discussion of mode-locking in an inhomogeneously broadened laser system such as a glass laser, before going on to describe our own results.

4.2.1 Mode-locking Of Inhomogeneously Broadened Lasers

The resonant frequencies (longitudinal modes) of a Fabry-Perot type laser resonator correspond to the situation where a wave making a complete round trip inside the resonator returns with the same phase except for some integral multiple of 2π . Thus the mode separation is given by,

$$\omega_s = \pi c/l \quad (4.1)$$

where l is the optical cavity length. The total optical electric field at an arbitrary point inside the resonator will be the summation of the individual oscillating modes,

$$E(t) = \sum_m E_m \exp \left\{ i \left[(\omega_0 + m\omega_s) t + \phi_m \right] \right\} \quad (4.2)$$

where ω_0 is an arbitrary reference mode frequency and ϕ_m is the phase of the m th mode.

If we now consider the case of N equal amplitude oscillating modes that have somehow been pulled in phase with each other such that $\phi_m = 0$ we obtain,

$$\begin{aligned}
 E(t) &= E_0 \sum_{m=-\infty}^{m=+(N-1)/2} \exp \left\{ i(\omega_0 + m\omega_s)t \right\} \\
 &= \exp(i\omega_0 t) E_0 \frac{\sin(N\omega_s t/2)}{\sin(\omega_s t/2)} \tag{4.3}
 \end{aligned}$$

where ω_0 is now the central mode frequency. Thus $E(t)$ behaves like a sinusoidal carrier wave at frequency ω_0 , whose amplitude is varied in time according to eqn.(4.3). The output power will be given by,

$$P(t) \propto \frac{\sin^2(N\omega_s t/2)}{\sin^2(\omega_s t/2)} \tag{4.4}$$

Fig.4.1 shows the time behaviour of the laser output for $N=10$. The signal is periodic in the round trip time $T=2L/c$ and the pulse duration, defined by the time from the peak to the first zero, is $\tau=T/N$. The number of oscillating modes is $N=\Delta\omega/\omega_s$, where $\Delta\omega$ is the oscillating linewidth. Thus,

$$\tau \sim 2\pi/\Delta\omega = 1/\Delta\nu \tag{4.5}$$

Since the oscillating bandwidth cannot exceed the gain bandwidth, the shortening of the pulses is fundamentally limited. If the same procedure is carried out for randomly varying phases the output consists of a set of a set of much weaker random impulses. Thus the signal is noise-like but it is still periodic in the round trip time, [1].

In practice the modes will be brought into phase with each other by the use of the active mode-locking techniques of amplitude (AM), [2,3], and phase (FM), [4], modulation.

i) Amplitude Modulation:

If an amplitude modulator is placed inside a laser cavity such that the losses are modulated at the mode

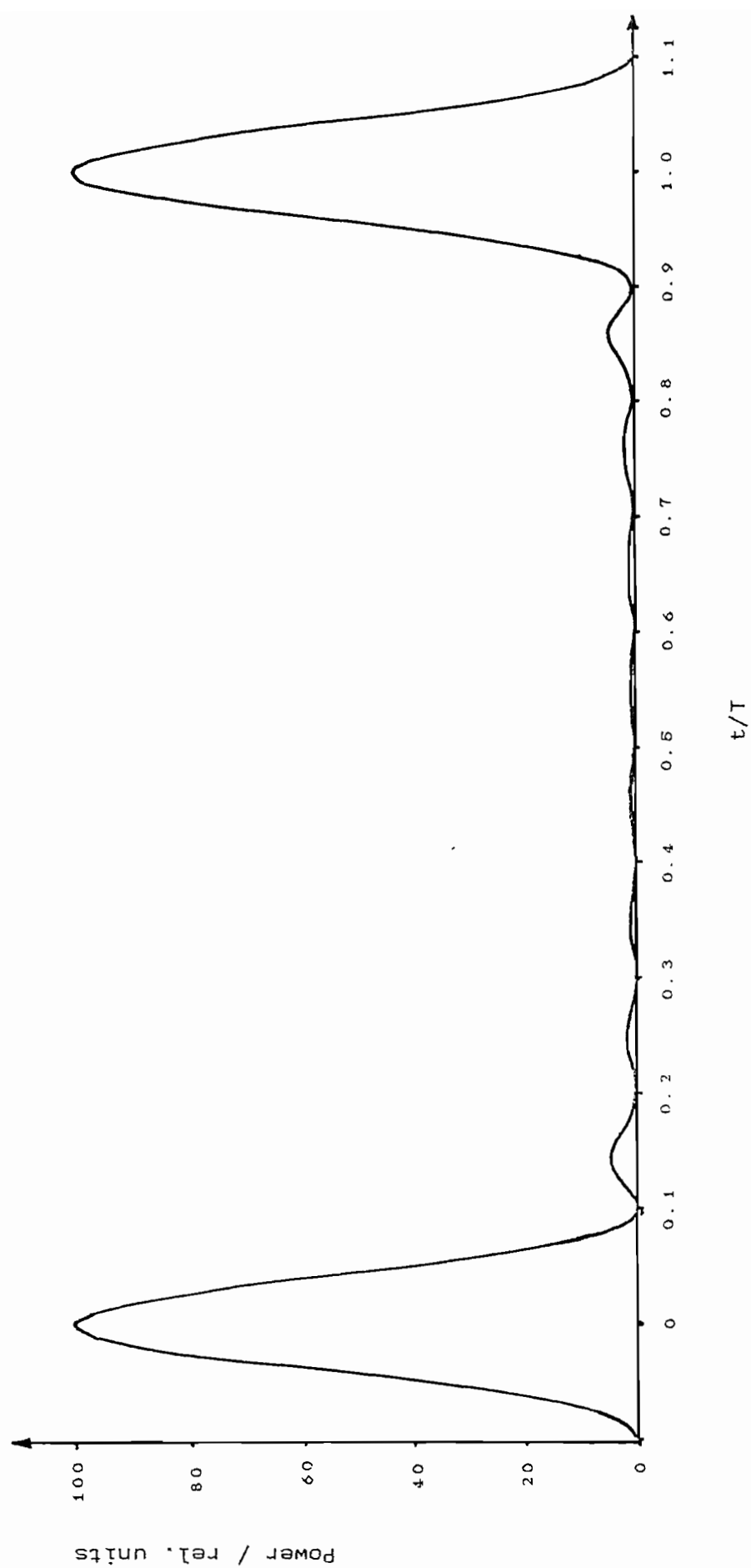


Fig 4.1 Laser Output For $N=10$

separation ω_s , it is then reasonable to expect that short pulses will be produced that pass through the modulator at its point of maximum transmission. In the frequency domain we can say that each oscillating mode ω_q acquires sidebands at $\omega_q \pm \omega_s$. Thus these sidebands fall on the adjacent modes, tending to couple them together by "injection locking".

ii) Phase Modulation:

In this method of mode-locking it is the cavity length that is modulated at the mode separation frequency. The easiest way of explaining how this produces a pulsed output is to realise that this is equivalent to the end mirror moving backwards and forwards at ω_s . A wave striking the mirror while it is moving will suffer successive Doppler frequency shifts on each round trip, pushing it out of the gain bandwidth. However a short pulse striking the mirror at either of the turning points will merely suffer a spectrum broadening frequency chirp rather than a general shift. Thus there are two possible short pulse operating points.

The mode-locked behaviour of a laser will also depend on whether it is homogeneously or inhomogeneously broadened. In the latter case each mode within the gain profile reaches threshold independently causing spectral "hole-burning" as the gain at those particular frequencies saturates to the losses. Thus we can have oscillation on a large number of longitudinal modes and the active modulator has merely to lock them together in phase, which requires a relatively small modulation strength.

However in a homogeneously broadened system the laser system tends to oscillate on one or, due to spatial hole burning, just a few longitudinal modes. Thus the active modulator must take on a much stronger role in creating the modulation sidebands and broadening the oscillating spectrum. This leads to a quite different dependance of the pulselwidth on the strength of modulation and the gain bandwidth. Kuizenga and Siegman, [5], have derived an analytical expression for the pulselwidth in such a system, assuming a Gaussian pulse shape, finding that a steady-state solution is obtained when the spectral broadening of the modulator is

balanced by the spectral narrowing of the gain medium. They give,

$$\tau_p(\text{homog}) = \frac{(2\ln 2)^{1/2}}{\pi} \left[\frac{2g_0}{\delta} \right]^{1/4} \left[\frac{1}{\nu_s \Delta\nu_g} \right]^{1/2} \quad (4.6)$$

where g_0 is the saturated gain coefficient at line centre, ν_s is the modulation frequency, $\Delta\nu_g$ is the gain bandwidth, and δ represents the modulation strength. For typical operating values of g_0 and δ (say 0.1 to 1.0) the factor $(g_0/\delta)^{1/4}$ is near to unity. Thus the pulselwidth is given by, [1],

$$\tau_p(\text{homog}) \sim \frac{0.5}{(\nu_s \Delta\nu_g)^{1/2}} \sim \frac{0.5}{N_0^{1/2} \nu_s} \quad (4.7)$$

where $N_0 \sim \Delta\nu_g / \nu_s$ is the total number of modes in the gain bandwidth. Unfortunately no such analytical expression has been found for an inhomogeneously broadened system but the limiting pulselwidth value can be expressed as, [1],

$$\tau_p(\text{inhomog}) \sim \frac{0.5}{\Delta\nu_g} \sim \frac{0.5}{N_0 \nu_s} \quad (4.8)$$

where, in comparison to eqn.(4.5), we have now assumed a Gaussian pulse shape. Thus we typically expect the pulselwidth in a homogeneously broadened system to be significantly larger than the gain bandwidth limited value of $\sim 0.5/\Delta\nu_g$. Whereas in an inhomogeneously broadened system we would expect to be able to approach this limit if we were able to get enough of the spectrum above threshold in the first place.

Using such active mode-locking techniques on cw pumped Nd doped glass lasers has recently given pulses of $< 10\text{ps}$ duration, [6-8], and there would appear to be no reason why similar results could not be obtained with the Yb:Er glass laser.

4.2.2 A Quasi-cw Mode-locked Yb:Er Glass Laser

(see appendix 6)

Using the pulsed Nd:YAG pump laser described in section 3.3.1 we set up the apparatus shown in fig.4.2. The resonator design needed to satisfy three major requirements,

(1). A small signal spot size at the plane input mirror to minimise the signal mode volume in the Yb:Er rod and give good overlap with the pump.

(2) .A collimated beam through the acousto-optic mode-locker, to give optimum diffraction efficiency and allow the tuning of the cavity length without significantly affecting the laser performance.

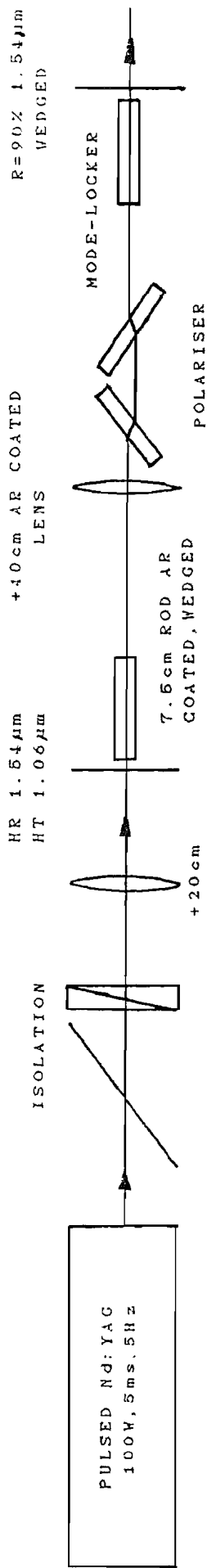
(3). Matching of the cavity length l to the fixed modulation frequency of the mode-locker $\omega/2$, ($l \sim 115\text{cm}$, $\omega/2 \sim 65\text{MHz}$).

These requirements were readily obtained through the use of a 40cm focal length lens which was AR coated at $1.5\mu\text{m}$, placed $\sim 40\text{cm}$ from the input mirror, as shown in fig.4.2. This gives a $\sim 170\mu\text{m}$ waist at the input mirror and a 0.8mm waist at the output mirror.

The acousto-optic modulator was a 7cm long fused silica slab originally designed for use in a Nd:YAG laser with wedged ends AR coated at $1.064\mu\text{m}$ [Intra Action ML-67J]. However it was found to also have low loss at $1.54\mu\text{m}$ and, with a pulsed rf drive power of 7W, it could give an average power, diffraction efficiency of 50%. Two fused silica plates set at Brewster's angle selected the correct linear polarisation state for the mode-locker.

Due to the good stability of our cavity design we were able to obtain lasing with the mirror placed on either side of the mode-locker. Thus by placing a (non-wedged) mirror before the mode-locker, we were able to optimise the diffraction efficiency with it outside the laser cavity. This mirror was then removed and the (wedged) output mirror was

Fig 4.2 Mode-locked Yb:Er Laser Resonator



positioned on the other side of the mode-locker such that the resonator length was matched to the modulation frequency.

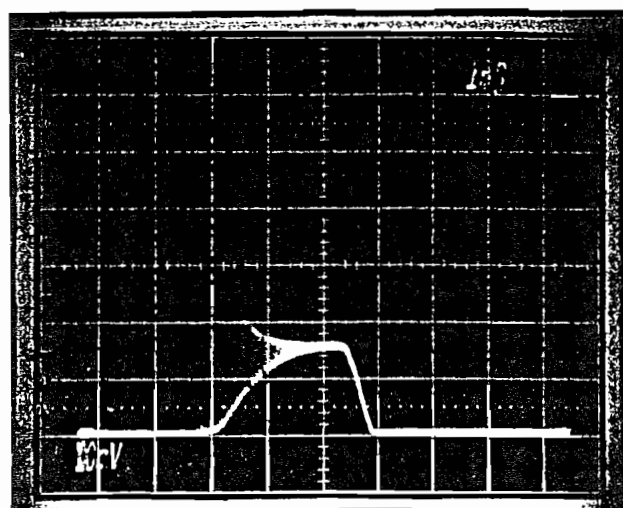
Two resonator length positions were found where driven relaxation oscillations occurred for the entire duration of the laser output, as described by Kuizenga, [9]. Optimum mode-locked performance was found at a resonator length mid-way between these two points. Fig 4.3(a) shows a typical output pulse train envelope, with an overall duration of $\sim 3\text{ms}$ and initial relaxation oscillations decaying away in $\sim 2\text{ms}$. Fig.4.3(b) shows the driven oscillations observed when the cavity length is detuned.

Using the autocorrelation procedure described in section 2.4.2 we obtained smooth autocorrelation traces of $\sim 70\text{ps}$ FWHM duration, assuming a Gaussian pulse shape. Fig4.4 shows a typical result, where the detection system is triggered such that the pulselength is measured over the latter part of the output pulse envelope, where the relaxation oscillations have died away. Using a scanning Fabry-Perot interferometer we found a corresponding bandwidth of $\sim 8\text{GHz}$. Thus we had a pulselength-bandwidth product of ~ 0.6 , comparable to that expected for bandwidth limited Gaussian pulses (0.44). With a 10% output coupler, average output powers of $\sim 3.2\text{mW}$ were obtained, corresponding to peak powers of $\sim 20\text{W}$.

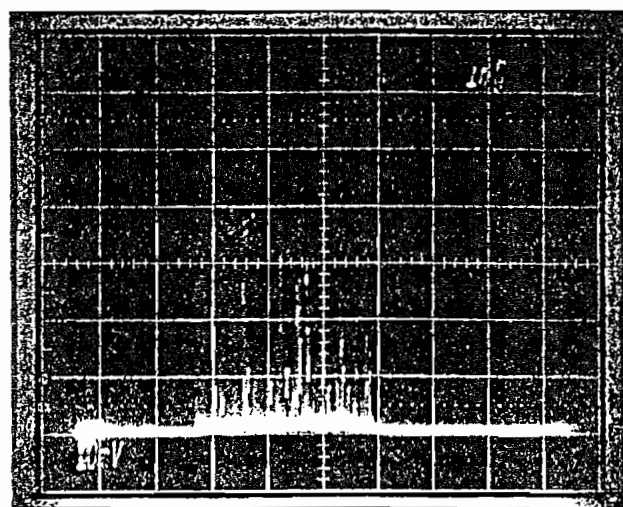
The input mirror was neither wedged or AR coated (unlike the output mirror, mode-locker, and Yb:Er rod), and, despite its high reflectivity at $1.54\mu\text{m}$, produced readily detectable etalon effects. Observation of the output spectrum with the Fabry-Perot interferometer showed that, when the cavity length was very slightly detuned, the output consisted of two $\sim 8\text{GHz}$ FWHM frequency bands separated by $\sim 30\text{GHz}$. The output seems to oscillate between the two frequencies as shown in fig.4.5. Fig.4.6 shows a corresponding autocorrelation trace. The modulation on the mode-locked pulse seems to correspond to beating between these two frequencies. The separation of the frequencies also seems to correspond to the transmission peaks of a $\sim 3\text{mm}$ thick etalon,

Fig 4.3 Mode-locked Output Train Envelope For Tuned And Detuned Cavity Lengths

a)



b)



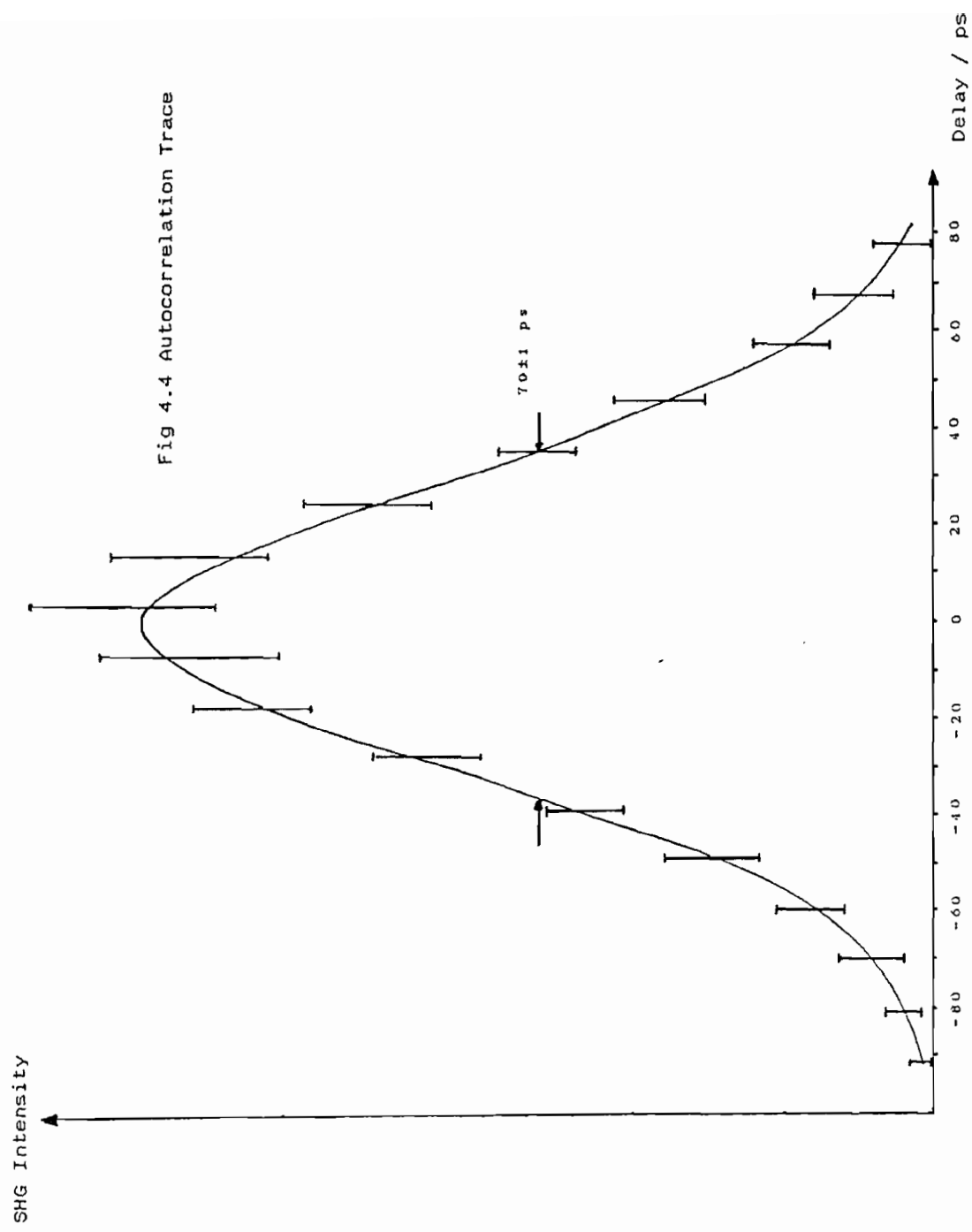
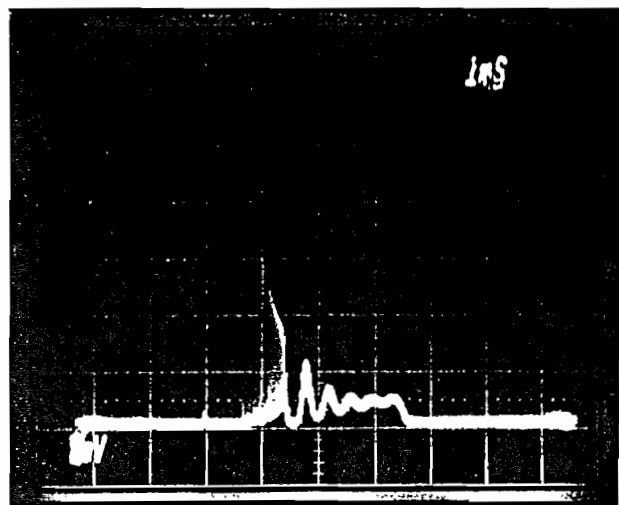
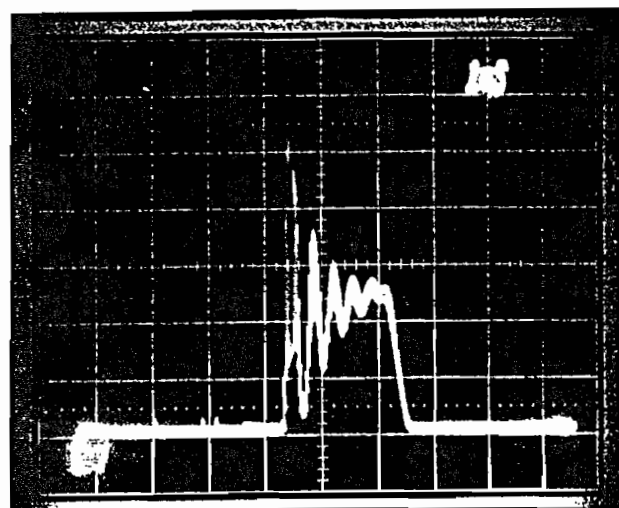


Fig 4.5 Time Behaviour Of The Two Oscilating Frequencies



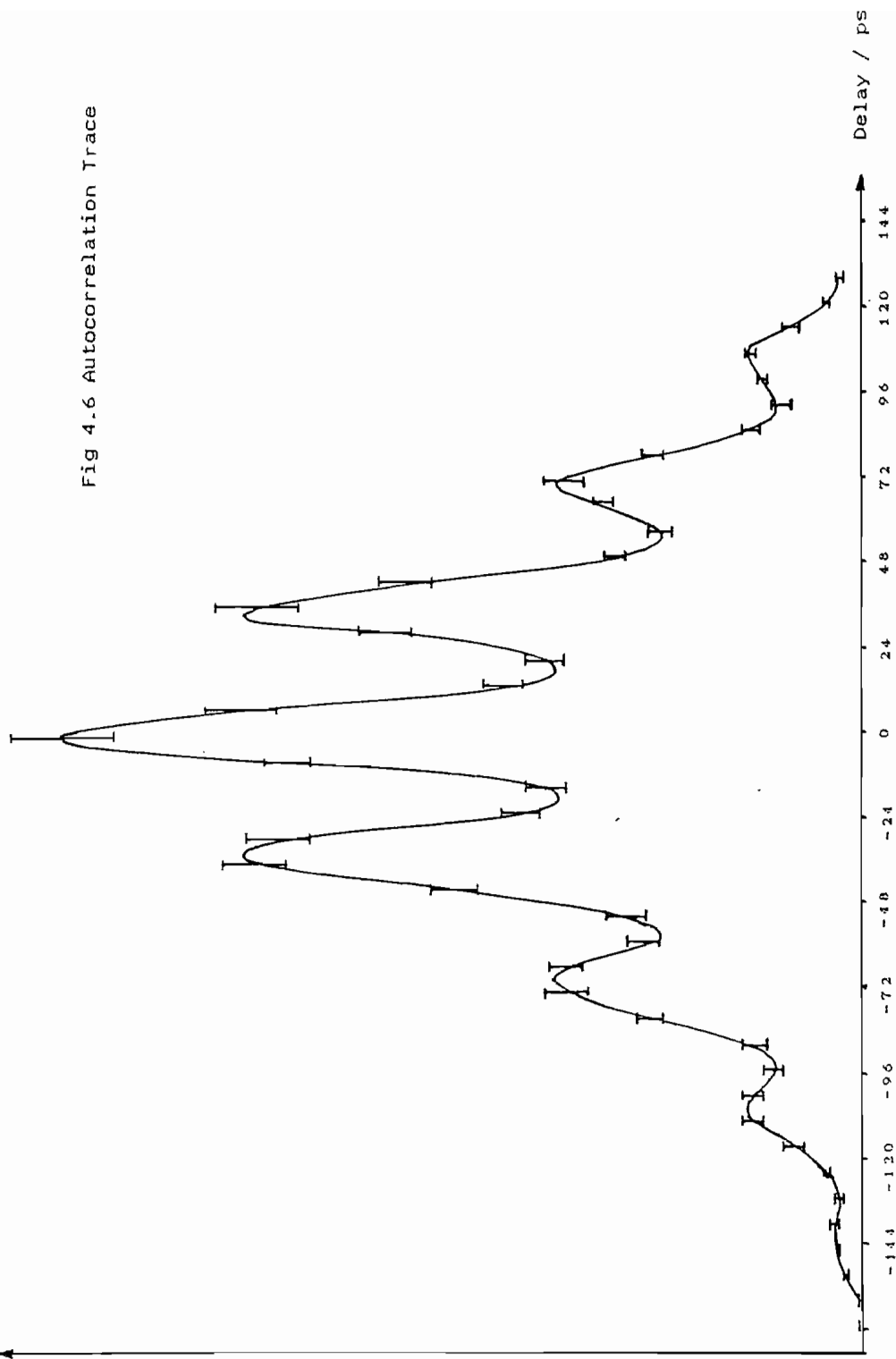
FREQUENCY 1



FREQUENCY 2

SHG Intensity

Fig 4.6 Autocorrelation Trace



(where the delay has not been divided by $\sqrt{2}$ as we have previously done for Gaussian pulse autocorrelations)

which is the thickness of the input mirror. However, at the optimum mode-locking cavity length one of the frequency bands is suppressed and we obtain the smooth autocorrelation trace shown in fig.4.4. Thus, despite the presence of this etalon, we have seen a reasonable mode-locked performance, obtaining bandwidth limited $\sim 70\text{ps}$ FWHM duration pulses of $\sim 20\text{W}$ peak power.

Using the cavity shown in fig.4.7 we were able to increase the available output peak power to $\sim 50\text{W}$ by feeding back the left-over pump power for further absorption. The output pulse envelope now lasts for $\sim 4\text{ms}$ with initial relaxations decaying away in $\sim 1\text{ms}$. Autocorrelation measurements show the pulselength to be unaffected by this change in cavity design.

If a wedged and/or AR coated pump input mirror were used it might be possible to significantly extend the mode-locked bandwidth and so obtain shorter pulses. For instance, if mode-locked oscillations could be obtained throughout the region separating the two currently observed frequency bands ($\sim 30\text{GHz}$), we could expect pulses of $\sim 20\text{ps}$ duration.

4.2.2.1 Mode-locked And Q-Switched Operation

Mode-locked and Q-switched operation at 5Hz was obtained with the same cavity as shown in fig.4.2 except for the addition of an AR coated LiNbO_3 crystal between the polarising plates and the intracavity lens. In contrast to the simple Q-switched operation described in section 3.3.3, the voltage applied to the crystal is carefully adjusted to allow a small level of "pre-lasing" to occur, [8], before the voltage is turned off and the large Q-switched pulse develops. The "pre-lasing" period of $\sim 2\text{ms}$ provided sufficient time for the mode-locker to establish a steady-state pulse duration. In this way we were able to obtain a $\sim 300\text{ns}$ FWHM duration Q-switched envelope of mode-locked pulses. Fig.4.8 shows a typical autocorrelation trace, giving an $\sim 85\text{ps}$ FWHM pulselength, assuming a Gaussian pulse shape. Measurements with a pyroelectric energy meter, taking care to subtract the

Fig 4.7 Mode-locked Yb:Er Laser Resonator With Pump Feedback

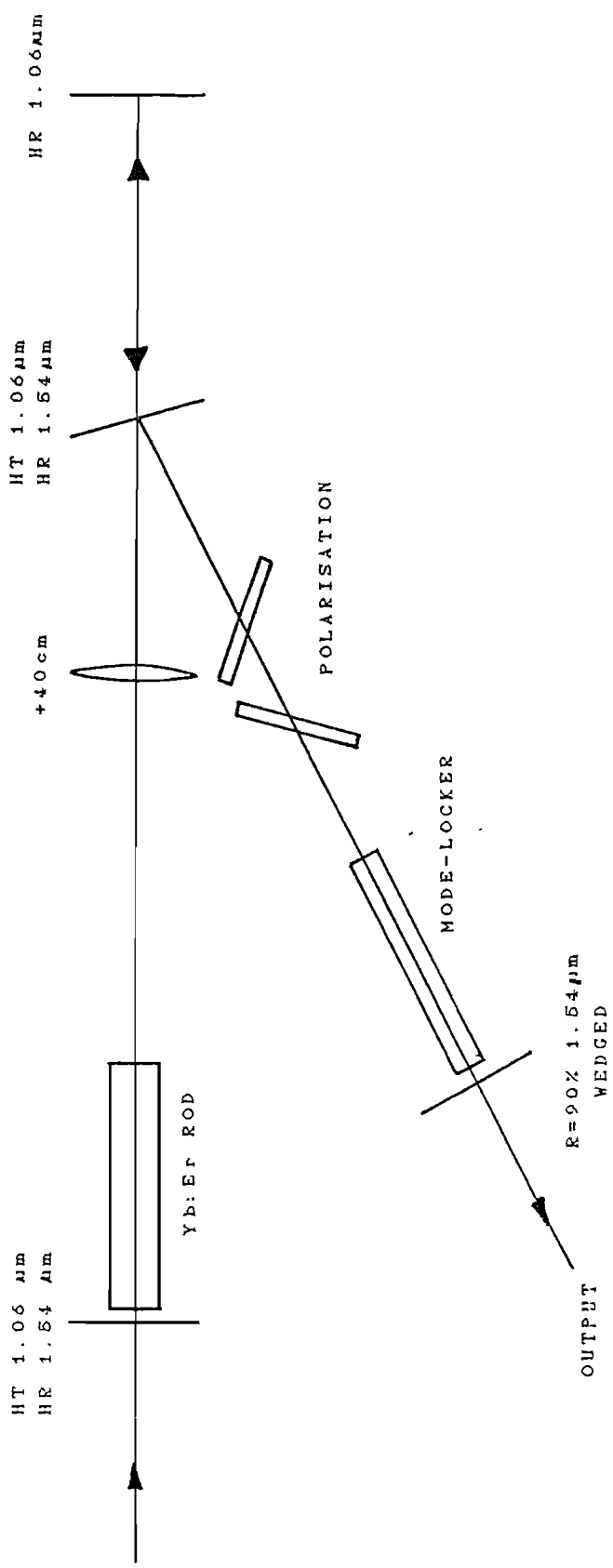
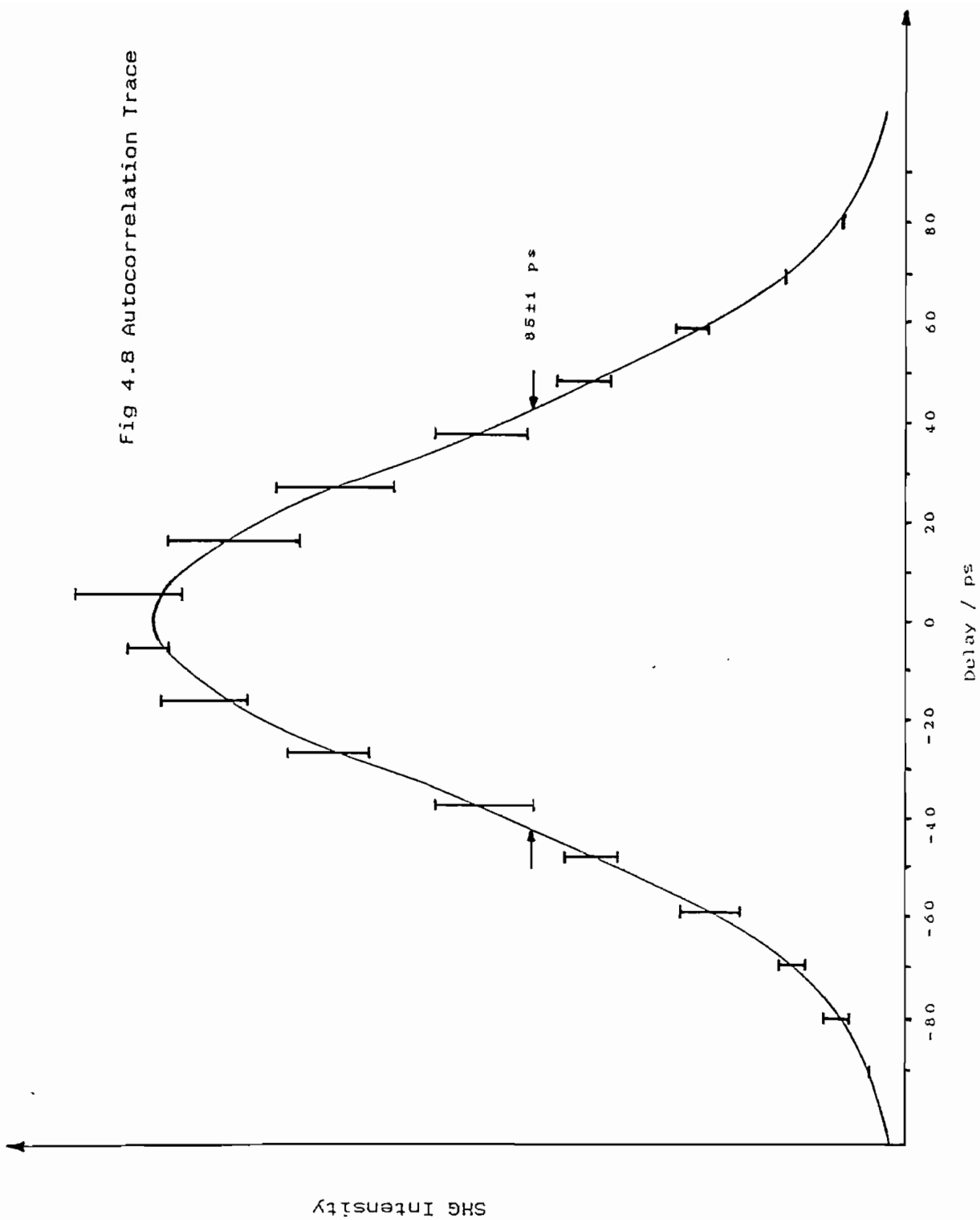


Fig 4.8 Autocorrelation Trace



pre-lase contribution, showed Q-switched pulse energies of $\sim 70\mu\text{J}$, indicating that peak powers of $\sim 20\text{kW}$ were now available.

It should be noted that if a similar cavity to that shown in fig.4.7 were used, it would be reasonable to expect a similar improvement in peak power, i.e. peak powers of $\sim 50\text{kW}$ could be available.

4.2.3 A Mode-locked Yb:Er Fibre Laser (see appendix 7)

Using a $\sim 60\text{cm}$ length of the Yb:Er doped fibre described in section 3.5, we set up the apparatus shown in fig.4.9. Following the approach of earlier workers, [10,11], we now decided to use the technique of F.M. mode-locking, [4], as described earlier. It should be noted however that it should also be possible to apply A.M. mode-locking to such a laser (for example see ref.[12]).

The phase modulator used was a 3cm long LiNbO_3 crystal with Brewster angled, 3mm by 3mm faces. It was mounted in a resonant LC circuit housing and the 98.5MHz rf signal was applied by inductive coupling. The signal polarisation and the applied voltage were chosen to be parallel to the crystal z axis in order to utilise the largest available electro-optic coefficient, r_{33} .

Unlike the fibre used in ref.[10], our fibre was not polarisation preserving. Thus, in order to allow the required polarisation of the signal, it was necessary to induce some birefringence in the fibre. This was achieved by wrapping a single loop of the fibre very tightly around a 3cm diameter disc, [11,13]. When the polarisation selecting element (the Brewster faced modulator) was in the cavity we found that we could minimise the laser threshold by twisting the disc, as shown in fig.4.10. Thus, through stress induced birefringence, we seem to be able to obtain some control over the polarisation of the light exiting the fibre, [14,15].

The pump light (limited to $\sim 300\text{mW}$ to avoid damage to the input mirror) was focussed into the fibre with a X10

Fig 4.9 Mode-locked Yb:Er Fibre Laser Resonator

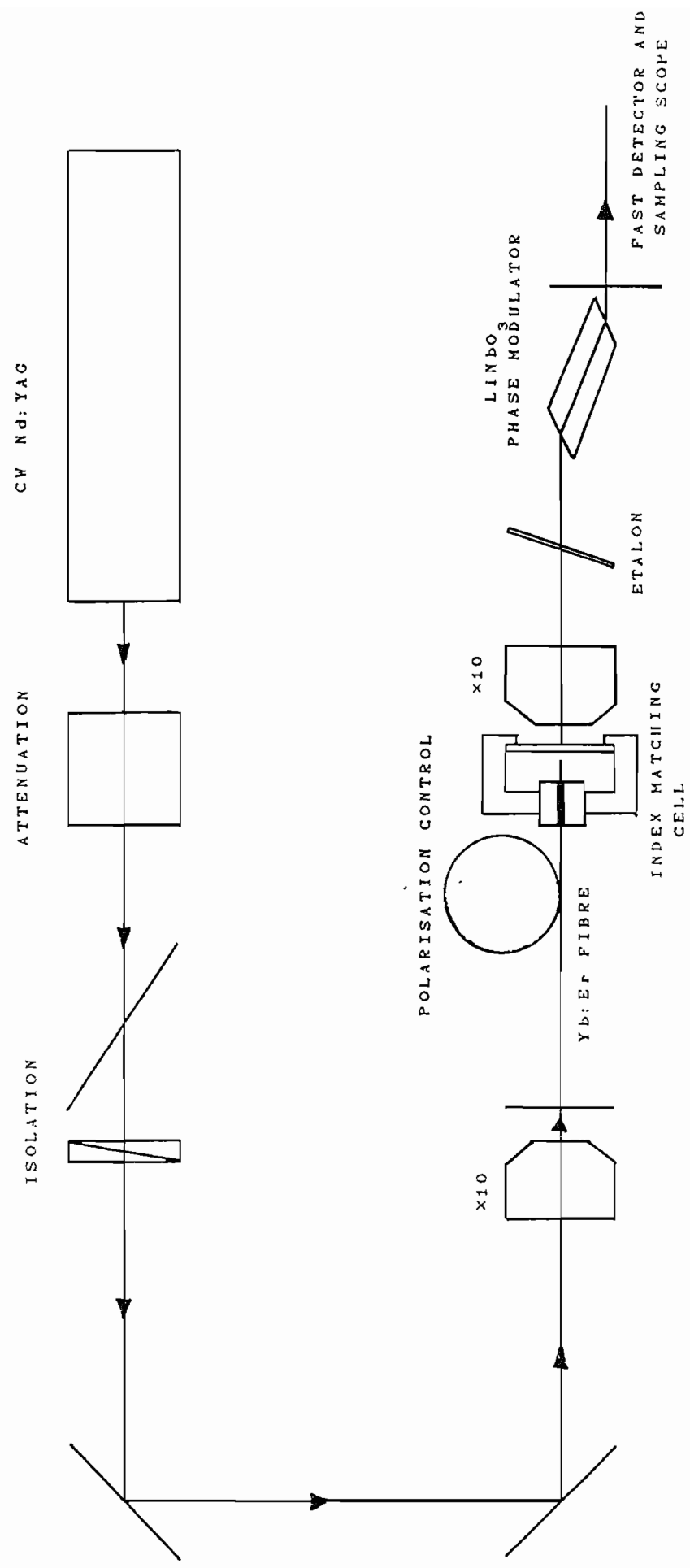
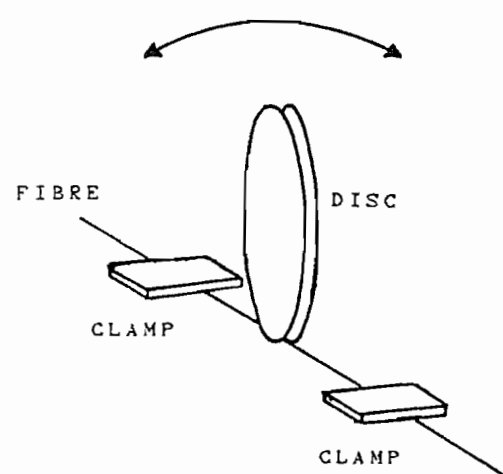


Fig 4.10 Polarisation Control



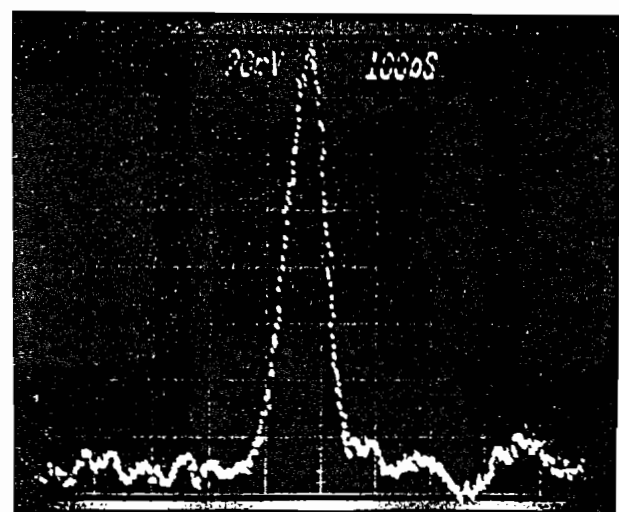
microscope objective through the wedged input mirror. The fibre was butted against the input mirror, and an overall launch efficiency of ~50% was achieved. ~35% of the launched light was absorbed by the fibre. Signal radiation from the other end of the fibre was collected by the intra-cavity X10 microscope objective, and focussed to an $\sim 85\mu\text{m}$ waist spot size on the plane, wedged, 95.5% reflectivity output mirror.

In order to suppress the possibility of an etalon caused by the two 4% reflections off the ends of the fibre, [10], the unbutted end was held in a cell containing index matching liquid. However, both the cell window and the intra-cavity microscope objective were not coated and may have been the source of unwanted etalon effects. In order to stabilise the lasing bandwidth we introduced a 0.25mm thick uncoated etalon as the final cavity element.

An InGaAs fast photodiode (G.E.C. Hurst prototype) was used in conjunction with a sampling scope to monitor the output pulsedwidth. The combined rise-time of the detection system was ~60ps. For r.f. powers of ~0.5W we were able to obtain a stable cw mode-locked output train. Fig.4.11 shows a picture of a typical sampling scope train, where the baseline structure is a result of the detection system used. Measured FWHM durations were typically ~90ps, indicating actual pulsedwidths of ~70ps. Using a scanning Fabry-perot interferometer we found a corresponding bandwidth of ~11.5GHz giving a time-bandwidth product of ~0.8. Kuizenga and Siegman, [5], show that the time-bandwidth product for F.M. mode-locked pulses is 0.626 (assuming a Gaussian pulse shape) for perfect tuning of the cavity length. The product is larger than in the loss modulation case due to a frequency chirp on the pulse.

As stated earlier (section 4.2.1) there are two possible operating points for the production of a mode-locked output train (at the maximum and the minimum of the swept cavity length). This was confirmed experimentally but we also found that it was possible to obtain stable single pulse operation.

Fig 4.11 Mode-locked Output Pulse



The average output power was found to be $\sim 0.1\text{mW}$, indicating peak powers of $\sim 15\text{mW}$. In section 3.5 we found average output powers of nearly 1mW for an Yb:Er fibre laser with butted mirrors. The drop in power in going to the mode-locked system is due in part to the use of uncoated intra-cavity elements (the index matching cell window and the microscope objective), and the fact that we had to use a shorter length of fibre so that we could match the cavity length to the modulator frequency. There would also have been losses off the Brewster faces of the modulator, as the cavity was not completely linearly polarised. Thus, through the use of better quality optics and polarisation preserving fibre, we might expect an order of magnitude improvement in available output power. Indeed later work by P.Suni (appendix 7), using an AR coated index matching cell window and a polarisation controller specifically designed for operation at $1.5\mu\text{m}$, led to increased peak output powers of $\sim 90\text{mW}$ and a polarisation extinction ratio in excess of 100:1. The corresponding intracavity peak power is now $\sim 2.0\text{W}$ which, with the possibility of further enhancement through Q-switching, may lead to interesting non-linear effects in the fibre lasing medium. This possibility will be dealt with in more detail in section 4.3.

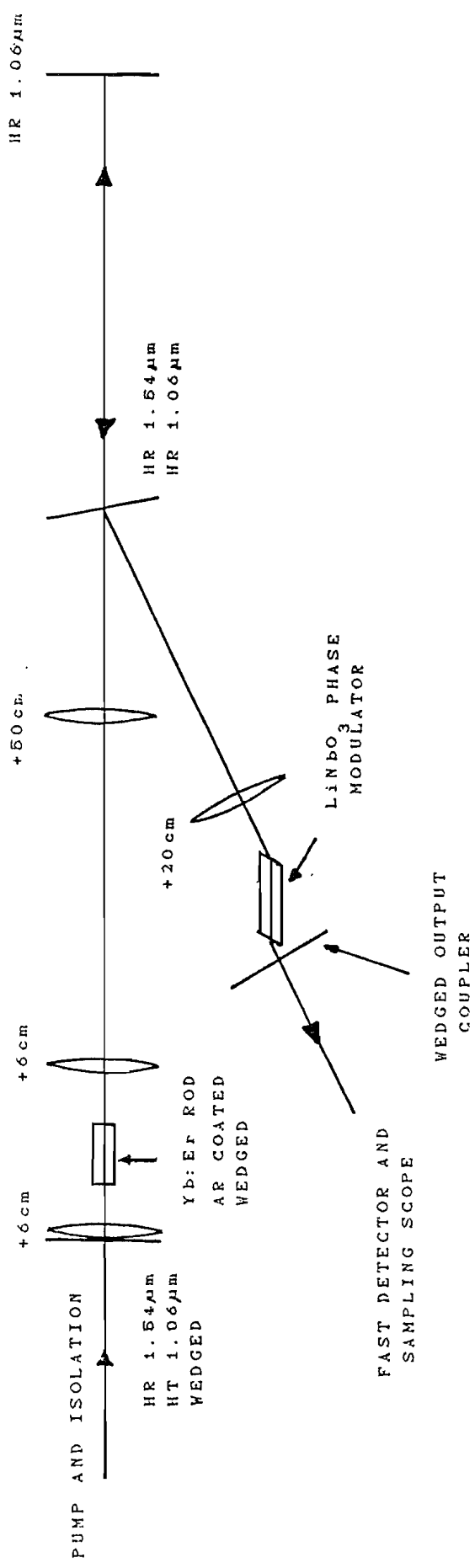
Another way of reducing the cavity losses (by allowing the use of mirrors butted to the ends of the fibre as in section 3.5) would be to use a modulator applied directly onto the fibre itself, [16], as has already been demonstrated with Nd doped fibres, [17].

4.2.4 A CW Mode-locked Yb:Er Glass Laser

Following the successful F.M. mode-locking of the Yb:Er fibre laser described in the previous section, we decided to also use this technique with the bulk cw Yb:Er laser. Fig.4.12 shows the cavity used in this experiment.

Once again we used the Spectra Physics 3000 cw Nd:YAG laser as the pump source. The cavity is the same as that described in section 3.4 (using the 2cm long AR coated

Fig 4.12 CW Mode-locked Yb:Er Resonator



rod), except for a 20cm focal length lens which is used to focus down the signal mode, through the LiNbO_3 phase modulator, to a $\sim 150\mu\text{m}$ waist at the output mirror. Both the rod and the input and output mirrors were wedged in order to avoid unwanted etalon effects. The detection system used is the same as that described in section 4.2.2, and has a combined rise time of $\sim 60\text{ps}$.

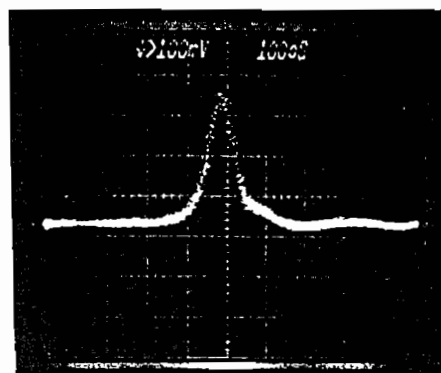
Using a 1% output coupler we obtained the results shown in fig.4.13 for rf powers of $\sim 0.9\text{W}$. Fig.4.13(a) shows a typical output pulse with a measured FWHM duration of $\sim 90\text{ps}$ indicating actual pulsedwidths of $\sim 70\text{ps}$. Fig 4.13(b) shows a train of pulses (detector limited) with pulse separation of $\sim 10.6\text{ns}$ corresponding to the rf modulation frequency of 94.2MHz. Output powers of $\sim 13\text{mW}$ were obtained, which was only slightly less than that obtained without the mode-locker in the cavity ($\sim 16\text{mW}$). Thus peak output powers of $\sim 1.9\text{W}$ were available. Fig.4.13(c) gives an indication of the pulse train stability, with amplitude fluctuations of $\sim 20\%$ being typically observed. This instability may have been due to vibration in the mountings of the numerous cavity elements, with similar fluctuation being observed for pure cw operation. Unfortunately bandwidth measurements were not taken but it was observed that the addition of a 0.25mm thick uncoated etalon, as used in the mode-locked fibre laser, caused no observable effect on the output pulsedwidth.

These results indicate that for mode-locked operation we can obtain similar output powers to those found for cw operation. Thus from the results of section 3.4.1 we might expect to be able to obtain slope efficiencies of $\sim 7\%$ for a $\sim 10\%$ output coupler. This would allow the production of much higher peak output power pulses if a slightly more powerful pump laser were available (see fig.4.14).

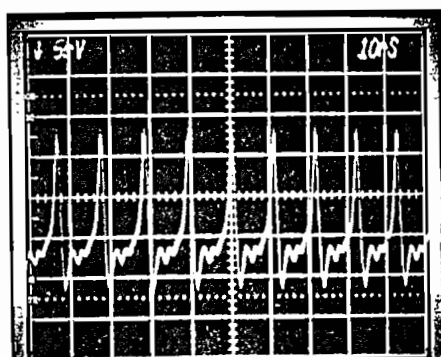
Thus we have achieved one of our main objectives ; the demonstration of cw mode-locked operation in the bulk Yb:Er glass laser. With pulsedwidths of $\sim 70\text{ps}$ and peak powers of $\sim 2\text{W}$ currently available, this source is thought to be a potentially useful research tool for the study of soliton

Fig 4.13 CW Mode-locked Output

a)



b)



c)

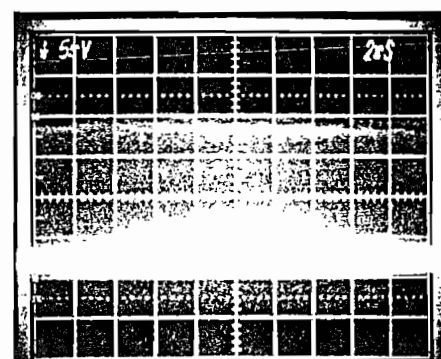
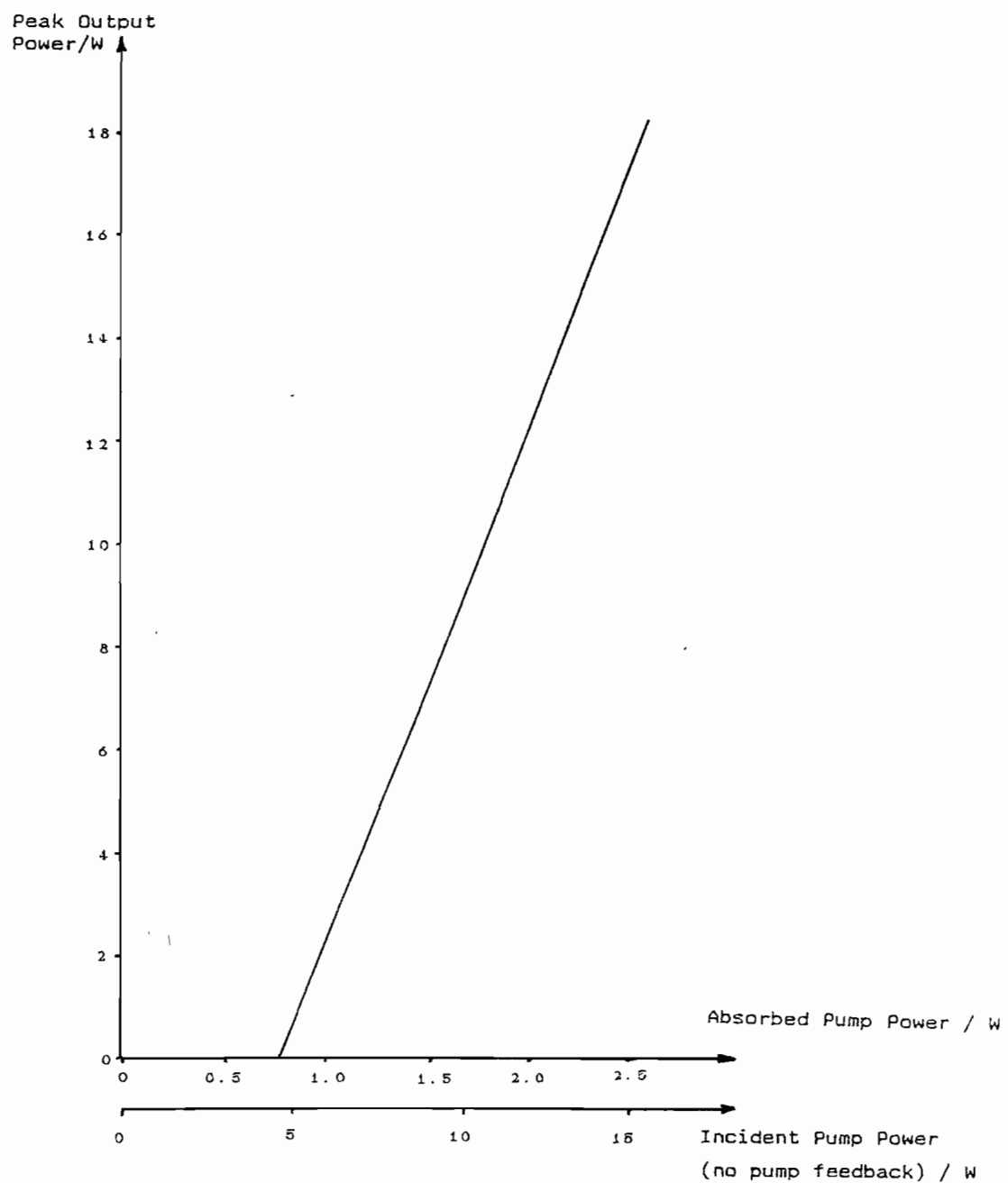


Fig 4.14 Theoretical Plot Of Peak Output Power Against
Pump Power For A 10% Output Coupler



effects. This potential is enhanced by the prediction that peak powers of ~10W could be achieved with the slightly more powerful pump lasers (~10W) that most communications research laboratories possess. This laser also has the capability of being efficiently Q-switched which, combined with mode-locking, could lead to peak powers of the order of 10^4 W at repetition rates of up to ~100Hz.

4.3 Non-linear Pulse Propagation In Optical Fibres

We have successfully shown how mode-locking of the Yb:Er glass laser, in bulk or fibre form, can lead to the production of short bandwidth limited pulses in the $1.5\mu\text{m}$ spectral region. We will now consider the use of these sources for studies of non-linear effects in silica based fibres with emphasis on the possibility of obtaining soliton propagation and pulse compression.

4.3.1 Non-linearity And Pulse Compression

The possibility of pulse narrowing and soliton propagation arises from the fact that the refractive index n is intensity dependent, as below,

$$n = n_0 + n_2 I \quad (4.9)$$

where n_2 is the Kerr coefficient ($= 3.2 \times 10^{-20} \text{m}^2 \text{W}^{-1}$ for silica). For an electric field of phase θ we have,

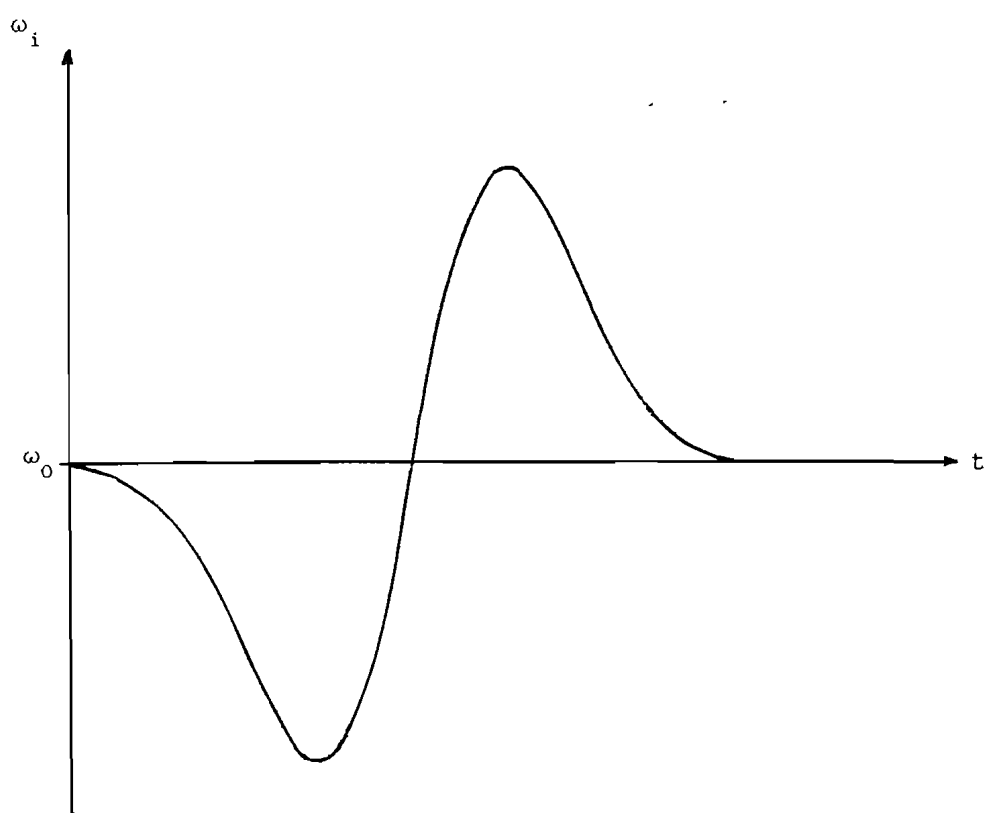
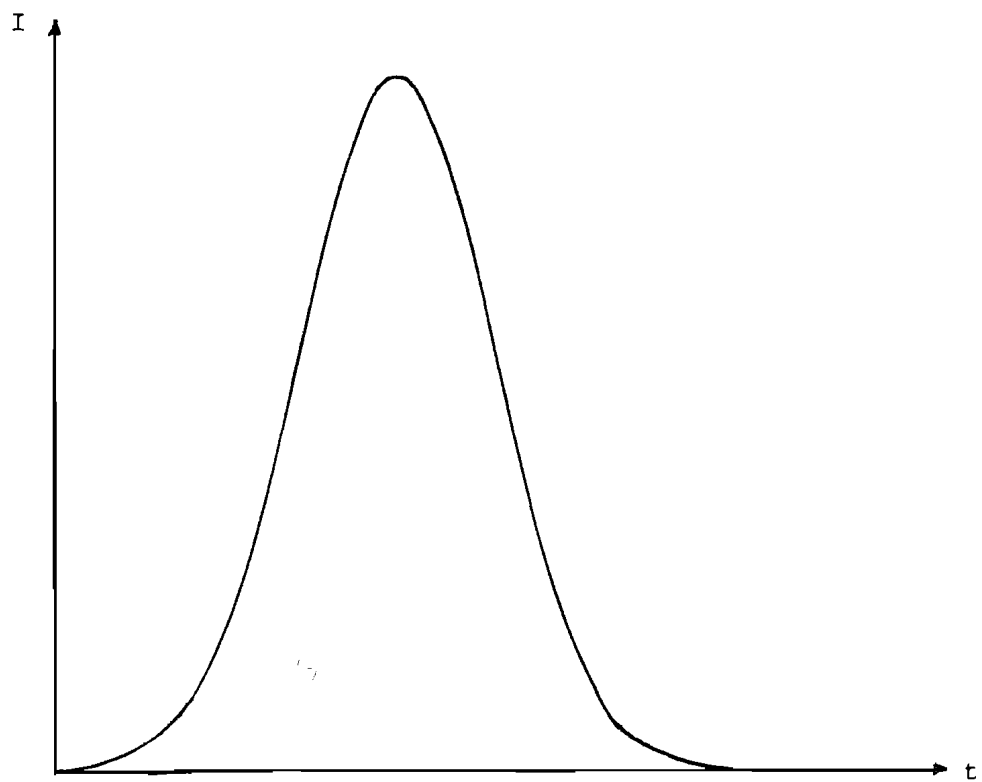
$$\begin{aligned} \theta &= \omega_0 t - kz \\ &= \omega_0 t - \omega_0 n_0 z / c - \omega_0 n_2 z I / c \end{aligned} \quad (4.10)$$

Thus the instantaneous frequency is given by,

$$\omega_1 = d\theta/dt = \omega_0 - (\omega_0 n_2 z / c) dI/dt \quad (4.11)$$

This effect is known as self-phase modulation, [18], and for a pulsed intensity it can lead to a frequency chirp and the broadening of the spectrum as shown in fig.4.15. Thus the

Fig 4.15 Self-Phase Modulation



pulse tends to have low frequencies in its leading edge and high frequencies in its trailing edge. If this chirped pulse is in the negative group velocity dispersion region ($\lambda > 1.3\mu\text{m}$ for standard silica fibres), then the high frequency components will tend to catch up with the low frequency components, leading to pulse compression.

4.3.2 The Non-linear Schrodinger Equation

In order to advance beyond this simple explanation and achieve a description of soliton propagation we need to write down the appropriate differential equations. Following Haus, [19], we assume that an optical field $e(z, \omega)$ is propagating along a single mode fibre such that,

$$\frac{\partial e(z, \omega)}{\partial z} = -i\beta(\omega)e(z, \omega) \quad (4.12)$$

where $\beta(\omega)$ is the propagation constant. If the spectrum is sufficiently narrow and centred around a carrier frequency ω_0 we can expand $\beta(\omega)$ as below,

$$\beta(\omega) = \beta(\omega_0) + \left[\frac{d\beta}{d\omega} \right] (\omega - \omega_0) + (1/2) \left[\frac{d^2\beta}{d\omega^2} \right] (\omega - \omega_0)^2 + \delta\beta \quad (4.13)$$

where $\delta\beta$ is the change in propagation constant due to an index perturbation δn . Thus,

$$\frac{\partial e}{\partial z} = -i \left[\beta(\omega_0) + \left[\frac{d\beta}{d\omega} \right] (\omega - \omega_0) + (1/2) \left[\frac{d^2\beta}{d\omega^2} \right] (\omega - \omega_0)^2 + \delta\beta \right] e \quad \dots (4.14)$$

As the narrow spectrum is centred around a carrier frequency ω_0 it is convenient to express the field as a function of $(\omega - \omega_0)$,

$$e(z, \omega) = E(z, \omega - \omega_0) \exp [-i\beta(\omega_0)z] \quad (4.15)$$

where $E(z, \omega - \omega_0)$ is the slowly varying, complex, wave envelope. If we compare eqns.(4.14) and (4.15) we obtain,

$$\frac{\partial E(z, \omega - \omega_0)}{\partial z} = -i \left[\left[\frac{d\beta}{d\omega} \right] (\omega - \omega_0) + (1/2) \left[\frac{d^2\beta}{d\omega^2} \right] (\omega - \omega_0)^2 + \delta\beta \right] E(z, \omega - \omega_0) \quad \dots (4.16)$$

Using the relation,

$$[i(\omega - \omega_0)]^n E(z, \omega - \omega_0) = F.T. \left[\frac{\partial^n}{\partial t^n} E(z, t) \right]$$

we can obtain the inverse Fourier transform of eqn.(4.16),

$$\left[\frac{\partial}{\partial z} + (1/v_g) \frac{\partial}{\partial t} \right] E(z, t) = (i/2) \left[\frac{d^2\beta}{d\omega^2} \right] \left[\frac{\partial^2 E(z, t)}{\partial t^2} \right] - i\delta\beta E(z, t) \quad (4.17)$$

where $E(z, t)$ is the space-time-dependant envelope defined by $e(z, t) = E(z, t) \exp\{-i[\beta(\omega_0)z - \omega_0 t]\}$, and $(1/v_g) = (d\beta/d\omega)$ is the inverse group velocity. If we now identify the index perturbation as being due to the non-linear refractive index, such that $\delta\beta \propto |E|^2$, we then have,

$$\left[\frac{\partial}{\partial z} + (1/v_g) \frac{\partial}{\partial t} \right] E(z, t) = (i/2) \left[\frac{d^2\beta}{d\omega^2} \right] \left[\frac{\partial^2 E(z, t)}{\partial t^2} \right] - ix|E(z, t)|^2 E(z, t) \quad (4.18)$$

where x is a constant dependant upon the single mode fibre used.

In eqn.(4.18) we can identify the two terms on the right hand side as due to group velocity dispersion and self-phase modulation respectively. For the case of negative

group velocity dispersion ($d^2\beta/d\omega^2 < 0$), and a pulse that is convex upwards ($\partial^2 E/\partial t^2 < 0$ over the centre portion of the pulse), it is possible to balance the dispersive and non-linear terms. It is then found that the pulse can approach a limiting pulseshape which does not change further with distance. This corresponds to the lowest order soliton solution of eqn.(4.18), which has the form of the non-linear Schrödinger equation (NLSE).

4.3.3 Solitons

Hasegawa and Tappert, [20], first considered the non-linear propagation of optical pulses in monomode fibres, and derived the NLSE for the slowly varying pulse envelope (eqn.(4.18)). This equation is known to support soliton solutions, [21,22], i.e. the solutions, which are characterised by a certain amplitude and pulseshape, can either propagate with a constant pulseshape or display a periodic oscillation through a set of recurring pulse shapes.

The NLS can be reduced to a dimensionless form through the following simple transformations, [23],

$$t' = (1/T)(t - z/v_g) \quad (4.19a)$$

$$z' = \left| \frac{d^2\beta}{d\omega^2} \right| \left[\frac{z}{T^2} \right] \quad (4.19b)$$

$$u = T x^{1/2} E \left| \frac{d^2\beta}{d\omega^2} \right|^{-1/2} \quad (4.19c)$$

where T is a scaling factor related to the pulselwidth. Thus we arrive at,

$$i \left[\frac{\partial u}{\partial z'} \right] = (\alpha/2) \left[\frac{\partial^2 u}{\partial t'^2} \right] + |u|^2 u \quad (4.20)$$

where $\alpha = -1$ for positive dispersion and $\alpha = +1$ for negative

dispersion. This equation was studied analytically by Satsuma and Yajima, [22], with the initial condition,

$$u(z'=0, t') = N \operatorname{sech}(t') \quad (4.21)$$

and it was found that solitary solutions are obtained for integer values of N . The fundamental, $N=1$, solution corresponds to an unchanging (sech) pulseshape as discussed earlier. For $N < 1$ the dispersion term dominates, with consequent pulse broadening with propagation. For $N > 1$ the pulse shape is periodic in $z' = \pi/2$ and will always initially undergo pulse compression. Direct large scale numerical solutions of the NLSE have proved to be practical up to $N \sim 4$ before they become just too large and time consuming (even on very powerful computer systems). However solutions up to $N \sim 20$ have been obtained, [24], for the exact $N = \text{integer}$ case using the method of ref. [21]. As an example of how the development of the pulseshape with propagation becomes much more complicated for higher order solitons the reader should consult fig. 2 of ref. [25], which shows the development of the $N=4$ soliton over the range $z' = 0$ to $z' = 2\pi$.

If we now transform these results back into "real world" dimensions it is found that the peak power required to propagate the fundamental $N=1$ soliton is, [21],

$$P_1 = 0.776 \frac{\lambda^3 |D|}{\pi^2 c n_2 \tau^2} A_{\text{eff}} \quad (4.22)$$

where τ ($= 1.76T$) is the FWHM duration of the input pulse, A_{eff} is the effective core area of the fibre, and D is the fibre dispersion parameter given by $d^2\beta/d\omega^2 = D\lambda^2/2\pi c$. We can also see that the soliton period is,

$$z_0 = 0.322 \pi^2 c \tau^2 / \lambda^2 |D| \quad (4.23)$$

and that the peak powers required for higher order solitons are related to P_1 via,

$$P_N = N^2 P_1 \quad (4.24)$$

4.4 Experimental Demonstration Of Soliton Pulse Compression

The first experimental observations of soliton pulse compression in optical fibres were made by Mollenauer et al in 1980, [23], while experimental confirmation of pulse restoration at the soliton period came a few years later in 1983, [26]. For our initial demonstration of soliton pulse compression we decided to use the quasi-cw mode-locked Yb:Er laser described in section 4.2.2. This version of the Yb:Er laser has given us the most stable and powerful train of mode-locked pulses to date and was thus ideally suited to soliton experiments.

Fig 4.16 shows the experimental set up. The Yb:Er laser output consisted of a 4ms train of 70ps FWHM duration pulses, with initial relaxation oscillations decaying away in ~1ms. Peak output powers of ~50W were available and after some beam steering optics and launching into the fibre we were left with peak powers of ~9W. Using eqns.(4.19),(4.20) and (4.21) we find the following,

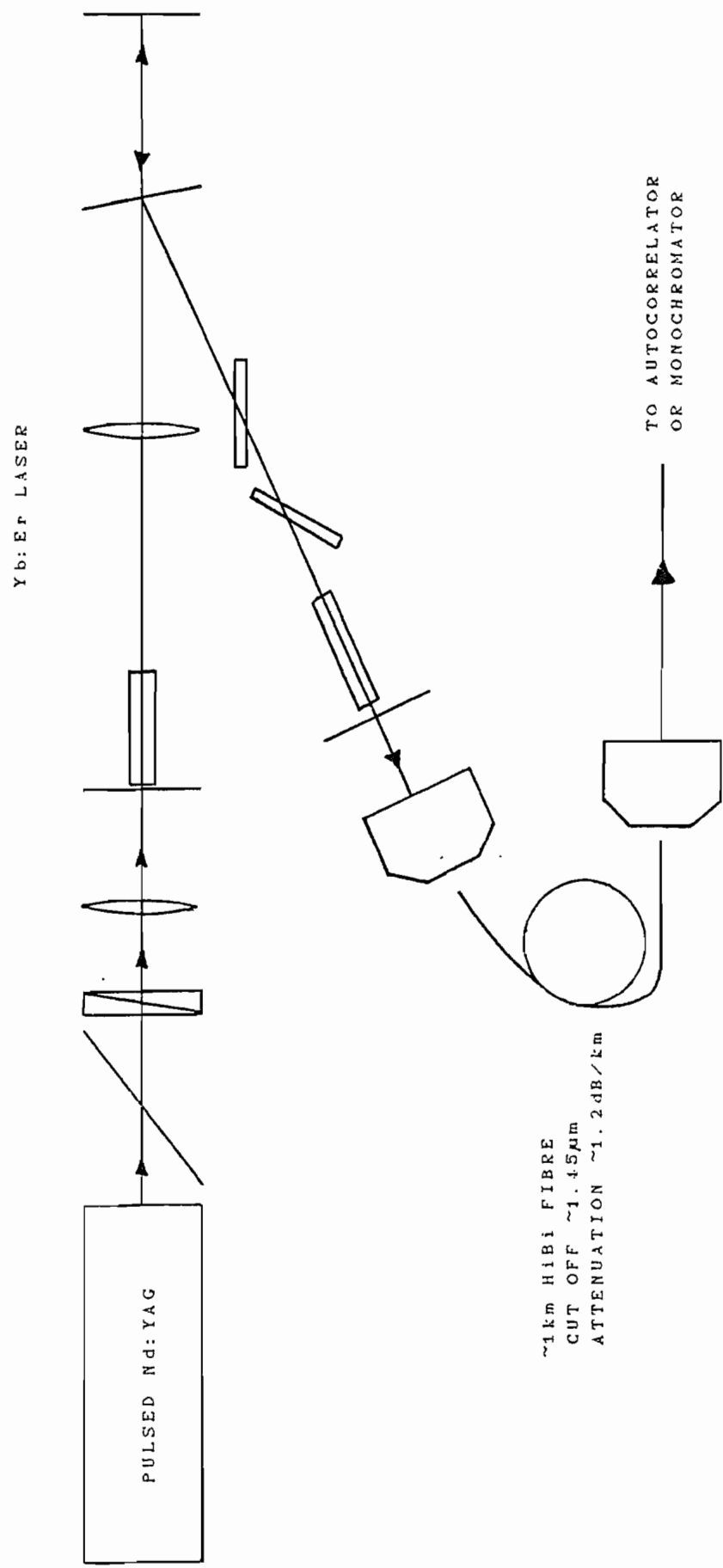
$$P_1 = 9.7 \text{mW}$$

$$z_0 = 124 \text{km}$$

$$N = 30$$

Where we have used typical single mode silica fibre values for D ($-16 \times 10^{-6} \text{sm}^{-2}$), A_{eff} ($1 \times 10^{-10} \text{m}^2$) and n_2 (3.2×10^{-20}). Dianov et al, [27], have estimated that an $N=30$ soliton should give an optimum compression of ~120 times, at a distance of $\sim 0.01z_0$. The order of magnitude of these estimates can be confirmed by assuming a linear continuation of the curves of fig 1 in ref [24]. This estimate also leads us to expect that ~0.1 of the original energy will be contained within the compressed pulse. Thus, after ~1km of fibre, we might expect to obtain pulses of ~600fs duration with peak powers of ~100W.

Fig 4.16 Soliton Pulse Compression

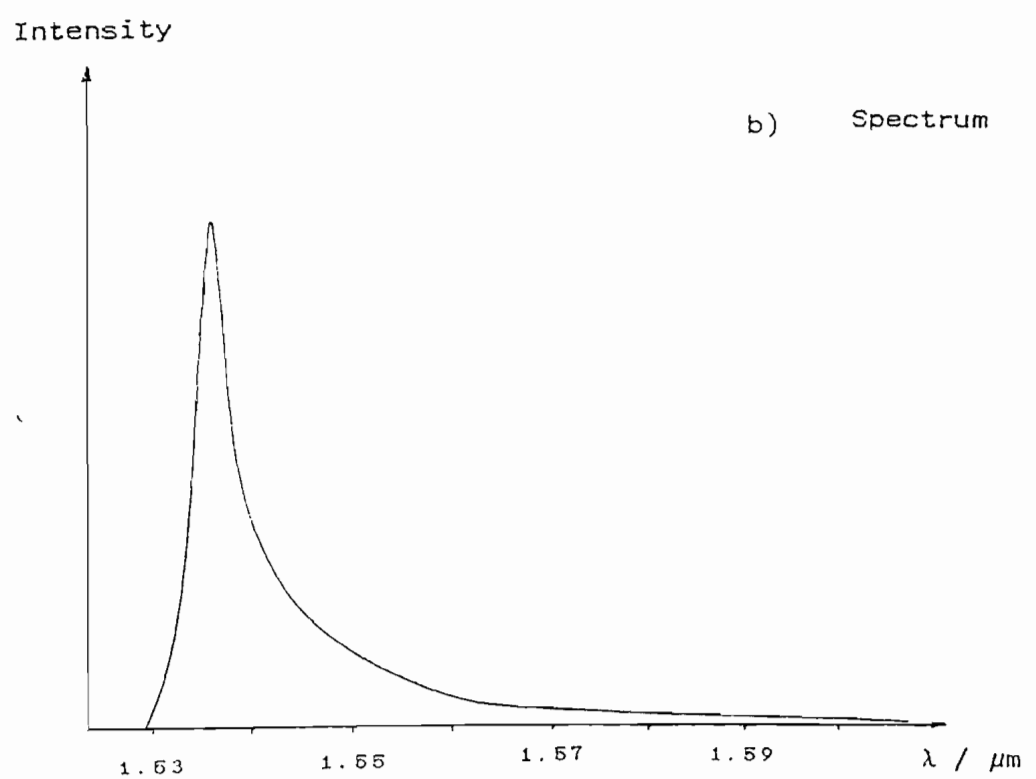
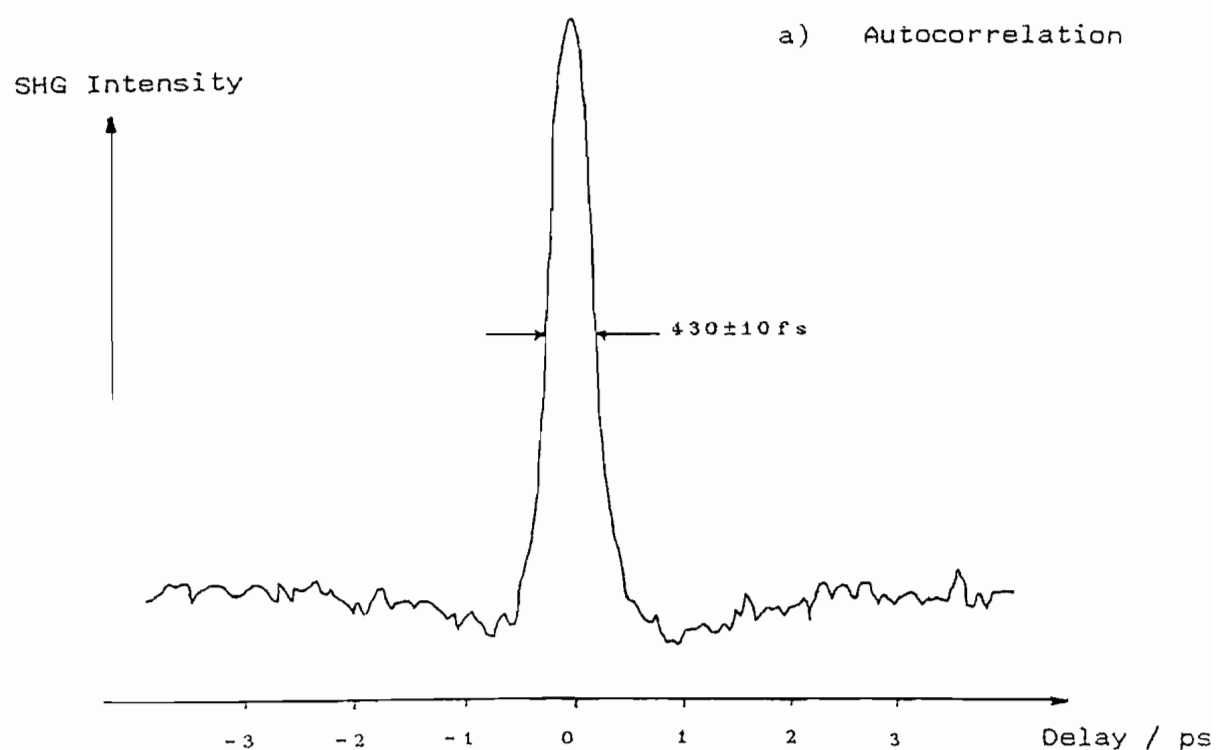


In practice we use a 1.025km length of HiBi fibre as shown in fig 4.16. This fibre had a cut off wavelength of $1.45\mu\text{m}$ and an attenuation of 1.2dB/km at $1.54\mu\text{m}$. It should be noted that our predictions are based on a lossless fibre and that loss will tend to broaden the soliton pulse (see ref [25], section 5.2, and references therein). We decided to use polarisation preserving fibre in order to avoid the effect of intensity-dependant birefringence. This effect can lead to the high intensity compressed pulse becoming differently polarised to any low intensity pedestal present. As the autocorrelator is polarisation sensitive this would lead to a false picture of the pulse shape, [24].

Fig 4.17 shows a typical output autocorrelation trace (using a 1mm LiIO_3 second harmonic crystal) and the corresponding frequency spectrum. It would appear that a very short pulse has developed together with a low-level background pedestal which has a similar width to the original input pulse. Assuming a sech^2 shape we find the compressed pulse has a FWHM duration of just $430\pm10\text{fs}$ representing a very large single stage compression factor of ~ 160 times. From fig 4.17(b) we can see that the spectrum has developed a long wavelength Stokes wing. These results agree very well with those of Dianov et al, [27]. They also launched pulses with enough peak power to propagate solitons of around $N \sim 30$ and used fibre length corresponding to the point of optimum compression.

The development of the Stokes wing can be explained by considering the interaction of the pulse bandwidth with the Raman gain of the silica fibre. Stolen et al, [28], have shown that silica fibres have a continuous Raman gain curve which stretches from frequency shifts of 0 to more than 1000cm^{-1} , with the main peak at 440cm^{-1} . Thus as the launched pulse begins to compress, and its spectrum is correspondingly broadened through self phase-modulation, part of the spectrum falls into the region of stimulated Raman amplification. Thus there is a "gain gradient" favouring the lower frequency part of the spectrum. In this way a continual channeling of energy from shorter to longer wavelengths is established. This

Fig 4.17 Fibre Output



effect has been called the soliton self-frequency shift (SSFS), [29,30]. A more complete explanation, both theoretical and experimental, is given by Beaud et al, [31], who show that an ultra-short pulse is formed from the Stokes wing which then separates both spectrally (due to the SSFS) and temporally (due to group velocity dispersion) from the remains of the input pulse. The ultra-short pulses are fundamental solitons and are free from a background pedestal. In fact this process limits the formation of very high order solitons, causing them to decay into one or more (depending on the input power and propagation distance) fundamental solitons at different wavelengths. Our results correspond to the onset of this behaviour and the autocorrelation we have obtained will contain information about both the initial and any Stokes pulse formed, (the spectral width of the second harmonic generation will be ~100nm due to the tight focussing of the light into the crystal).

Under similar conditions Dianov et al, [27], found the Stokes wing to contain such a fundamental soliton pulse. In order to make such a measurement one would need to send the autocorrelation second harmonic signal through a monochromator to select the specific part of the spectrum which is of interest. Unfortunately our detection system was not sensitive enough to allow this improvement. However it is not unreasonable to assume that we have generated a Stokes pulse of around ~400fs duration. This pulse would be a fundamental soliton and would thus have a peak power of ~300W.

This is as far as our initial experiments have progressed, however one simple way of obtaining further compression and studying the propagation of lower order solitons in the femtosecond region would be to launch the fundamental soliton we have already obtained into a dispersion shifted fibre, [32]. For instance if we chose a fibre such that $D = -1 \times 10^{-6} \text{ sm}^{-2}$ then from eqns (4.22) and (4.23) we find,

$$P_1 = 19W$$

$$z_0 = 65\text{m}$$

where we have assumed $\tau=400\text{fs}$. Thus with a launch efficiency of $\sim 50\%$ (i.e. initial peak powers of $\sim 150\text{W}$), we could propagate solitons of up to $N \sim 3$ with optimum pulse compression factors of 8.4, [24], giving pulsewidths down to $\sim 50\text{fs}$. The relatively small value for z_0 would also allow a more careful study of pulse shape versus propagation length.

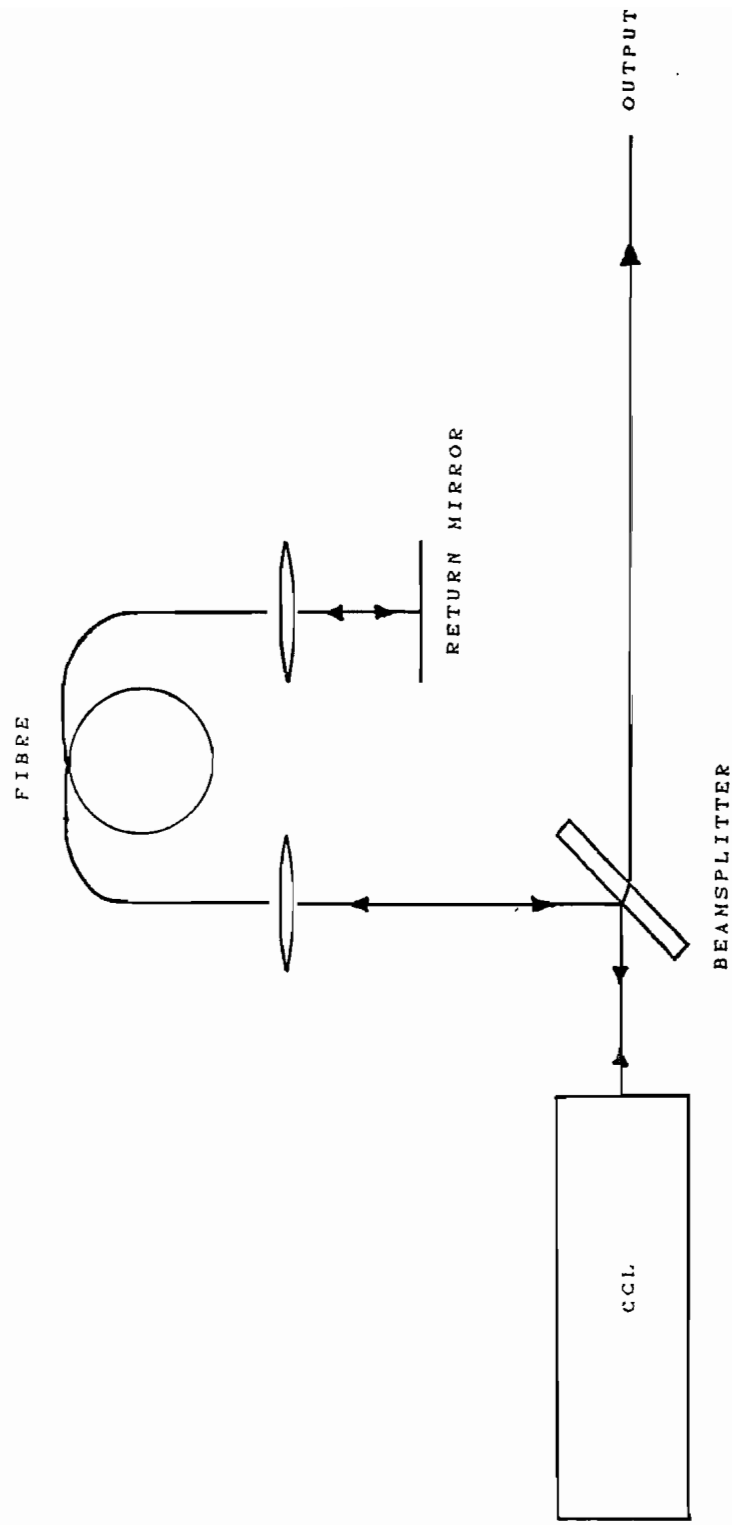
It should be noted that there is an even simpler route to these single pass soliton pulse compression studies avoiding the need for an Yb:Er laser (or colour-centre laser) altogether. Grudinin et al, [32], have shown that by launching a $1.06\mu\text{m}$ mode-locked and Q-switched Nd:YAG laser into a silica fibre the consequent Raman scattering spectrum extends well into the negative dispersion region. Autocorrelation measurements around the $1.6\mu\text{m}$ region show that pulses of $<100\text{fs}$ can be generated which, again, propagate as fundamental solitons.

Having demonstrated the viability of using the Yb:Er laser as a research tool for investigating single pass soliton propagation, we will now go on to the more complicated situation where the compressed pulse is fed back into the main cavity eventually leading to a "soliton laser" as first described by Mollenauer and Stolen in 1984, [33].

4.5 Design Considerations For An Yb:Er Glass Soliton Laser

As we have already seen the pulse compression that can be obtained via propagation of $N > 1$ soliton pulses leads to uncompressed "wings" (because $\partial^2 E / \partial t^2$ is only negative over the central portion of the pulse). This energy loss can be avoided by setting up a soliton laser where the source laser itself can be forced to produce much shorter pulses at its normal average output power. The soliton laser as described by Mollenauer and Stolen, [33], consists of a mode-locked laser at $\sim 1.5\mu\text{m}$ (a colour centre laser (CCL)) coupled to an external cavity consisting of a length of single mode fibre, as shown in fig 4.18.

Fig 4.18 The Soliton Laser



The initial explanation of this effect was that the fraction of the CCL output fed into the fibre had enough peak power to be compressed via high order soliton effects. The slightly compressed pulse (as the fibre length is very much shorter than the initial soliton period) is then re-injected into the CCL cavity in synchronism with the existing mode-locked pulses, stimulating the production of narrower pulses from the laser itself, (this method of injection mode-locking is described in ref [34]). This process continues until the pulses entering and leaving the fibre have essentially the same shape, i.e. when the pulselwidth compresses to the point where the soliton period is equal to twice the fibre length.

Experimentally it was found that the laser wanted to work on the $N=2$ rather than $N=1$ soliton which, from this simple explanation, should have been a stable operating point. It was also found that it was necessary to use a servo stabilisation scheme on the return mirror to ensure that the returned pulse had the correct relative phase for stable soliton laser operation, [35]. Nevertheless the soliton laser represents a method of producing high energy ultra-short pulses whose pulse shape is well determined (sech^2) and whose pulselwidth can be altered by simply changing the length of fibre used in the external cavity. In this way pulses near to the limit set by the gain bandwidth of the CCL have been produced, [36]. It is also interesting to note that once soliton laser action has been initiated the system becomes passively mode-locked, allowing the removal of the relatively weak, main cavity, active mode-locking process, [35].

However it was soon realised that the operating conditions for the soliton laser were more complicated than has been suggested above. Further experimental work by Mitschke and Mollenauer, [35], showed that it was possible to obtain pulses for which the fibre length was considerably less than $z_0/2$, i.e. the pulses returned from the fibre were shorter than those launched into it. For a fixed fibre length they found the pulselwidth varied with the reflectivity of the

CCL output mirror, and that the shortest pulse that could be obtained corresponded to a soliton period z_0 of just greater than twice the fibre length. Thus there is always some narrowing in the fibre, which might explain why the $N=1$ operating point is never achieved.

Later theoretical and experimental work by Blow et al, [37,38], suggested that soliton formation in the external cavity was, in fact, not crucial to the successful operation of a "soliton" laser. Instead they show that shortened mode-locked pulses (if permitted by the gain bandwidth) can be produced by coupling a laser to an external cavity containing any element that has a non-linear response to the optical field. They also predict that this improvement is not limited to pulse shortening nonlinear effects, i.e. the improved mode-locking is not due to the injection of energy into modes far from the peak of the gain, but rather is due to induced coupling between the modes allowing phase information to be more efficiently communicated to the edges of the gain bandwidth. These predictions were experimentally confirmed by Kean et al, [39], who successfully demonstrated enhanced mode-locking with an external cavity containing an optical fibre with positive group velocity dispersion. They also achieved similar performance with the external cavity containing an InGaAsP semiconductor diode amplifier acting as a saturable amplifier.

Thus the soliton laser appears to be a specific case of the general effect of enhanced mode-locking via nonlinear external cavities. However, in considering whether the Yb:Er laser is suitable for a soliton laser, we will use the very simple model described earlier. It is valid to do this because, in the case of a fibre with negative group velocity dispersion, the external cavity pulse does, in practice, approximate to an $N=2$ soliton, [35]. Also, as stated earlier, the condition that $z_0/2$ is equal to the fibre length is approached under certain experimental conditions. Thus we will be able calculate whether we are within the correct power regime for soliton laser operation and roughly what fibre length is required.

Fig 4.19 shows a graph of how the peak power, P_2 , required to launch an $N=2$ soliton, and how the soliton period varies with respect to the pulsedwidth, τ (assuming $\lambda=1.54\mu\text{m}$). We can now apply the line corresponding to the peak power in the fibre, [33],

$$\hat{P} = 0.88\eta\bar{P}T / \tau \quad (4.25)$$

where \bar{P} is the Yb:Er laser average output power, η is the fraction of the power launched into the fibre, and T is the time between pulses.

In fig 4.19 we use the values corresponding to the quasi-cw version of the Yb:Er laser and take a typical value for η of 0.2. This value, and hence the slope of the line \hat{P} , can be finally adjusted through the launching microscope objective. Thus we find that the values of \hat{P} and P_2 cross at a point corresponding to a pulsedwidth, τ , of ~290fs and a fibre length, l , of ~1.06m. Similarly in fig.4.20 we find a cross-over at $\tau=7.8\text{ps}$ and $l=768\text{m}$ for the cw Yb:Er laser. However using the improved output power values that would be available with a slightly higher power pump laser (see section 4.2.4), we would predict a cross-over of $\tau=1.5\text{ps}$, $l=28.4\text{m}$.

Thus it would appear that the bulk Yb:Er laser is an ideal candidate for the setting up of a soliton laser. Unfortunately this has not, as yet, been properly tested experimentally. Some initial investigations with the quasi-cw pumped Yb:Er laser resulted in the observation of driven oscillations (~2 μs duration, 50 μs period) rather than enhanced mode-locking. However, as we have already seen in section 4.2.2, this version of the laser suffers from etalon effects which could possibly restrict any attempted pulse shortening. There may also be problems due to the fact that the cavity length will be changing during the pump pulse due to the heating of the laser rod.

One laser in which a kind of soliton laser has

Fig 4.19 Soliton Laser Operating Conditions For The
Quasi-cw Yb:Er Laser

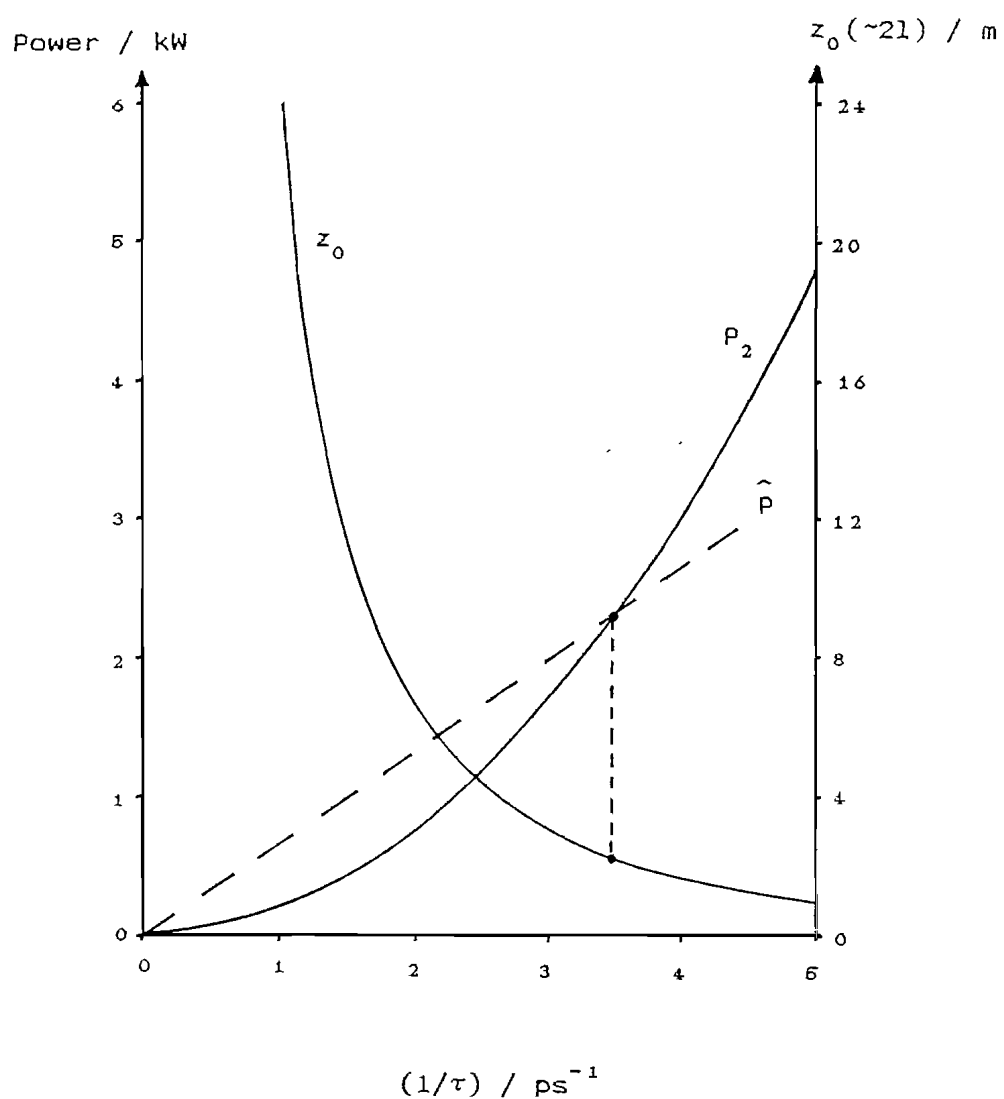
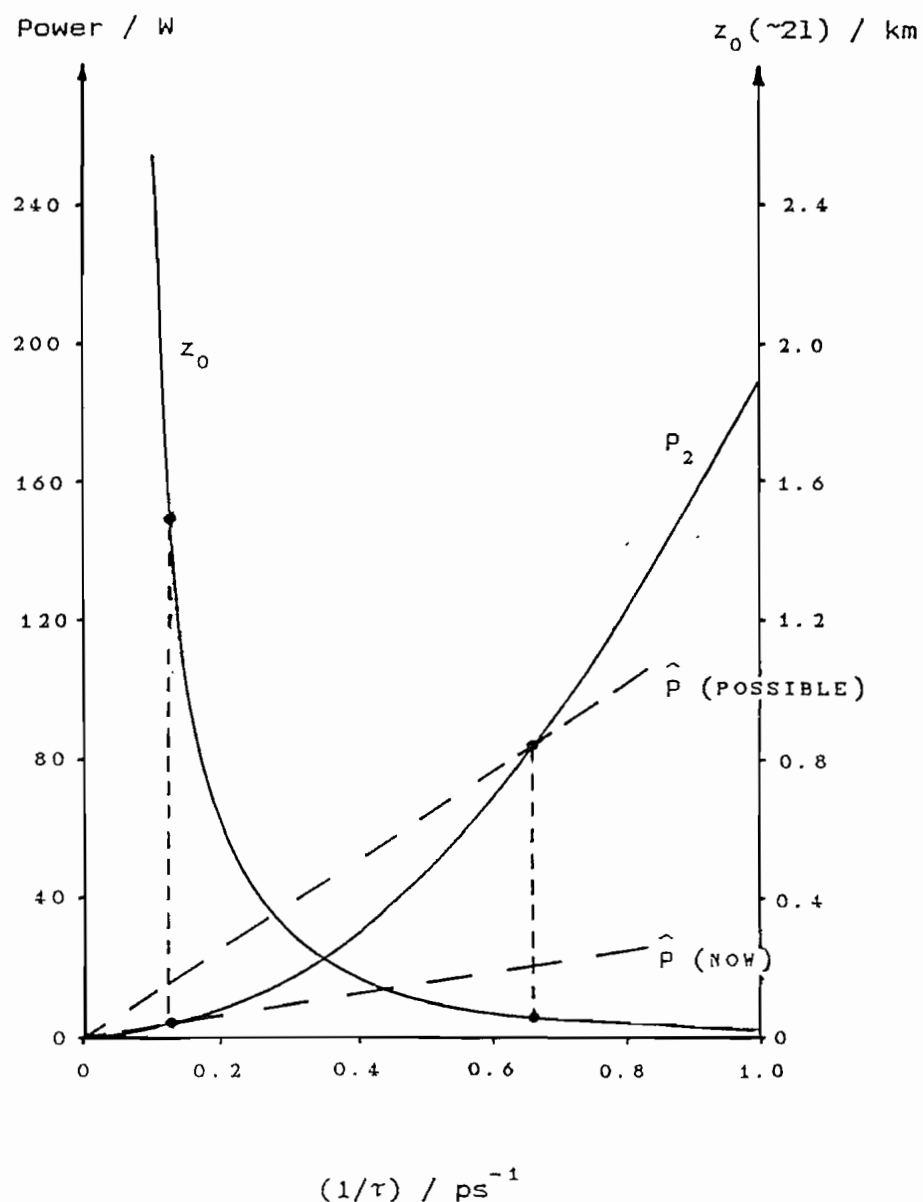


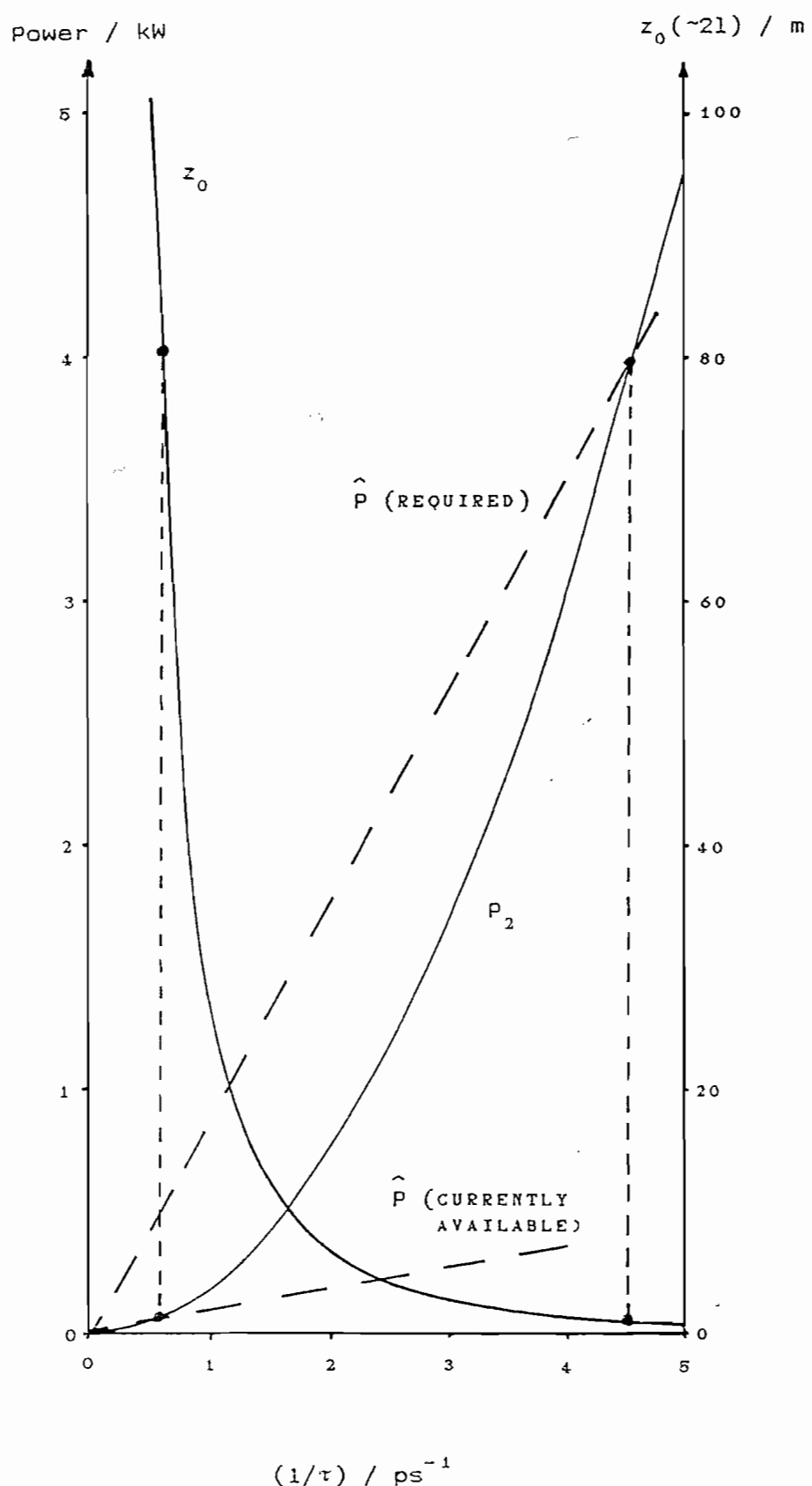
Fig 4.20 Soliton Laser Operating Conditions For The CW Yb:Er Laser



automatically been attempted is the mode-locked Yb:Er fibre laser. If we take the same simplistic reasoning as we have used above, we might expect that the pulses inside the fibre laser cavity would be continually shortened by passage through the fibre until the pulses have essentially the same shape on entering and leaving the fibre. Thus the pulses would be solitons with a period equal to twice the doped fibre length. If we again assume they are $N=2$ solitons, and remember that the operating wavelength is $1.56\mu\text{m}$, we can obtain the results shown in fig.4.21. These show that at the power levels currently available within the fibre laser cavity, we would need over 40m of fibre to achieve soliton laser action (pulsewidth $\sim 1.8\text{ps}$). Due to the limitations of matching the cavity length to the modulation frequency, we have so far only used fibre lengths of $\sim 60\text{cm}$. To achieve soliton laser action with this length (pulsewidth $\sim 220\text{fs}$) would require an over eight times increase in average power. Thus it is not surprising that we have not seen any dramatic improvement in mode-locking by going to a fibre laser configuration. However it should be noted that it may be possible to significantly increase the power available by moving away from the butted mirror configuration (see fig.4.9) which limits the safe pumping power to $\sim 300\text{mW}$. With greater pump power we would also need a longer length of fibre to avoid saturation of the pump absorption (see section 3.5). Both these considerations could combine to create conditions under which soliton laser action may be possible.

It is, of course, important to realise that we have ignored the fact that the pulse-shaping fibre is now also the gain medium. In a recent paper, [40], Haus and Silberberg have theoretically predicted a possible mode-locking enhancement of just a factor of two by the addition of a non-linear refractive index medium to a laser cavity. However it should be noted that, strictly speaking, this analysis is only for homogeneously broadened lasers. Even with this rather pessimistic prediction it is obvious that the mode-locked Yb:Er fibre laser is a very interesting system with which to experimentally investigate such intracavity mode-locking enhancement. With the use of combined

Fig 4.21 Soliton Laser Operating Conditions For The Yb:Er Fibre Laser



mode-locking and Q-switching it should also be possible to generate other non-linear effects, such as Raman scattering and Raman amplification.

4.6 Summary

We have successfully demonstrated the active mode-locking of the Yb:Er glass laser in both bulk and fibre forms, obtaining near bandwidth limited pulses of \sim 70ps FWHM duration in both cases. The suitability of these sources for soliton propagation experiments has been demonstrated obtaining compressed pulses of \sim 400fs duration, whose spectrum showed significant Raman amplification effects. However, the Yb:Er glass laser itself, with a gain bandwidth of the order of 10^{13} Hz (see appendix 8) is theoretically capable of supporting pulses down to \sim 100fs. Thus we have also considered the possibility of a soliton/non-linear external cavity laser, finding that the bulk Yb:Er glass lasers are ideal candidates for such a mode-locking enhancement scheme. At the present time the fibre laser version appears to have too little power for significant non-linear pulse-shaping to occur. However several ways of increasing the available power have been suggested, which could make the Yb:Er fibre laser a very interesting system for studying the behaviour of mode-locked lasers with internal non-linear index elements.

4.7 References

- [1] A.E.Siegman, "Lasers", University Science Books, Oxford University Press (1986)
- [2] M.DiDomenico Jr., J. Appl. Phys. 35 (1964) 2870
- [3] A.Yariv, J. Appl. Phys. 36 (1965) 388
- [4] S.E.Harris and O.P.McDuff, IEEE J. Quantum Electron. QE-1 (1965) 388
- [5] D.J.Kuizenga and A.E.Siegman, IEEE J. Quantum Electron. QE-6 (1970) 694
- [6] L.Yan, J.D.Ling, P.-T.Ho and C.H.Lee, Opt.Lett. 11 (1986) 502
- [7] L.Yan, J.D.Ling, P.-T.Ho, C.H.Lee and G.L.Burdge, IEEE J. Quantum Electron. QE-24 (1988) 418
- [8] S.Basu and R.L.Byer, Opt. Lett. 13 (1986) 458
- [9] D.J.Kuizenga, IEEE J. Quantum Electron. QE-17 (1981) 1694
- [10] M.W.Phillips, A.I.Ferguson and D.C.Hanna, Opt. Lett. 14 (1989) 219
- [11] G.Geister and R.Ulrich, Opt. Comm. 68 (1988) 187
- [12] I.N.Duling, L.Goldberg and J.F.Weller, Electr. Lett. 24 (1988) 1333
- [13] R.Ulrich, S.C.Rashleigh and W.Eickhoff, Opt. Lett. 5 (1980) 273
- [14] H.C.Lefevre, Electr. Lett. 16 (1980) 778
- [15] B.G.Koehler and J.E.Bowers, Appl. Opt. 24 (1985) 349
- [16] D.B.Patterson, A.A.Godil, G.S.Kino and B.T.Khuri-Yakub, Opt.Lett. 14 (1989) 248
- [17] M.W.Phillips, A.I.Ferguson, G.S.Kino and D.B.Patterson, submitted to Opt. Lett. (1989)
- [18] R.H.Stolen and C.Lin, Phys. Rev. A 17 (1978) 1448
- [19] H.A.Haus, "Waves And Fields In Optoelectronics", Series In Solid State Physical Electronics, Prentice Hall (1984)

[20] A.Hasegawa and F.Tappert, *Appl. Phys. Lett.* 23 (1973) 142

[21] V.E.Zakharov and A.B.Shabat, *Sov. Phys. JETP* 34 (1972) 62

[22] J.Satsuma and N.Yajima, *Prog. Theor. Phys. Supp.* 55 (1974) 284

[23] L.F.Mollenauer, R.H.Stolen and J.P.Gordon, *Phys. Rev. Lett.* 45 (1980) 1095

[24] L.F.Mollenauer, R.H.Stolen, J.P.Gordon and W.J.Tomlinson, *Opt. Lett.* 8 (1983) 289

[25] K.J.Blow and N.J.Doran, *IEE Proc. Pt.J.* 134 (1987) 138

[26] R.H.Stolen, L.F.Mollenauer and W.J.Tomlinson, *Opt. Lett.* 8 (1983) 186

[27] E.M.Dianov, A.Ya.Karasik, P.V.Mamyshev, A.M.Prokhorov, V.N.Serkin, M.F.Stel'makh and A.A.Fomichev, *JETP Lett.* 41 (1985) 295

[28] R.H.Stolen, C.Lee and R.K.Jain, *J. Opt. Soc. Am. B* 1 (1984) 652

[29] F.M.Mitschke and L.F.Mollenauer, *Opt. Lett.* 11 (1986) 659

[30] J.P.Gordon, *Opt. Lett.* 11 (1986) 662

[31] P.Beaud, W.Hodel, B.Zysset and H.P.Weber, *IEEE J. Quantum Electron.* QE-23 (1987) 1938

[32] A.B.Grudinin, E.M.Dianov, D.V.Korobkin, A.M.Prokhorov, V.N.Serkin and D.V.Khaidarov, *JETP Lett.* 45 (1987) 260

[33] L.F.Mollenauer and R.H.Stolen, *Opt. Lett.* 9 (1984) 13

[34] P.A.Belanger, *J. Opt. Soc. Am. B* 5 (1988) 793

[35] F.M.Mitschke and L.F.Mollenauer, *IEEE J. Quantum Electron.* QE-22 (1986) 2242

[36] F.M.Mitschke and L.F.Mollenauer, *Opt. Lett.* 12 (1987) 407

[37] K.J.Blow and D.Wood, *J. Opt. Soc. Am. B* 5 (1988) 629

[38] K.J.Blow and B.P.Nelson, *Opt. Lett.* 13 (1988) 1026

- [39] P.N.Kean, X.Zhu, D.W.Crust, R.S.Grant, N.Langford and W.Sibbett, Opt. Lett. 14 (1989) 39
- [40] H.A.Haus and Y.Silberberg, IEEE J. Quantum Electron. QE-22 (1986) 325

5. Concluding Remarks

5.1 Summary Of Results Achieved

In chapter two we described the successful achievement of low threshold operation of a capillary waveguide CH_4 Raman laser at $1.544\mu\text{m}$. Table 1 summarises the results obtained,

Table 5.1

	Unguided	Single Pass, Guided	Synchronously Pumped, Guided
Predicted Peak Power Threshold	2.5MW	200kW	60kW
Experimental Peak Power Threshold	-	190kW	50kW
Output Pulse Duration	-	100ps	100ps
Output Peak Power	-	66kW	12kW

These results clearly show the advantage of going to a guided configuration. The experimental thresholds agree very well with theoretical predictions and are now easily within reach of a cw pumped Nd:YAG laser (typical peak mode-locked and Q-switched powers $\sim 0.5\text{MW}$) which should have allowed high repetition rate operation. However an unforeseen problem involving breakdown of the CH_4 gas limited operation to a 5Hz repetition rate. Although this source has enough power to launch extremely high order solitons it has some practical drawbacks which led us to find a more versatile alternative. The main disadvantage being that the output train consists of pulses of varying peak powers which would thus all undergo different amounts of pulse compression, leading to a

confused autocorrelation picture (as this would be some average of all these pulses). Nevertheless the fact that such low thresholds were achieved could make this system generally attractive as a method of frequency conversion of short pulses.

In chapters three and four we have described the operation of a Nd:YAG pumped Yb:Er phosphate glass laser at $1.54\mu\text{m}$. This laser can be operated pulsed or cw, Q-switched and/or mode-locked, in bulk or fibre form. The results obtained to date are summarised in table 5.2.

Table 5.2

	7.5cm Long Rod , Quasi-cw Pumped	2cm Long Rod , cw Pumped	Fibre Laser
Threshold	4.5W	500mW	12mW
Absorbed Power	(HR mirrors)	(HR mirrors)	(10% output)
Mode-locked			
Pulsewidth	70ps	70ps	70ps
Mode-locked	50W	2W	90mW
Output Peak Power	(20kW when mode- locked and Q- switched)		
Q-Switched Performance	10kW Peak Power 60ns duration 5Hz Rep. Rate	25W Peak Power 750ns duration 125Hz Rep Rate (Using a mechanical chopper)	-

Thus some of the most interesting points we have been able to demonstrate are,

- i) The first pumping of an Yb:Er glass laser by the widely available $1.064\mu\text{m}$ Nd:YAG laser.

- ii) The first active mode-locking of an Yb:Er glass laser.
- iii) The efficient cw and cw, mode-locked operation of a bulk 3-level glass laser.
- iv) The efficient operation of a co-doped fibre laser.

This versatile source is thought to match the necessary requirements for a research tool with which to investigate the non-linear propagation of pulses in the negative group velocity dispersion regime of silica optical fibres. As a demonstration of this capability we have launched the pulses from the quasi-cw mode-locked bulk Yb:Er glass laser into a 1km length of single mode fibre. A very large single stage pulse compression factor of 160 was obtained leading to pulse durations of ~400fs. The corresponding frequency spectrum indicated the onset of soliton self frequency shift effects due to the fibre Raman gain.

5.2 Proposed Further Developments

It is clear that many of the figures given in table 5.2 are preliminary results taken to show the Yb:Er laser's capability, and could certainly be improved upon. Some of the most interesting possibilities are given below,

- i) We have shown (section 4.2.4) that the power available from the bulk cw Yb:Er laser would be greatly improved if a slightly more powerful cw pump laser was available.
- ii) With the very large gain bandwidth available it should be possible to improve the mode-locked performance obtained so far. Eliminating the observed unwanted etalon effects should allow the production of pulses of similar duration to those found with Nd doped glass lasers (~10ps), using standard active mode-locking techniques. We have also considered the possibility of using a non-linear external cavity to enhance the mode-locked performance and have shown the Yb:Er laser to be a good candidate for such operation.

iii) The power available in the mode-locked Yb:Er fibre laser could also be greatly enhanced by using an alternative pumping scheme where the fibre is no longer butted to the pump input mirror, allowing the use of higher pump powers. Alternatively the use of a modulator applied directly to the fibre would allow the butting of mirrors to both ends of the fibre giving a very low loss (and very compact) cavity. Thus this would also lead to an increase in available output power. With such improvements would also come an increase in the power circulating in the laser cavity which could lead to significant non-linear pulse shaping by the fibre itself, as discussed in section 4.5.

The use of the sources we have already obtained in order to study non-linear propagation in optical fibres has been demonstrated. We have also suggested that launching the pulses obtained into another length of dispersion shifted fibre would allow the careful study of lower order soliton propagation in the sub-picosecond regime, leading to pulses as short as ~50fs.

Low-threshold operation of a waveguide CH_4 Raman laser at $1.54 \mu\text{m}$

D.P. Shepherd
D.C. Hanna
S.G. Mussett
M.T.T. Pacheco

Indexing terms: Optical waveguides, Lasers, Nonlinear optics

Abstract: A convenient source of high-power ($\sim 20 \text{ kW}$) stable mode-locked pulses at $1.54 \mu\text{m}$, suitable for pulse-compression studies in the negative group-velocity-dispersion region of optical fibres, is described. The source is based on a capillary-waveguide Raman laser, using CH_4 gas, and pumped by a mode-locked Q -switched CW Nd:YAG laser. Initial results for a synchronously pumped Raman laser are also presented.

1 Introduction

The spectral region around $1.5 \mu\text{m}$ is of particular interest in optical communications since fused-silica fibres have very low loss in this region. The negative group-velocity dispersion in this region is also of interest since it offers the possibility of soliton pulse propagation. There are few sources of mode-locked pulses of sufficient power to induce nonlinear propagation effects in this $1.5 \mu\text{m}$ region, and studies of soliton behaviour have so far relied on colour-centre lasers [1, 2]. In this paper we report the development of a rather simple source of high-power mode-locked pulses at $1.54 \mu\text{m}$ which should prove suitable for studies of nonlinear propagation behaviour.

The source is based on stimulated Raman scattering (SRS) in CH_4 gas, pumped by the $1.06 \mu\text{m}$ output from a mode-locked Q -switched continuously pumped Nd:YAG laser (Spectra Physics 3000). To reduce the threshold to a level that could be reached by the output from such a CW pumped laser, the CH_4 gas was contained in a capillary waveguide, thus providing guidance for both the pump and Stokes waves [3-7]. Working at a CH_4 gas pressure of 7 MPa (70 atmospheres), the threshold pump power was measured to be $\sim 200 \text{ kW}$; an order of magnitude reduction in threshold compared with an unguided geometry, and more than a factor of two lower than the available output power from the pump laser. Peak power of the generated $1.54 \mu\text{m}$ pulses was $\sim 20 \text{ kW}$ with amplitude stability equal to that of the pump laser. The output beam was diffraction limited. Since this type of Nd:YAG laser is widely used in optical-communications research laboratories and since

Paper 5353J (E13), first received 23rd October 1986 and in revised form 18th March 1987

D.P. Shepherd, D.C. Hanna and S.G. Mussett are, and M.T.T. Pacheco was formerly, with the Department of Physics, The University, Southampton SO9 5NH, United Kingdom. M.T.T. Pacheco is now with Centro Técnico Aeroespacial, Instituto De Estudos Avançados, Radovia Dos Tamoios, K.M. 5.5 12200-São José dos Campos-SP, Brazil

operation is in principle possible up to $\sim 1 \text{ kHz}$, this Raman laser provides a potentially attractive and simple source.

2 Background

Under plane-wave pumping conditions the steady-state power gain for the scattered Stokes wave, of frequency ω_s , is $\exp G$, where $G = g_R I_p l$. Here I_p is the pump intensity, l is the length of medium and g_R , the Raman gain coefficient, is given by [8]

$$g_R = \frac{16\pi^2 c^2 \Delta N}{n_s^2 \hbar \omega_s^3 \Delta \omega_R} \left(\frac{d\sigma}{d\Omega} \right) \quad (1)$$

Here ΔN is the difference in population density between the initial and final levels (in this case simply the number density of CH_4 molecules), $\Delta \omega_R$ is the Raman linewidth and $(d\sigma/d\Omega)$ is the Raman-scattering cross-section. For CH_4 it has been shown that the linewidth $\Delta \omega_R$ is given by [9]

$$\Delta \omega_R = \pi c (64 + 2.4 P) \quad (2)$$

where P is the pressure in atmospheres. The Raman cross-section $(d\sigma/d\Omega)$ is here defined in terms of the ratio of scattered to incident intensity as in Reference 3. The threshold for stimulated Raman scattering is reached when $G_{th} = 25$. From eqn. 1 and the relation $G = g_R I_p l$, the threshold pump intensity can be calculated. In practice, two further modifications to the analysis are needed, to account for the nonuniform intensity within the pump beam and the transient character of the Raman scattering when the pump pulse durations are comparable to the inverse of the Raman linewidth. With these modifications the threshold pump power, for an unguided beam focused at the centre of a Raman medium of length l to give a confocal parameter b , is given by Reference 3:

$$P_{th} = \frac{F \lambda_t}{4 g_R} \left[1 + \left(1 - \frac{G_{th} \lambda_p}{\lambda_t \tan^{-1}(l/b)} \right)^{1.2} \right]^2 \quad (3)$$

The numerical factor F accounts for the transient behaviour, and the procedure for calculating F is given in Reference 3. Using eqn. 3, it is found that the predicted threshold pump intensity, for a $1.06 \mu\text{m}$ pump of $\sim 100 \text{ ps}$ duration generating $1.54 \mu\text{m}$ 1st Stokes radiation in CH_4 gas at $\sim 7 \text{ MPa}$, is $\sim 2 \text{ MW}$, in good agreement with experimental results [3]. This is significantly greater than the 0.5 MW peak power available from a typical CW pumped Nd:YAG laser. The necessary reduction in threshold can however be achieved by an appropriate choice of capillary waveguide [4, 5].

The capillary used in this work was a thin-walled capillary made of fused silica, with a bore diameter of $2a = 180 \mu\text{m}$. To support the capillary and hold it straight, it was fitted inside another glass capillary of large outside diameter ($\sim 6 \text{ mm}$) and then placed inside a high-pressure cell. The end windows of the pressure cell were of fused silica, $\sim 12 \text{ mm}$ thick, allowing operation up to CH_4 gas pressures of 7 MPa.

The pump laser provided an output energy of $\sim 1.4 \text{ mJ}$ in a Q -switched envelope of $\sim 200 \text{ ns}$ duration. Within this envelope the mode-locked pulses had a repetition rate of 82 MHz. The duration of these pulses was measured, see Fig. 1, using a background-free second-

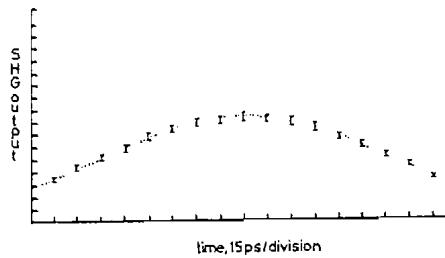


Fig. 1 Pump-pulse autocorrelation
FWHM = $150 \pm 1 \text{ ps}$

harmonic autocorrelation technique, and found to be $\sim 150 \text{ ps}$ (assuming a Gaussian temporal profile), thus implying a peak power of 0.5 MW in the most energetic pulses. This autocorrelation was performed over the full Q -switched pulse envelope, and so represents an average pulse duration. Measurements on a single pulse in the train were not made. The output was in the form of a clean TEM_{00} mode. This is important for efficient launching into the EH_{11} mode of the capillary. The beam was focused to a waist of spot size $w_0 = 60 \mu\text{m}$ at the capillary entrance, thus satisfying the launch condition [10].

$$3w_0 = 2a \quad (4)$$

The theoretical transmission T of the capillary for the EH_{11} mode is given by [11]

$$T = \exp(-\alpha_s l) \quad (5)$$

where $\alpha_s = 0.43\lambda_p^2/a^3$ is the pump attenuation coefficient. For Raman scattering in the capillary waveguide of length l the power gain exponent G is given by [3]

$$G = g_R l_p l_{eff} - \alpha_s l \quad (6)$$

where α_s is the Stokes attenuation coefficient and the 'effective length' l_{eff} is given by [3]

$$l_{eff} = (1 - T)\alpha_s l \quad (7)$$

The threshold pump power P_{th} for SRS is therefore

$$P_{th} = F A_{eff} (G + \alpha_s l) / g_R l_{eff} \quad (8)$$

where, following Reference 5, $A_{eff} = \pi w_0^2$.

The capillary waveguide allows a small threshold to be achieved by virtue of the fact that even if A_{eff} is made small, l_{eff} can be kept significantly longer than the effective length of approximately one confocal parameter ($\equiv 2\pi w_0^2/\lambda$) that would apply for unguided conditions.

3 Experimental results

A capillary transmission of 38% was achieved in practice for the $1.06 \mu\text{m}$ pump, to be compared with a calculated

theoretical transmission of 58%. The discrepancy was probably due to slight bending of the capillary [4] and imperfect launching, although care was taken to ensure the capillary ends were cleaved cleanly. The remaining transmitted pump beam was in the form of a clean circular spot of diffraction-limited divergence. The predicted threshold for SRS, $\sim 160 \text{ kW}$, was in good agreement with the experimentally observed value of 205 kW. Fig. 2a shows the undepleted pump pulse train observed at

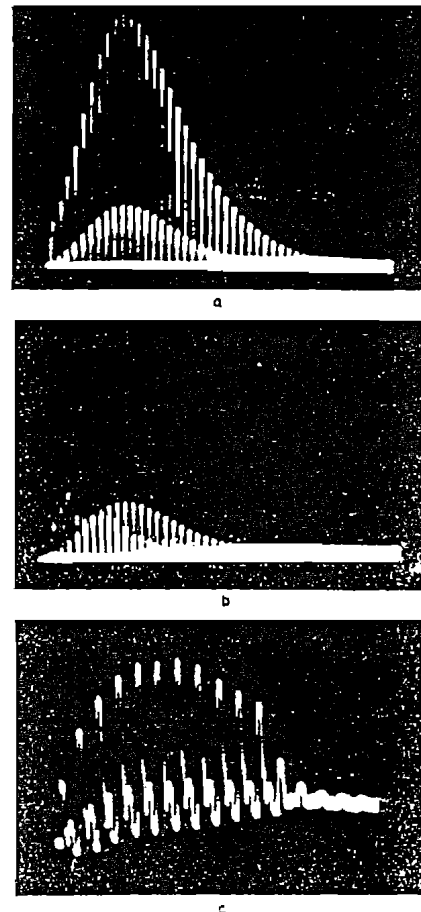


Fig. 2 Pulse trains
a Undepleted pump transmitted by capillary. The smaller, interleaved pulses are due to pump light launched into the capillary walls. Mode-locked pulse separation is 12.2 ns
b Strong depletion of transmitted pump when operating at 2.5 times threshold power. The original interleaved pulses have the same intensity as in Fig. 2a
c Train of 1st Stokes pulses at $1.54 \mu\text{m}$

the capillary output when the pump intensity was below the SRS threshold. The smaller interleaved train of pulses is due to pump light travelling through the walls of the capillary rather than down the bore and hence is delayed by $\sim 1 \text{ ns}$. Fig. 2b shows the heavily depleted pump pulse train when the maximum available pump power was used (~ 2.5 times the threshold). The pulses travelling through the capillary walls are unchanged in intensity (they enter the wall at the launch) and provide a useful reference to quantify the pump depletion. They are also useful for achieving optimum alignment by adjusting the capillary so that their intensity is minimised. Fig. 2c

shows the corresponding $1.54\text{ }\mu\text{m}$ output pulses. These displayed excellent amplitude stability, with amplitude variations being no greater than those of the pump pulse itself. The DC level on the tail of these pulses is an artefact of the recording process. Second-harmonic autocorrelation measurement of the Stokes pulse duration gave a value of 130 ps (assuming Gaussian shape) for a 150 ps input pump pulse, see Fig. 3. A bandwidth measurement

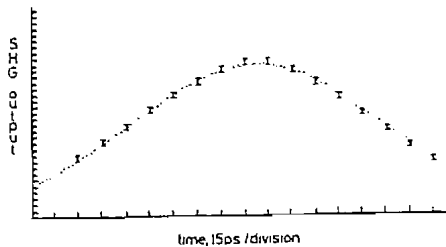


Fig. 3 Raman pulse autocorrelation
FWHM = 133 ± 1 ps

of the generated Stokes radiation gave an upper limit of 5.5 GHz, although this was instrument limited owing to the low finesse of the spectrum analyser used. The pulses are therefore close to being bandwidth limited (within a factor of ~ 2). Peak output pulse energies of $\sim 3\text{ }\mu\text{J}$ were observed implying peak output powers of $\sim 20\text{ kW}$.

Although the Q -switched repetition rate can go up to $\sim 1\text{ kHz}$, all the measurements reported here have been carried out at 5 Hz. Initial measurements at the 1 kHz rate revealed a gas breakdown behaviour leading to a deposit of 'soot' on the inside surface of the window where the pump beam entered and also at the capillary entrance. The cause of this breakdown is not yet understood. It appears to depend on the average power of the pump and not the peak power. The maximum safe operating rate has not been established, although in view of the dependence on average power it is expected that if a single pulse switchout were used to take one pulse from each Q -switched envelope, repetition rates of several hundred hertz would be free from breakdown.

The single-pass Raman-scattering scheme described above has given threshold pump powers of 200 kW. A further reduction of threshold is possible by operating the Raman laser as a synchronously pumped oscillator. This involves feeding back the Stokes radiation to arrive at the entrance of the capillary in synchronism with the next pump pulse in the mode-locked train. We have used a ring configuration to achieve this. In this way the threshold pump power has been reduced to 54 kW, in good agreement with the predicted value of 40 kW, and thus almost an order of magnitude lower than the available

pump power from our laser. This arrangement gave a stable 1st Stokes output, but at a lower peak power ($\sim 3\text{ kW}$) than the single-pass scheme. Further details of the operation of this synchronously pumped Raman oscillator are to be given in a further publication.

4 Conclusion

We have demonstrated a simple high-power source of mode-locked pulses at $1.54\text{ }\mu\text{m}$. The good amplitude stability, diffraction-limited beam quality and high power make these pulses particularly interesting for studies of pulse-compression phenomena in fibres under conditions of very high soliton number.

5 Acknowledgments

This work has been supported by the SERC under the Joint Optoelectronics Research Scheme. One of us (D.P.S.) wishes to acknowledge SERC and British Telecom for support in the form of a CASE studentship. We are grateful to Dr. A.I. Ferguson for a number of useful discussions.

6 References

- 1 MOLLENNAUER, L.F., STOLEN, R.H., and GORDEN, J.P.: 'Experimental observation of picosecond pulse narrowing and solitons in optical fibres', *Phys. Rev. Lett.*, 1980, 45, pp. 1095-1098
- 2 MOLLENNAUER, L.F., STOLEN, R.H., GORDEN, J.P., and TOMLINSON, W.J.: 'Extreme picosecond pulse narrowing by means of soliton effect in single-mode optical fibres', *Opt. Lett.*, 1983, 8, pp. 289-291
- 3 HANNA, D.C., POINTER, D.J., and PRATT, D.J.: 'Stimulated Raman scattering of picosecond light pulses in hydrogen, deuterium, and methane', *IEEE J. Quantum Electron.*, 1986, QE-22, pp. 332-336
- 4 BERRY, A.J., HANNA, D.C., and HEARN, D.B.: 'Low threshold operation of a waveguide H_2 Raman laser', *Opt. Commun.*, 1982, 43, pp. 229-232
- 5 BERRY, A.J., and HANNA, D.C.: 'Stimulated Raman oscillation in capillary waveguide resonators', *Opt. Commun.*, 1983, 45, pp. 357-360
- 6 RABINOWITZ, P., KALDOR, A., BRICKMAN, R., and SCHMIDT, W.: 'Waveguide H_2 Raman laser', *Appl. Opt.*, 1976, 15, pp. 2005-2006
- 7 HARTIG, W., and SCHMIDT, W.: 'A broadly tunable IR waveguide Raman laser pumped by a dye laser', *Appl. Phys.*, 1979, 18, pp. 235-241
- 8 MAIER, M.: 'Applications of stimulated Raman scattering', *Appl. Phys.*, 1976, 11, pp. 209-231
- 9 TAIKA, Y., IDE, K., and TAKUMA, H.: 'Accurate measurement of the pressure broadening of the v_1 Raman line of CH_4 in the 1-50 atm region by inverse Raman spectroscopy', *Chem. Phys. Lett.*, 1982, 91, pp. 299-302
- 10 ABRAMS, R.L.: 'Coupling lasers in hollow waveguide laser resonators', *IEEE J. Quantum Electron.*, 1972, QE-8, pp. 838-843
- 11 MARCATILI, E.A.J., and SCHMELTZER, R.A.: 'Hollow metallic and dielectric waveguides for long distance optical transmission and lasers', *Bell Syst. Tech. J.*, 1964, 43, pp. 1783-1809

A SYNCHRONOUSLY PUMPED WAVEGUIDE CH₄ RAMAN LASER AT 1.54 μmD.C. HANNA, S.G. MUSSETT ¹, M.T.T. PACHECO ² and D.P. SHEPHERD*Department of Physics, University of Southampton, Southampton SO9 SNH, UK*

Received 2 October 1987; revised manuscript received 20 November 1987

The threshold for stimulated Raman scattering (SRS) in CH₄ gas with a 1.06 μm pump has been reduced to only ~50 kW using an arrangement involving synchronous pumping and confinement in a capillary waveguide. This corresponds to a threshold reduction of ~50 compared to an unguided, single pass device. This Raman laser has produced stable mode-locked 1.54 μm pulses of ~12 kW power and pulse duration ~100 ps.

1. Introduction

The use of a capillary waveguide to reduce the threshold of stimulated Raman scattering in gases has been the subject of a number of publications [1-5]. In particular it has been shown that stimulated Raman scattering in CH₄ gas can be achieved with the output power available from a continuously pumped Nd:YAG laser, when Q-switched and mode-locked [6]. In this paper we describe a synchronously pumped waveguide Raman laser in CH₄ gas where the introduction of synchronous pumping has led to a further factor of four reduction of threshold. The overall reduction of threshold compared with a single pass unguided arrangement is ~50, and the threshold power requirement for a 1.06 μm pump is now ~50 kW. Agreement between predicted and observed threshold is good. Output pulses of ~12 kW and 100 ps are obtained at the 1.54 μm 1st Stokes wavelength.

2. Background

Following ref. [6], the stimulated Raman threshold power P_{th} for a single pass arrangement in a capillary waveguide of length l is

$$P_{th} + FA_{eff}(G_{th} + \alpha_s l)/g_R l_{eff}, \quad (1)$$

where α_s , α_p are the Stokes and pump attenuation coefficients respectively, the effective length $l_{eff} = [1 - \exp(-\alpha_p l)]/\alpha_s$, and the effective area $A_{eff} = \pi W_0^2$ where W_0 is the spot size of the EH₁₁ mode. G_{th} is the gain exponent needed to reach threshold, usually taken to be $G_{th}=25$. F is a factor which takes account of the increase in threshold relative to the steady state value, due to the transience of the medium response. The value of F as a function of the ratio of pump pulse duration to the medium T_2 is given in ref. [5]. g_R is the Raman gain coefficient [7,6].

Expression (1) for the single-pass case can be readily extended to the synchronously pumped case by noting that the net gain of Stokes power after n round trips is

$$P_{st}/P_{s0} = (R)^{n-1} \times \exp\left((g_R l_{eff}/F A_{eff}) \sum_{i=1}^n P_{pi} - n\alpha_s l\right), \quad (2)$$

where P_{pi} is the pump in the i th pulse of the pump train and R is the fraction of Stokes power fed back into the capillary entrance as a result of mirror and launching losses. The threshold power is expressed as the value reached by P_{st} at the peak of the pump train envelope, where $P_{st}/P_{s0} = \exp(G_{th})$.

¹ Now at Pirelli General PLC, Western Esplanade, Southampton, UK.

² Now at Centro Técnico Aeroespacial, Instituto De Estudo Avançados, Rodovia Dos Tamoios, KM 5.5, 12200 São José dos Campos, SP-Brasil.

3. Experimental arrangement

The pump laser was a continuously pumped Nd:YAG laser (Spectra Physics 3000), operating at 1.06 μm and producing a $\sim 1.6 \text{ mJ}$ Q-switched mode-locked train of 200 ns (fwhm), with mode-locked pulse duration measured to be 120 ps. The peak pulse power was thus calculated to be $\sim 700 \text{ kW}$. The Raman cell consisted of a fused silica capillary of bore diameter $2a = 200 \mu\text{m}$ and length 75 cm, supported and held straight inside another capillary, which in turn was held inside a pressure cell with fused silica windows. Operating pressures up to 70 atm of CH_4 were used. High pressures are advantageous in reducing the threshold since this result in a shorter T_2 and hence a smaller factor F . At 70 atm, with 120 ps pump pulses, F is estimated to be ~ 1.4 [5]. It should be noted that with the short T_2 , $\sim 9 \text{ ps}$ at 70 atm, the vibrational excitation of the medium decays virtually completely between pump pulses ($\sim 12 \text{ ns}$ separation).

The TEM_{∞} pump beam was launched into the capillary with a waist spot size at the guide input chosen to satisfy $3W_0 = 2a$ [8]. The theoretical transmission T of the capillary guide for the EH_{11} mode is given by [9]

$$T = \exp(-\alpha_p l), \quad (3)$$

where $\alpha_p = 0.43 \lambda_p^2/a^3$. In practice we achieve a measured transmission of 57%, compared to the theoretical value of 70%. Slight bending of the capillary and/or imperfect launch may have accounted for the slight discrepancy. In calculation of threshold we have used an empirical α_p value which, when substituted in eq. (3) gives the observed transmission. The transmitted pump beam was in the form of a clean circular spot of diffraction-limited divergence.

Results obtained for the single pass arrangement gave a threshold of $\sim 190 \text{ kW}$, in excellent agreement with the theoretical value from eq. (1). Fig. 1(a) shows a typical depleted pump pulse observed at the capillary output and fig. 1(b) shows the corresponding 1st Stokes 1.54 μm output pulses. The Stokes output has good amplitude stability, similar to that of the pump, when the Raman medium is pumped well above threshold. Energy measurements indicated that single mode-locked pulse energies of $\sim 7 \mu\text{J}$ were generated.

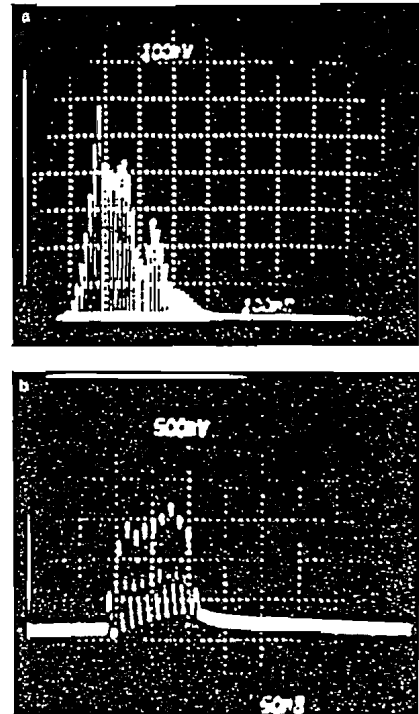


Fig. 1. (a) Depleted pump pulse for single pass Raman laser. (100 ns/division). (b) 1st Stokes 1.54 μm output pulses. (50 ns/division).

The single pass arrangement was then modified to the synchronously pumped arrangement shown in fig. 2. The 1st Stokes pulses were fed back to the capillary entrance via the prisms P_1 , P_3 , P_4 and the beam-

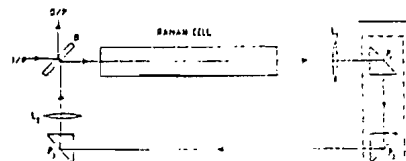


Fig. 2. The synchronously pumped Raman laser resonator with beam splitter (B), lenses (L_1 , L_2) and prisms (P_1 , P_3 , P_4). The pump input is denoted by I/P and the Raman output by O/P.

splitter B. The ability to achieve single pass operation with the feedback loop misaligned proved a considerable help in setting up the synchronous pumping. Lenses L_1 and L_2 were used respectively to collimate and focus the Stokes beam for relaunch, again taking $3W_0 = 2a$ as the launch condition. Fine control of the cavity length, to achieve synchronism, was achieved with a micrometer adjustment on the common mounting of prisms P_1 , P_2 . When correctly adjusted the observed threshold was found to be ~ 50 kW, a factor of four less than for the single pass arrangement, and in fair agreement with the value of 58 kW predicted via eq. (2). At threshold the largest Stokes pulse occurs after the peak of the pump envelope, as predicted by eq. (2).

The effect that Stokes feedback has on pump depletion is shown in fig. 3(a) and 3(b). Fig. 3(a) shows the transmitted pump when just above the single pass threshold and with the feedback blocked, while fig. 3(b) shows the heavily depleted transmitted pump when, under the same pump conditions, the feedback is restored. Fig. 4 shows the train of 1st Stokes pulses for an input pump power of 310 kW. The pulses show good amplitude stability, as good as that of the pump pulse, and a measurement of pulse energy indicated $\sim 1.3 \mu\text{J}$ in each mode-locked pulse. The mode selection of the waveguide and feedback resonator ensure diffraction limited output. The pulselwidth, averaged over the whole output pulse train, was measured by a background free second harmonic autocorrelation measurement using a LiIO_3 doubling crystal. Pulse duration, assuming a gaussian temporal shape, was found to be ~ 100 ps, see fig. 5, implying peak powers of ~ 12 kW.

Anti-Stokes radiation ($\lambda = 812$ nm) was also observed in the output, but 2nd Stokes radiation at $\lambda = 2.8 \mu\text{m}$ was not detected, despite it probably being generated in significant amounts, as the 12 mm thick fused silica windows had a very low transmission at that wavelength.

Two features of the Stokes behaviour are as yet unexplained. One is the fact that typically a maximum of ~ 10 pulses are observed in the Stokes output train, whereas a simultaneous observation of pump depletion indicates that ~ 20 or more pump pulses are strongly depleted. This is seen by comparing figs. 3(a) and (b), which were taken under identical pump conditions, and differing only in that

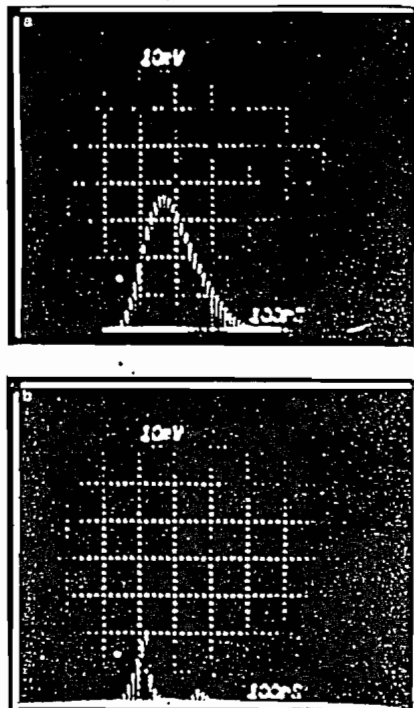


Fig. 3. (a) Transmitted pump pulse with feedback blocked. (b) Heavily depleted pump pulse with feedback operating.

fig. 3(a) corresponds to the feedback being blocked. After the first 6 or 7 pump pulses, all remaining pulses are heavily depleted, many to the base line, and even the late pulses in fig. 3(b) are depleted to below the 20% level. It appears that the Stokes output corresponds to the initial part of the pump depletion. A second observation, found in single pass operation, is that depletion of the pump train is not symmetric about the envelope peak (fig. 1(a)), as one might have expected since pump pulses of the same power would be expected to produce the same behaviour.

A final comment is on a practical but important aspect of this source. We have found that when operating at higher repetition rates (the pump laser is capable of 1 kHz or more) the CH_4 gas rapidly undergoes decomposition, leading to a deposit of soot

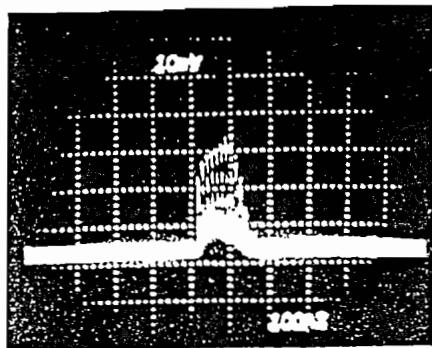


Fig. 4. 1st Stokes $1.54 \mu\text{m}$ output pulses for synchronously pumped Raman laser.

on the inside of the cell entrance window and at the entrance of the capillary guide. We have therefore confined our measurements to a repetition rate of 5 Hz, where operation over periods of many weeks is possible without such decomposition occurring. The underlying cause of this decomposition is not yet understood.

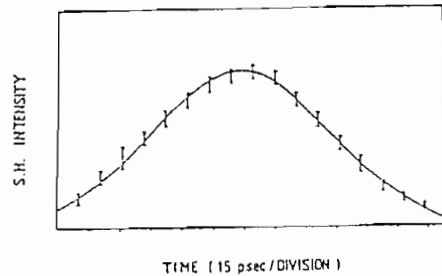


Fig. 5. Second harmonic autocorrelation measurement of pulse duration. FWHM = $104 \pm 1 \text{ ps}$.

4. Summary

We have demonstrated that very low threshold operation of a CH_4 Raman laser at $1.54 \mu\text{m}$ can be achieved by the combination of capillary waveguiding and synchronous pumping. Similar techniques should work successfully with a number of gases. The particular source based of CH_4 provides output at a wavelength, and in a form, which would be suitable for nonlinear propagation studies and measurements in the negative group velocity dispersion region of fused silica fibre.

Acknowledgements

This work has been supported by the SERC under the Joint Optoelectronics Research Scheme. D.P.S. wishes to acknowledge SERC and BTRL for support in the form of a Case studentship. We are grateful to Dr. A.I. Ferguson for a number of useful discussions.

References

- [1] P. Rabinowitz, A. Kaldor, R. Brickman and W. Schmidt, *Appl. Optics* 15 (1976) 2005.
- [2] W. Hartig and W. Schmidt, *Appl. Phys.* 18 (1979) 235.
- [3] A.J. Berry, D.C. Hanna and D.B. Hearn, *Optics Comm.* 45 (1982) 229.
- [4] A.J. Berry and D.C. Hanna, *Optics Comm.* 45 (1983) 357.
- [5] D.C. Hanna, D.J. Pointer and D.J. Pratt, *IEEE J. Quant. Electron.* QE-22 (1986) 332.
- [6] D.P. Shepherd, D.C. Hanna, S.G. Mussett and M.T.T. Pacheco, *IEEE Proc. J.* 134 (1987) 187.
- [7] M. Maier, *Appl. Phys.* 11 (1976) 209.
- [8] R.L. Abrams, *IEEE J. Quant. Electron.* QE-8 (1972) 338.
- [9] E.A.J. Marcatili and R.E. Schmelzer, *Bell Syst. Tech. J.* 43 (1964) 1783.

A 1.54 μm Er GLASS LASER PUMPED BY A 1.064 μm Nd:YAG LASER

D.C. HANNA, A. KAZER and D.P. SHEPHERD

Department of Physics, University of Southampton, Highfield, Southampton SO9 5NH, UK

Received 20 May 1987

Laser oscillation in Er-glass, co-doped with Yb sensitiser, has been achieved by pumping with the 1.064 μm output of a Nd:YAG laser.

1. Introduction

The current interest in optical communication systems operating around 1.5 μm has generated a requirement for coherent sources in this spectral region. Given the variety of measurements and investigations to which such sources would be applied, there is a need for a convenient versatile source, capable of operating cw, pulsed, mode-locked and Q-switched. With such a source in mind, we have looked at the possibilities of an Er glass laser pumped by a Nd:YAG laser. In this paper we report the preliminary results of lasing at 1.54 μm from a commercially available Er glass rod pumped by a pulsed Nd:YAG laser. The performance data indicate that cw lasing using a cw Nd:YAG laser should also be possible, and that a fibre laser based on this same glass should have a very low threshold, compatible with pumping by a diode-pumped miniature Nd:YAG laser.

The possibility of using a Nd laser to pump an Er glass laser, via absorption by Yb sensitizers with subsequent energy transfer to Er (see fig. 1), was first demonstrated by Gaponov et al. [1]. In that work, and subsequent related work (see Gaponov et al. [2] for numerous references) the emphasis has been on efficient conversion and high energy operation, using Nd glass lasers (usually phosphate) as the pump. By contrast our emphasis has been to assess the potential for low threshold operation with, for convenience and availability, a Nd:YAG laser as pump. To our knowledge this is the first report of

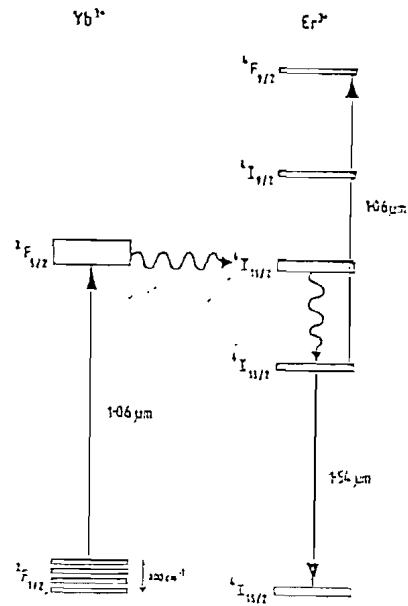


Fig. 1. Pump radiation is absorbed by Yb^{3+} from the highest sublevel of $^2\text{F}_{7/2}$. Nonradiative energy transfer occurs from Yb^{3+} ($^2\text{F}_{7/2}$) to Er^{3+} ($^1\text{I}_{1/2}$) and then nonradiative decay to Er^{3+} ($^1\text{I}_{3/2}$). Lasing at 1.54 μm is from Er^{3+} ($^1\text{I}_{1/2}$) to the ground level ($^1\text{I}_{1/2}$). Excited state absorption of the pump can occur from the metastable level Er^{3+} ($^1\text{I}_{1/2}$) to Er^{3+} ($^2\text{F}_{5/2}$).

lasing in Er glass pumped by a Nd:YAG laser. In fact, apart from the convenience and availability of Nd:YAG, the wavelength of 1.064 μm is not ideal

since it lies in the steeply falling long-wavelength wing of the $Yb\ ^2F_{7/2}\rightarrow ^2F_{5/2}$ absorption and lies in the short wavelength wing of the unwanted $^{4I_{13/2}}\rightarrow ^4F_{9/2}$ absorption in Er [2], see fig. 1. On both of these accounts a somewhat shorter pump wavelength is to be preferred, and it is for this reason that with Nd glass laser pumping, phosphate glass ($\lambda\sim 1.055\ \mu m$) has been used in preference to silicate glass [2]. It is therefore likely that replacement of Nd:YAG by, for example, the shorter wavelength Nd:YLF will prove beneficial.

2. Pump energy requirement

The advantages of using a laser to longitudinally pump another laser are well known: the small pumped volume minimises the pump power requirement and this in turn minimises the thermal input to the medium. For a glass host medium with its relatively low thermal conductivity the reduced thermal load is particularly important and especially so for high repetition rate or cw operation.

To make a rough estimate of the pump energy requirements to reach threshold we calculate the number of pump photons that must be absorbed in order to pump half of the Er ground state population to the $^{4I_{13/2}}$ level. The laser medium we have used is a 7.5 cm long cylindrical rod of Kigre QE-7 Er phosphate glass, with an estimated Er concentration $N_0\sim 1\times 10^{23}\ m^{-3}$. This estimate is based on the measured unpumped absorption coefficient of $\sim 7\ m^{-1}$ at $1.54\ \mu m$ and an assumed value of $7\times 10^{-23}\ m^2$ for the stimulated emission cross section [2]. With the pump beam focussed to a waist spot size w_0 , so as to have a confocal parameter equal to the rod length l ($2\pi w_0^2 n/\lambda_p = l$, where n is the refractive index), the pumped volume is $\sim \lambda_p^2 l/n$, thus indicating a minimum possible pump energy of $\lambda_p^2 N_0 h\nu_p/2n$. Inserting the relevant parameter values yields a predicted pump energy of $\sim 4\ mJ$. However, the pump light is only weakly absorbed ($\sim 18\%$ of the $1.064\ \mu m$ pump being absorbed in a rod 7.5 cm in length at room temperature) leading to an increased predicted threshold of $\sim 20\ mJ$ incident on the rod.

This estimate assumes 100% transfer efficiency from Yb to the upper laser level in Er. While mea-

urements of fluorescence lifetime shortening for Yb indicate near 100% transfer from Yb to Er [1], it has been pointed out [3] that this transfer is not necessarily all to the $^{4I_{13/2}}$ upper laser level. In fact absorption of pump light from the $^{4I_{13/2}}$ level is one process which reduces net transfer efficiency to $^{4I_{13/2}}$. Estimates by Gaponov [3] indicate a net transfer efficiency to $^{4I_{13/2}}$ of somewhat less than 50%, but this figure may be lower in the case where Nd:YAG is used as the pump since the longer pump wavelength leads to stronger absorption from the $^{4I_{13/2}}$ level [2].

In practice we have measured a threshold of $\sim 300\ mJ$ incident pulse energy (at room temperature) suggesting a significantly lower transfer efficiency. At elevated temperatures a threshold of $\sim 150\ mJ$ has been achieved, indicating that a cw threshold of $\sim 20\ W$ is to be expected.

3. Experimental arrangement

Given the predicted pumping requirements indicated above we chose to carry out an initial investigation using a long pulse Nd:YAG laser as the pump source, having a pulse duration of 5 ms, comparable to the $\sim 8\ \mu s$ lifetime of the Er $^{4I_{13/2}}$ level. This provided significantly higher power than usually available from a cw Nd:YAG laser, but on the other hand allowed operation at lower intensity and hence with lower damage risk than for typical non-Q-switched Nd:YAG lasers of 100–200 μs pulse duration.

To maximise the available TEM_{00} power from the Nd:YAG laser, a telescopic resonator was used [4,5]. With a plane 80% reflectivity output coupler, $\times 3$ telescope, and 6 mm \times 75 mm Nd:YAG rod, this laser gave 5 ms pulses of up to 90 W, in a linearly polarised TEM_{00} mode, at a repetition rate of 5 Hz. The linear polarisation produced by means of two Brewster angle plates in the resonator, was necessary to enable efficient isolation of the Nd:YAG laser from the Er laser using a polariser and quarter wave plate (fig. 2). With the generous power available from the pump laser the pump focussing condition in the Er rod could be relaxed somewhat from the confocal condition ($2\pi w_0^2 n/\lambda_p = l$, implying a waist size $w_0 = 90\ \mu m$) and a waist size of $170\ \mu m$ was actually used, achieved with a lens of focal length 20 cm. The

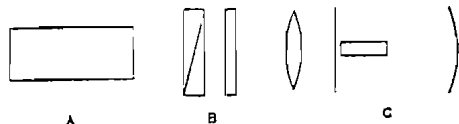


Fig. 2. Arrangement of telescopic resonator Nd:YAG pump laser (A) and Er glass laser resonator (C), with isolation (B) provided by a polariser and quarter wave plate.

erbium laser resonator, fig. 3, consisted of a plane mirror (pump input mirror) and a concave mirror, 20 cm radius, spaced by 22 cm, with the laser rod adjacent to the plane mirror. This resonator was chosen to give a calculated TEM_{00} spot size, at 1.54 μ m, of 130 μ m at the plane mirror, and hence comparable to the pump spot size in the rod. The plane mirror had $\sim 99\%$ reflectivity at 1.54 μ m and $\sim 90\%$ transmission at 1.064 μ m. The concave mirror had $>99\%$ reflectivity at 1.54 μ m. To investigate the optimum output mirror transmission (for maximum power) an inclined plate was placed in the resonator, providing a known loss as a function of tilt angle.

With the arrangement described above, threshold for 1.54 μ m oscillation with the glass rod at room temperature corresponded to ~ 64 W incident on the input mirror, and hence ~ 10 W of absorbed pump power. A significant increase in absorption, and corresponding decrease in threshold was obtained by heating the rod, thus increasing the thermal population in the upper levels of the Yb $^3F_{7/2}$ manifold. Most of the results have therefore been taken at a temperature of $\sim 90^\circ\text{C}$, where the absorption of pump radiation was $\sim 30\%$ over the rod length. The threshold power incident on the input mirror was thereby reduced to ~ 32 W. Further increase in temperature, while producing stronger absorption, did not lead to further significant threshold reduction.

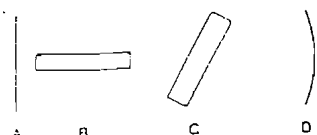


Fig. 3. Er glass laser resonator, with plane pump input mirror (A), Er rod (B), concave mirror (C), and inclined plate (D) to provide a calibrated output coupling.

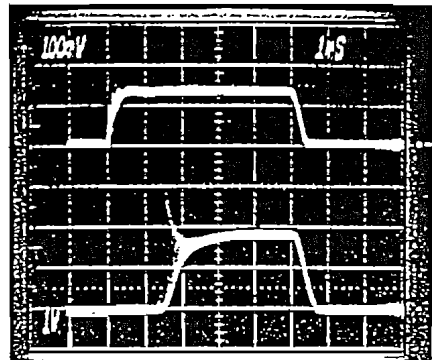


Fig. 4. Upper trace shows the 1.064 μ m pump pulse, lower trace the 1.54 μ m Er laser output. The Er rod was at 90°C and the input pump power of 90 W was $\sim 3\times$ the threshold value.

Fig. 4 shows a typical output pulse from the Er laser, with initial ringing behaviour, settling to steady state output in ~ 1 ms. Fig. 5 shows in more detail the trailing edge of the Er output and the pump pulse. It is interesting to note that lasing continues after the pump pulse has terminated and ringing can be produced on the trailing edge of the Er laser pulse. The output from the inclined plate was monitored by a Ge photodetector and the reflected power from one surface of the inclined plate, measured with an average power meter, was used to calculate the total output power. By varying the plate angle, and hence the output coupling, we found a maximum average output power of ~ 45 mW for a total output coupling of $\sim 8\%$, corresponding to a total peak output power of ~ 2.2 W. Under these optimum coupling conditions the photon conversion efficiency, from absorbed pump photons to emitted 1.54 μ m photons is $\sim 10\%$, a result which suggests a rather low transfer efficiency from Yb to the $^4I_{13/2}$ level of Er.

4. Conclusion

We have shown that, despite its rather weak absorption at 1.064 μ m, Yb :Er phosphate glass can be pumped sufficiently hard by a Nd:YAG laser to achieve lasing with reasonable gain and efficiency. Clearly a number of improvements in the perform-

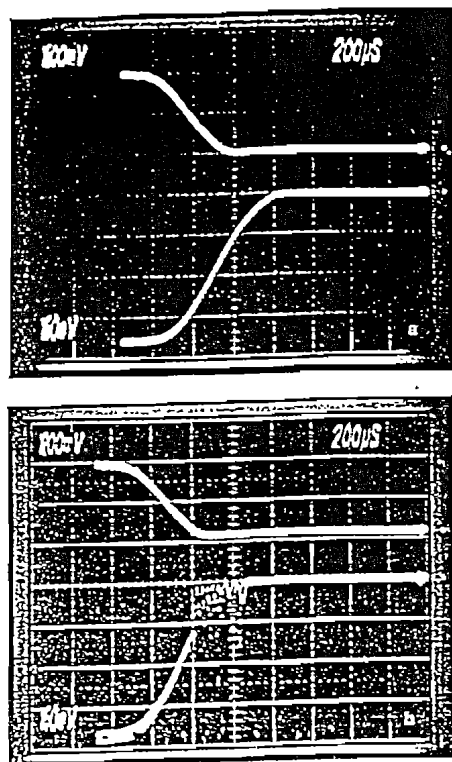


Fig. 5. Detail of the trailing edge of the Er laser output (lower trace inverted): (a) shows lasing continuing after the pump pulse has finished; (b) shows the ringing which can be produced by the transient effect of the falling pump pulse.

ance reported here can be made with an optimised arrangement. The low degree of observed (and estimated [6]) thermal lensing and birefringence and the low threshold indicate that pumping with a cw Nd:YAG laser should be possible. Improved utilisation of the available pump power could be achieved by placing the Er rod in the Nd laser resonator [2].

The long fluorescence lifetime makes the Er laser

well suited to energy storage and Q-switching. Using a mechanical chopper we have readily produced a pulse of ~ 400 ns duration. The long pumping pulse used for this laser is also suitable for the development of steady state actively mode-locked operation and experiments are planned to test such performance. Combined mode-locking and Q-switching should readily produce multikilowatt peak powers.

Very low threshold operation as seen in Er doped fibres [7] should ultimately be possible by fabricating the Yb:Er glass in the form of a monomode fibre. This would offer the opportunity of pumping by means of a diode pumped Nd:YAG or Nd:YLF laser. These various possibilities suggest that laser-pumped Er glass lasers could provide a convenient and versatile source of radiation in the $1.5 \mu\text{m}$ region.

Acknowledgements

This work has been supported by the Science and Engineering Research Council. A.K. acknowledges support in the form of a SERC studentship and D.P.S. in the form of a SERC CASE studentship, sponsored by BTRL. Acknowledgement is also given of valuable discussions with A.I. Ferguson and A.C. Tropper.

References

- [1] V.P. Gaponov, M.E. Zhabotinskii, A.A. Iznyev, V.B. Kravchenko and Yu.P. Rudnitskii, JETP Lett. 18 (1973) 251.
- [2] V.P. Gaponov, S.M. Matisin, A.A. Iznyev and V.B. Kravchenko, Optics and Laser Technology, Aug. 1982, p. 139.
- [3] V.P. Gaponov, S.M. Matisin and A.A. Iznyev, Optics Comm. 46 (1983) 226.
- [4] D.C. Hanna, C.G. Sawyers and M.A. Yuratich, Optics Comm. 37 (1981) 359.
- [5] D.C. Hanna, C.G. Sawyers and M.A. Yuratich, Optics and Quantum Electron. 13 (1981) 493.
- [6] W. Koechner, Solid-state laser engineering, Springer Series in Optical Sciences, Vol. 1, 1976.
- [7] R.J. Mears, L. Reekie, S.B. Poole and D.N. Payne, Electron. Lett. 22 (1986) 159.

CW OPERATION OF Nd:YAG PUMPED Yb:Er PHOSPHATE GLASS LASER AT 1.54 μ m

D. ESPIE, D.C. HANNA, A. KAZER and D.P. SHEPHERD

Department of Physics, University of Southampton, Highfield, Southampton SO9 5NH, UK

Received 11 July 1988

CW lasing at 1.54 μ m has been obtained by longitudinal pumping of an Yb:Er doped phosphate glass with a 1.064 μ m Nd:YAG laser. The threshold absorbed pump power was ~ 1.6 W and a cw output power of ~ 17 mW was obtained. Q-switched operation, at repetition rates of up to 125 Hz, gave peak output powers of ~ 25 W in ~ 750 ns fwhm pulses.

1. Introduction

In previous publications [1,2] we have reported the operation of a 1.54 μ m Er glass laser, pumped by a pulsed 1.064 μ m Nd:YAG laser, in which 1.064 μ m radiation is absorbed by Yb³⁺ sensitizers which then transfer their excitation to the Er³⁺ ions. Recently cw operation has been reported at 1.6 μ m on the same Er³⁺ transition ($^4I_{11/2} \rightarrow ^4I_{13/2}$) in a short length (4 mm) of doubly-sensitised Cr:Yb:Er fluoroaluminate glass [3]. A 647.1 nm krypton laser was used to pump into the Cr³⁺ absorption band, with subsequent energy transfer to Yb³⁺ and then to Er³⁺. In this paper we now report cw operation of the Nd:YAG laser pumped Yb:Er phosphate glass laser. This work and the work of Heumann et al. [3] clearly demonstrates the benefits of longitudinal laser pumping, which allows the pump power requirements to be minimised, thus reducing thermal distortions to a level which permits cw operation of the 3-level Er laser. Using a 2.5 cm long rod of Kigre QE-7 glass, we obtained a threshold of ~ 1.6 W of absorbed pump power from the cw Nd:YAG laser. With an unoptimised output mirror transmission of 1%, we have obtained a cw output of ~ 17 mW and using a mechanical chopper and Q-switch we have obtained pulses of ~ 750 ns and 25 W peak power at up to 125 Hz repetition rate.

2. Experimental arrangement

The resonator arrangement is shown in fig. 1. Its design was dictated by the following major requirements: (i) The pump beam and laser beam waists should be at the centre of the laser rod and should be of such a size that their confocal parameters are of the order of the rod length. This minimises the pumped volume. (ii) For the same reason one should use as short a laser rod as possible, the minimum length being dictated by the requirement that there be sufficient gain available. We have used a 2.5 cm length of rod, for which the maximum gain with the Er³⁺ population complete inverted, would be $\sim 17.5\%$ per pass. (iii) Since the ultimate intention is to mode-lock this laser with a 67 MHz acousto-optic modulator, the optical length of the resonator level

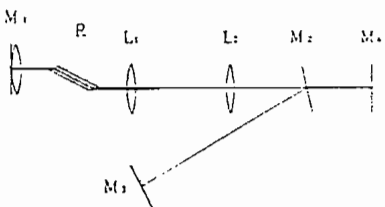


Fig. 1. CW resonator consisting: M₁, plane input mirror HT @ 1.064 μ m HR @ 1.54 μ m with a 6 cm lens; R, 2.5 cm Yb:Er rod; L₁, 6 cm lens; L₂, 50 cm lens; M₂, plane mirror HT @ 1.064 μ m HR @ 1.54 μ m (at 5° angle of incidence); M₃, plane output mirror 1% transmission @ 1.54 μ m; M₄, pump feedback mirror HR @ 1.064 μ m.

had to be fixed at 1.12 m. (iv) Since the available TEM_{00} pump power from the Nd:YAG laser was limited to ~ 7 W (Spectra Physics Model 3000), and only $\sim 20\%$ of this was absorbed in the glass rod on a single pass, an arrangement was chosen whereby unabsorbed pump power could be fed back to the glass rod. To achieve this a three mirror resonator was used (M_1, M_2, M_3), M_1 being the output mirror, M_3 having high reflectivity at $1.54 \mu\text{m}$ but transmitting $1.064 \mu\text{m}$ and mirror M_4 , of high reflectivity at $1.064 \mu\text{m}$ was used to feed back the unabsorbed pump light. The advantage of this arrangement is that devices such as Q-switch or mode-locker can be inserted between M_2 and M_3 without blocking the feedback of the pump light. With more pump power available, say 10 W or more, it would not be necessary to resort to this pump feedback arrangement.

The TEM_{00} pump beam was focussed into the laser rod, so as to give a waist at the rod centre, with $w_0 \sim 70 \mu\text{m}$. Mirror M_1 consisted of a plane mirror and adjacent positive lens of focal length 6 cm, AR coated for $1.54 \mu\text{m}$, thus simulating a 6 cm concave mirror. Since only plane mirrors were available it was necessary to use an intracavity lens to provide a sta-

ble resonator. A lens L_1 , of 6 cm focal length, placed at ~ 12 cm from mirror M_1 , provided the required tightly focussed spot in the laser rod. In practice it was found, both by numerical calculation, and experimental observation that a resonator containing a second lens L_2 (50 cm focal length) placed at ~ 40 cm from L_1 was much less sensitive to position of mirror M_1 and lens L_1 , so this two lens resonator design was used. Both lenses L_1 and L_2 were AR coated for $1.54 \mu\text{m}$.

The cylindrical laser rod of QE-7 glass is 2.5 cm long and approximately 2 mm in diameter, with its end faces at Brewster's angle. The rod is held in an oven at a temperature of $\sim 110^\circ\text{C}$. As described in ref. [1] this elevated temperature increases the pump absorption and hence reduces the pump power requirement. Since the absorbed power is also a significant source of heat it is necessary to avoid too high a temperature within the pumped region of the rod. This problem is avoided by using a small diameter rod, thus reducing the temperature difference between the rod walls and its centre, and also by ensuring good thermal contact between the rod and the body of the oven.

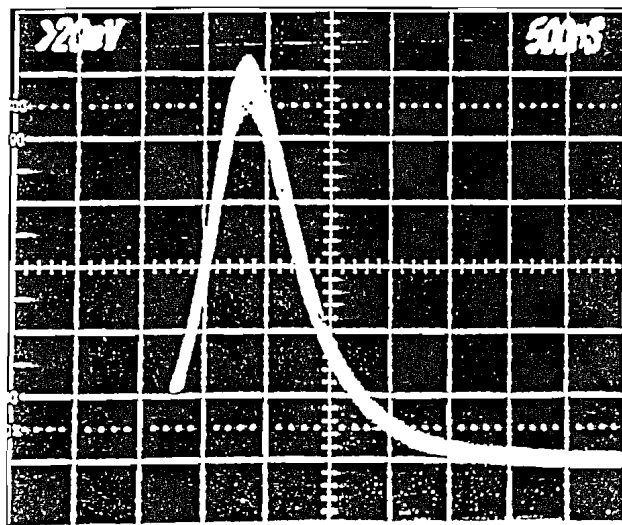


Fig. 2. Oscilloscope photograph of several Q-switched output pulses.

Using mirrors of nominally 100% reflectivity, threshold was found to occur at 1.6 W of absorbed pump power, which corresponds to 5.4 W output from the pump laser. A measurement of reflected power from the Brewster faces indicated a loss of less than 0.2%, thus indicating that depolarisation due to thermally induced birefringence was not a problem at this pump power level. Using a 1% transmission output mirror a cw output power of ~17 mW was obtained for an absorbed pump power of ~2.7 W. A simple mechanical chopper placed between mirrors M_2 and M_3 provided a simple means of Q-switching and output pulses of ~25 W, in pulses of ~750 ns duration, were observed at repetition rates up to 125 Hz (the inverse of the upper laser level lifetime). Fig. 2 shows an oscilloscope photograph containing several pulses and gives an indication of the good amplitude stability. The observed variation is thought to be due to fluctuations arising from feedback of the 1.064 μm pump light into the Nd:YAG laser. With greater available pump power this problem could be eliminated, by dispensing with mirror M_4 , and using a quarter-wave plate/polariser combination to act as isolator to prevent feedback from mirror M_1 .

Clearly a number of further improvements can be made, with losses reduced by replacing the lenses with

appropriate curved resonator mirrors and by choosing an optimum output transmission. With these improvements and given the higher pump powers now available from commercial Nd:YAG lasers, a significant increase in output power can be anticipated. Mode-locked operation, which has previously been demonstrated with the pulsed Er glass laser [2], should provide a convenient source of high power short pulses from this laser, and experiments are now in progress to demonstrate this.

Acknowledgement

This work has been supported in part by a SERC JOERS programme. Support in the form of SERC studentships is acknowledged by A.K., D.E. and D.P.S. The loan of mirrors by BTRL is also gratefully acknowledged.

References

- [1] D.C. Hanna, A. Kazer and D.P. Shepherd, *Optics Comm.* 63 (1987) 417.
- [2] D.C. Hanna, A. Kazer and D.P. Shepherd, *Optics Comm.* 65 (1988) 355.
- [3] E. Hewmann, M. Ledig, D. Ehr, W. Seeger, E.W. Duczynski, H.J. v.d. Heide and G. Huber, *Appl. Phys. Lett.* 52 (1988) 255.

has significant implications in the development of metal-insulator-semiconductor systems in general, and may possibly be generically applied to a broad class of materials systems, especially those that are based on substrate materials whose native oxides are unstable and detrimental to a good interface formation.

Acknowledgments: The authors wish to thank Paul Enquist for providing the GaAs substrates with the MOCVD-grown epilayers. This work was supported by SDIO/IST through the Office of Naval Research Contract Number N00014-86-C-0421.

G. G. FOUNTAIN
 S. V. HATTANGADY
 D. J. VITKAVAGE
 R. A. RUDDER
 R. J. MARKUNAS
*Research Triangle Institute
 Research Triangle Park, NC 27709, USA*

18th July 1988

* Present address: AT&T Laboratories, Allentown, PA 18102, USA

References

- 1 FRESE, K. W., JUN., and ROY MORRISON, S.: 'Passivation and interface state studies on *n*-GaAs', *Appl. Surf. Sci.*, 1981, 8, pp. 266-271
- 2 MEINERS, L. G.: 'Electrical properties of the gallium arsenide-insulator interface', *J. Vac. Sci. Technol.*, 1978, 15, pp. 1402-1407
- 3 SENGUPTA, D., and KUMAR, V.: 'Study of *n*-GaAs MOS diodes with spin-on SiO₂', *Phys. Stat. Sol. A*, 1982, 73, pp. K279-K280
- 4 KAMIMURA, K., and SAKAI, Y.: 'The properties of GaAs-Al₂O₃ and InP-Al₂O₃ interfaces and the fabrication of MIS field-effect transistors', *Thin Solid Films*, 1979, 56, pp. 215-221
- 5 CASEY, H. C., JUN., CHO, A. Y., LANG, D. V., NICOLLIAN, E. H., and FOY, P. W.: 'Investigation of heterojunctions for MIS devices with oxygen-doped Al_{1-x}As on *n*-type GaAs', *J. Appl. Phys.*, 1979, 50, pp. 3484-3491
- 6 TSANG, W. T.: 'Self-terminating thermal oxidation of AlAs epilayers grown on GaAs by molecular beam epitaxy', *Appl. Phys. Lett.*, 1978, 33, pp. 426-429
- 7 SUZUKI, N., HARIU, T., and SHIBATA, Y.: 'Effect of native oxide on the interface property of GaAs MIS structures', *Appl. Phys. Lett.*, 1978, 33, pp. 761-762
- 8 FOUNTAIN, G. G., RUDDER, R. A., HATTANGADY, S. V., MARKUNAS, R. J., and LINDORME, P. S.: 'Low interface state density SiO₂ deposited at 300°C by remote plasma enhanced CVD on reconstructed Si surfaces', *J. Appl. Phys.*, 1988, 63, pp. 4744-4746
- 9 FOUNTAIN, G. G., RUDDER, R. A., HATTANGADY, S. V., VITKAVAGE, D. J., and MARKUNAS, R. J.: 'Electrical and microstructural characterisation of an ultra-thin silicon interlayer used in a SiO₂/Ge-based MIS structure', *Electron. Lett.*, 1988, 24, pp. 1010-1011
- 10 VITKAVAGE, D. J., FOUNTAIN, G. G., RUDDER, R. A., HATTANGADY, S. V., and MARKUNAS, R. J.: 'Gating of Germanium surfaces using pseudomorphic Silicon interlayers', to appear in *Appl. Phys. Lett.*, 1988, 53, (8)
- 11 HATTANGADY, S. V., RUDDER, R. A., FOUNTAIN, G. G., VITKAVAGE, D. J., and MARKUNAS, R. J.: 'In situ cleaning of Ge(111) and Si(100) surfaces', Materials Research Society Symposium Proceedings, Vol. 102 (Symposium C): Epitaxy of Semiconductor Layered Structures, Boston, Mass., Nov. 1987, pp. 319-322

EFFICIENT OPERATION OF AN Yb-SENSITISED Er FIBRE LASER AT 1.56 μm

Indexing terms: Lasers and laser applications, Optical fibres, Optical properties of substances, Doping

We report operation of a high-efficiency Yb:Er single-mode fibre laser. Pumping at wavelengths of 1064 nm and at 820 nm has shown low pump power thresholds (<7 and 4 mW) and high slope efficiencies (4.2 and 7.0%).

Introduction: Erbium-doped glass has long been recognised as an important laser material, particularly for applications in optical fibre communications. The 1.5 μm transition is well

matched to the so-called third transmission window in silica-based communications fibres and erbium-based systems are consequently of great interest both as sources and inline amplifiers. Despite its potential usefulness, one drawback of the Er laser is its lack of absorption bands where low cost pump sources, e.g. semiconductor laser diodes or diode-pumped Nd:YAG lasers, emit. Furthermore Er is known to have strong excited-state absorption (ESA) which constrains the choice of useful pump wavelengths.

One way around these problems is to use glass which is codoped, or sensitised, with materials which absorb in desirable spectral bands. Optically pumping a suitable codopant can lead to efficient transfer of excitation to the laser active material. Very early on ytterbium was shown¹ to be a suitable sensitiser for Er, giving efficient energy transfer. Recently operation of the first Yb:Er fibre laser has been reported.²

We describe here the operating characteristics of an Yb:Er fibre laser which has produced significant output powers and a high slope efficiency and which can be pumped either at the Nd:YAG wavelength of 1.064 μm (as demonstrated in bulk glass)³ or at wavelengths and with powers available from commercial laser diodes emitting in the 820-850 nm region.

Details of the energy transfer behaviour in the Yb:Er fibre used in our experiments will be described elsewhere* and only a summary will be provided here. Because of the significant inhomogeneous line broadening in glass and because several levels of the Yb ground state multiplet ²F_{5/2} are thermally populated at room temperature, both Nd:YAG and semiconductor diode lasers can efficiently pump into the Yb ¹F_{3/2} doublet, whose lower level has a 0.75 ms intrinsic radiative lifetime.

From the ²F_{5/2} state energy is transferred by multipole interactions to nearby Er ions resulting in population of the ⁴I_{11/2} level. A fast nonradiative decay from this level prevents significant back-transfer of energy to the Yb and leads to population trapping in the long-lived (14 ms) ⁴I_{13/2} level. Lasing action subsequently takes place between this level and the ground state manifold ⁴I_{15/2}.

Experimental details: The probability of energy transfer between ions decays rapidly with ion separation. Efficient transfer consequently requires high doping levels. Recent developments of the solution doping technique⁴ have made possible the production of low scattering loss, cluster-free fibres with dopant concentrations of several percent. The host glass used in our fibre was silica based with doping levels of 5 mole percent Al₂O₃ (to enhance the solubility of rare-earth ions) and 5 mole percent P₂O₅ and had Yb and Er concentrations of approximately 1.7% and 0.080%, respectively (21:1 ratio). The fibre had an NA of 0.25 and a core radius of 2.3 μm. The cutoff wavelength was designed to be 1.5 μm to ensure single-mode operation of the Er laser and a good launch efficiency of the pump light.

A Spectra-Physics CW Nd:YAG laser or a Coherent argon-ion pumped Styryl 9M dye laser provided the pump light. The latter could be tuned with significant power (>100 mW) over the wavelength range 800-850 nm, thus stimulating the performance of a diode laser. A microscope objective focused the pump light into the fibre and mirrors were butted to both fibre ends to form a low-loss cavity. The input mirror had a reflectivity of 98% at the lasing wavelength and was highly transmitting at the pump. Output couplers with 1.5 μm transmissions of 10% and 27% were used. These had reflectivities of 10% at the pump wavelength.

Since Er operates essentially as a three-level laser, end-pumped fibre laser performance depends strongly on the fibre length. The optimum fibre length can be found by cutting back a long length of fibre while monitoring the laser performance in terms of threshold pump power, slope efficiency and lasing wavelength. When pumping at 1.064 μm, a length of ~1 m showed a good compromise between minimum threshold power and maximum output power. This length corresponds roughly to one absorption length at the pump wavelength. Small fibre length variations do not significantly alter the lasing characteristics. Larger variations increase the pump threshold and lead to a shift in lasing wavelength. This

* FERMANN, M. E.: in preparation

shift, from $1.568\text{ }\mu\text{m}$ at 2.8 m to $1.549\text{ }\mu\text{m}$ at 25 cm , results from preferential lasing to lower levels in the Er ground state multiplet.⁵

Laser performance with $1.064\text{ }\mu\text{m}$ pumping was evaluated using a 91 cm length (27% output coupling) and an 84 cm length (7% output coupling) of fibre. The absorbed (launched) power at threshold was found to be 8.0 (16) mW and 6.6 (12) mW for the two cases and slope efficiencies, measured with respect to absorbed (launched) power, were found to be 4.2% (2.0) and 2.8% (1.5), respectively. Fig. 1 shows plots of the output power against launched power for the two output couplers. It is evident that the amount of output coupling is

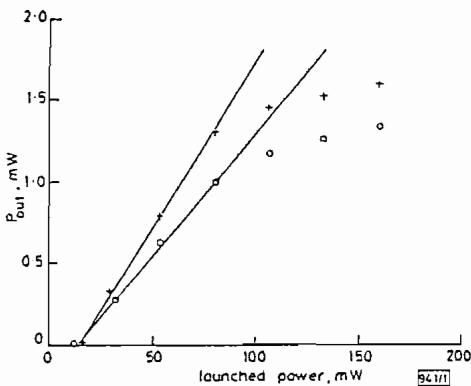


Fig. 1 Output power against launched power for output mirror transmissions of 27% (+) and 7% (○) when pumped at 1.064 nm

not very critical. The saturation seen at high pump powers is believed to be due to pump saturation of the Yb ions. Higher output powers than those shown can be achieved with higher Yb concentrations or simply by using longer fibre lengths.

Pumping a 70 cm length of the same fibre with the dye laser also showed a low threshold. With a 99% reflector as the input mirror and a 27% transmitting output coupler the threshold with 820 nm pumping was found to be 3.7 mW and a slope efficiency (absorbed power) of 7.0% was measured. More detailed results from the dye laser experiments will be published separately.

Discussion: The results described are significant in a number of ways. First, it has been shown that efficiency energy transfer lasers can be made in fibre form using doping levels of only 1–2%. The only previous mention² of such a laser had a significantly lower (0.7%) slope efficiency and produced only small amounts of power ($100\text{ }\mu\text{W}$) using a higher ion doping level (4% Yb). We note that ESA has not strongly impeded the laser performance. Further investigations are aimed at studying the influence of pump-induced ESA. This can conveniently be done using the dye laser since ESA peaks have been identified in its wavelength range at 800 and 840 nm .⁶

Secondly, the Yb:Er system is not unique and many other sensitisation schemes are possible. This opens up new possibilities for fabrication of fibre lasers and amplifiers which can be pumped by convenient and inexpensive sources. As shown here the pump powers required for operation are small enough to be well within the reach of mini-YAGs or diode lasers.

Finally we note that significantly higher output powers for a given pump power can be achieved by feeding the unabsorbed pump light into the output end of the fibre; this is simply a matter of appropriate mirror design. The slope efficiency with respect to launched power can then approach the value calculated with respect to absorbed power.

Acknowledgments: We are grateful to R. M. Percival, I. R. Perry and R. G. Smart for assistance in performing some of the experiments. We thank E. Tarbox of Pirelli General plc for assistance in the development of the fibre design. Funding

for this work was provided by the UK SERC, part of the support being provided by JOERS.

M. E. FERMANN[†]

D. C. HANNA

D. P. SHEPHERD

P. J. SUNI

J. E. TOWNSEND[†]

Department of Physics

[†]Department of Electronics & Information Engineering

University of Southampton

Southampton SO9 5NH, United Kingdom

29th June 1988

References

1. SNITZER, E., and WOODCOCK, R.: 'Yb³⁺-Er³⁺ glass laser', *Appl. Phys. Lett.*, 1966, 6, pp. 45–46
2. SNITZER, E., PO, H., HAZIM, F., TUMMINELLI, R., and MCCOLLUM, B. C.: 'Erbium fiber laser amplifier at $1.55\text{ }\mu\text{m}$ with pump at $1.49\text{ }\mu\text{m}$ and Yb sensitized Er oscillator', Paper PD2-1, OFC '88 Optical Fibre Communications Conference, New Orleans, 1988
3. HANNA, D. C., KAZER, A., and SHEPHERD, D. P.: 'Active mode-locking and Q-switching of a $1.54\text{ }\mu\text{m}$ Er:glass laser pumped by a $1.064\text{ }\mu\text{m}$ Nd:YAG laser', *Opt. Commun.*, 1988, 65, pp. 355–358
4. TOWNSEND, J. E., POOLE, S. B., and PAYNE, D. N.: 'Solution-doping technique for fabrication of rare-earth-doped optical fibres', *Electron. Lett.*, 1987, 23, pp. 329–331
5. REEKIE, L., JAUNCEY, I. M., POOLE, S. B., and PAYNE, D. N.: 'Diode-laser-pumped operation of an Er³⁺-doped single-mode fibre laser', *Electron. Lett.*, 1987, 23, pp. 1076–1078
6. LAMING, R. L., POOLE, S. B., and TARBOX, E. J.: 'Excited-state absorption in erbium-doped fibres', submitted to *Optics Letters*

PROPAGATION MODELLING IN THE TROPOSPHERE: PARABOLIC EQUATION METHOD

Indexing terms: Radiowave propagation, Atmospheric propagation, Modelling, Microwave radiation

The parabolic equation is a simplification of the wave equation that admits an efficient full wave solution to the problem of microwave propagation in a two-dimensional refractive index structure. Field strength diagrams for propagation in the presence of typical elevated ducting layers are given. The fields are significantly more complicated than can be predicted by one-dimensional mode methods.

Introduction: Predictions of variations in signal level at microwave frequencies caused by complex refractive index structures are usually based on ray tracing or mode theory. Both of these have severe limitations. Ray tracing, derived from geometrical optics, can give reasonable qualitative results, but quantitative calculations are expensive and difficult to automate as all ray paths linking transmitter and receiver must be found and the ray amplitudes added coherently. While two-dimensional refractive index structures can be handled,¹ the generation of two-dimensional field strength diagrams is very expensive. In addition, the assumptions of geometrical optics may not be satisfied if strong ducting layers are present. Quantitative results are obtained directly from mode theory—a full wave method based on the solution of Maxwell's equations. In practice, only one-dimensional refractive index structures are tractable, and most implementations use simple analytical profiles.² Again two-dimensional field strength diagrams are very expensive to produce.

The parabolic equation is an alternative full wave approach, first introduced into radiowave propagation in 1946.³ Numerical methods of solving the equation were not available at that time, and only recently has the application to tropospheric propagation been revived; the success is due to the application of an efficient numerical technique that has previously been applied to an analogous problem in underwater acoustics.⁴

**ACTIVE MODE-LOCKING AND Q-SWITCHING OF A $1.54 \mu\text{m}$ Er:GLASS LASER
PUMPED BY A $1.064 \mu\text{m}$ Nd:YAG LASER**

D.C. HANNA, A. KAZER and D.P. SHEPHERD

Department of Physics, University of Southampton, Highfield, Southampton SO9 5NH, UK

Received 11 September 1982

A Nd:YAG pumped Yb:Phosphate glass laser oscillator has been actively mode-locked and Q-switched, producing stable ~ 70 ps fwhm mode-locked pulses at $1.54 \mu\text{m}$. Peak powers of ~ 20 kW are achieved when Q-switched and mode-locked and ~ 30 W when quasi-cw mode-locked, thus providing a convenient source suitable for investigation of nonlinear propagation behaviour in the negative dispersion region of silica optical fibres.

1. Introduction

In a previous paper [1] we have reported operation of a $1.54 \mu\text{m}$ Er glass laser pumped by a $1.064 \mu\text{m}$ Nd:YAG laser, via absorption by Yb sensitizers. Here we report mode-locked and Q-switched operation of this laser, at power levels which are suitable for studies of nonlinear propagation and pulse compression in the negative velocity dispersion region of silica fibre [2,3]. Mode-locked pulse durations of 70 ps have been measured, having a time-bandwidth product of 0.6, and a peak power of 20 W. When Q-switched and mode-locked, a peak power of ~ 20 kW has been achieved.

2. Experimental arrangement

The laser medium is the same as reported in ref. [1], consisting of a 7.5 cm long rod of Kigre QE-7 glass, with end faces anti-reflection coated for $1.5 \mu\text{m}$ and wedged by $1/2^\circ$ relative to the axis of the rod. The pump laser is a pulsed Nd:YAG, providing pulses of 5 ms duration, of up to 90 W, in a linearly polarised TEM_{00} mode, at a repetition rate of 5 Hz [1]. As in ref. [1], the Er laser was isolated from the pump laser by means of a quarter wave plate and polariser. Through all of the measurements reported here the pump beam was focussed to a spot-size (radius, w) of 170 μm . The various resonators used for

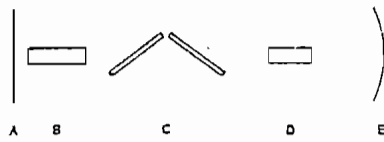


Fig. 1. Resonator for Q-switched operation. (A) plane pump input mirror, (B) Er rod, (C) Brewster plates, (D) LiNbO_3 crystal, (E) concave output mirror.

the Er laser have been designed to provide a comparable spot size in the laser rod for the laser wavelength of $1.54 \mu\text{m}$, so as to achieve good beam overlap. To enhance absorption of the $1.064 \mu\text{m}$ radiation in the Er glass we have operated with the glass rod maintained at a temperature of $\sim 90^\circ\text{C}$.

Q-switching has been achieved using a LiNbO_3 Pockels cell, with field applied transversely, in the x_1 direction, and propagation in the x_2 direction. The crystal, of dimensions $9 \times 9 \times 25$ (x_1) mm, had anti-reflection coatings for $1.5 \mu\text{m}$ on the end faces. Applying a quarter wave voltage (~ 2.5 kV) was sufficient, in conjunction with a polariser consisting of two Brewster-angled silica plates, to suppress laser action during the entire pumping pulse. The Pockels cell voltage was removed at the end of the pumping pulse to produce a Q-switched output. Using the resonator of fig. 1, with a concave (50 cm) output mirror of $\sim 10\%$ transmission, and a resonator length of ~ 50 cm (i.e. a near hemi-spherical resonator), gave

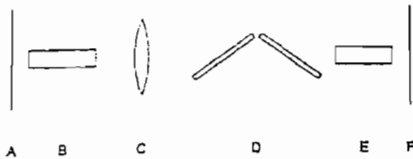


Fig. 2. Resonator for mode-locked operation. (A) plane pump input mirror. (B) Er rod, (C) 40 mm lens. (D) Brewster plates, (E) modelocker, (F) plane output mirror.

a TEM₀₀ output pulse of ~0.7 mJ in a ~60 ns (fwhm) pulse, hence a peak power of ~10 kW. This corresponds to ~20% of the energy obtained in long pulse operation (~4 ms) being available as Q-switched output. Amplitude stability was good, with <5% fluctuation in output.

Active mode-locked operation has been tested both under long-pulse, i.e. quasi-cw conditions, and under Q-switched operation. First we consider quasi-cw operation. The resonator for quasi-cw operation is shown in fig. 2. The resonator design was constrained by three considerations. First there was the need for a resonator length of 115 cm, to match the modulation frequency ($\omega_m \sim 67$ MHz) of the acousto-optic modulator available to us. Also there was the need for an appropriate spot size (~170 μm) in the glass rod, and a sufficiently collimated beam in the acousto-optic modulator. A 40 cm lens, anti-reflection coated for 1.5 μm achieved the desired resonator, with a ~0.8 mm waist spot-size at the plane output mirror. This output mirror was wedged, effectively suppressing etalon effects. The input mirror was not wedged, or anti-reflection coated, and despite its high reflectivity (~99%) at 1.5 μm , it produced readily detectable etalon effects which may have degraded the mode-locking performance. In arriving at the resonator design, allowance was made for the effect of thermally induced lensing in the laser rod, following the analysis of Gordon et al. [4].

The acousto-optic modulator consisted of a 7 cm long fused silica slab originally intended for use at 1.06 μm and therefore having wedged end faces anti-reflection coated for 1.06 μm operation [Intra Action ML-675]. It was found that these AR coatings gave sufficiently low loss to permit satisfactory operation at 1.5 μm . Using a pulsed rf drive power of 7 W, it was found by measurement that the depth of

modulation for 1.5 μm radiation corresponded to a value of $\theta_m \approx 1.2$ (using the notation of Kuizenga [5] who defines the single-pass amplitude transmission $m(t)$ as $m(t) = \cos(\theta_m \sin \omega_m t)$). The Brewster plate polariser was retained in this resonator to constrain the laser polarisation to that for which the modulator produced strongest modulation.

To obtain mode-locked operation the resonator length was adjusted to match the modulation frequency. Two resonator length positions were found where driven relaxation oscillations occurred for the entire duration of the laser output as described by Kuizenga [5], the correct resonator length corresponded to a position midway between. Fig. 3 shows a typical pulse train obtained under these conditions, with an overall duration of ~3 ms, and with initial relaxation oscillation decaying away in ~2 ms. Measurements of mode-locked pulse duration were made using background-free second-harmonic autocorrelation, in a LiIO₃ crystal. The entire pulse train was used in this measurement and fig. 4 shows a typical result with the curve corresponding to a best fit assuming a gaussian pulse shape. The pulse duration deduced from fig. 4 is 70 ps. By using a Pockels cell shutter external to the laser, the initial part of the pulse envelope, containing the relaxation oscillations, could be suppressed in the autocorrelation measurement, however it was found that the measured pulse duration was still 70 ps. The bandwidth of the output, measured using a scanning Fabry-Perot interferometer, was 8 GHz, corresponding to a time bandwidth product of ~0.6. From measurement of output energy in the pulse train, and the measured mode-locked pulse duration, a peak power of ~20 W is deduced.

For combined Q-switching and mode-locking the resonator is as shown in fig. 2 but with the LiNbO₃ Pockels cell placed between the Brewster plates and the intracavity lens. The Pockels cell voltage was adjusted to allow 'prelasing' to occur [5]. The prelase lasted for ~2 ms, thus providing sufficient time for the mode-locker to establish a steady state pulse duration. The voltage was then removed from the Pockels cell near the end of the pumping pulse, resulting in a Q-switched envelope of ~300 ns duration (fwhm) and pulse energy of ~70 μJ . Auto-correlation measurement of pulse duration yield ~85 ps, hence indicating peak power of ~20 kW.

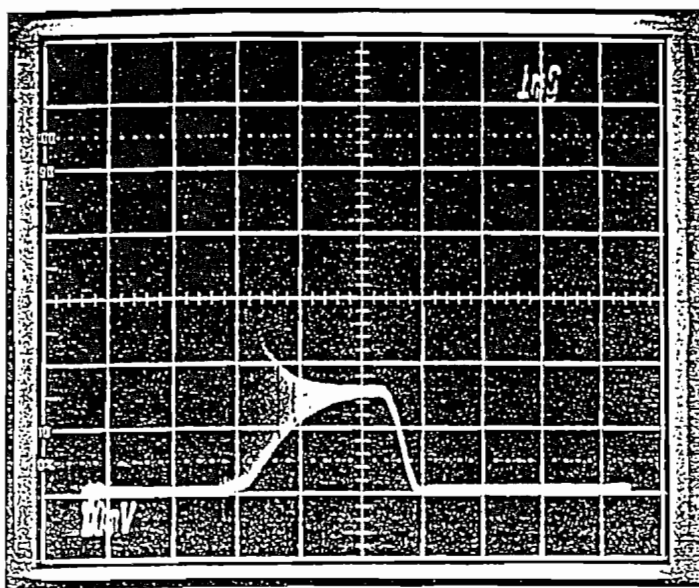


Fig. 3. Envelope of mode-locked pulse train, showing initial relaxation oscillations decaying after ~ 2 ms.

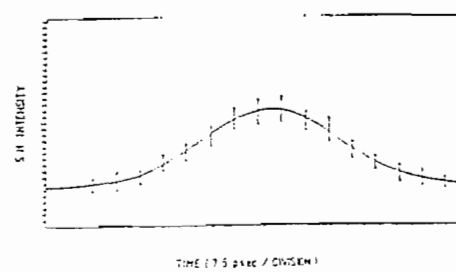


Fig. 4. Second harmonic autocorrelation measurement of pulse duration, $fwhm = 70 \pm 1$ ps. The background level observable on this trace is due to ambient room light.

3. Conclusion

The results reported here give further confirmation that the Nd:YAG-pulsed Er glass laser is a versatile and convenient source of $1.54 \mu\text{m}$ radiation. Significant improvements on our results should be

possible as a number of the components we have used were not optimally designed for operation at $1.54 \mu\text{m}$. The power levels and pulse durations suggest that this source should be useful for investigations of nonlinear propagation in silica fibre, and, in particular the mode-locked laser could form the basis of a soliton laser, as described by Mollenauer and Stoien [6].

Acknowledgements

This work has been supported in part by a SERC/JOERS grant. A.K. receives support from the SERC in the form of a studentship and D.P.S. receives support from both SERC and BTRL in the form of a CASE studentship. We also wish to record our gratitude to BTRL for the loan of the Pockels cell and a number of lenses and mirrors.

References

- [1] D.C. Hanna, A. Kazer and D.P. Shepherd, *Optics Comm.* 63 (1987) 417.
- [2] L.F. Mollenauer, R.H. Stolen and J.P. Gordon, *Phys. Rev. Lett.* 45 (1980) 1095.
- [3] L.F. Mollenauer, R.H. Stolen, J.P. Gordon and W.J. Tomlinson, *Optics Lett.* 8 (1983) 289.
- [4] J.P. Gordon, R.C.C. Leite, R.S. Moore, S.P.S. Porto and J.R. Whinnery, *J. Appl. Phys.* 36 (1965) 3.
- [5] D.J. Kuizenga, *IEEE J. Quantum Electron.* QE-17 (1981) 1694.
- [6] L.F. Mollenauer and R.H. Stolen, *Optics Lett.* 9 (1983) 13.

The established orthonormality and completeness of $\{W_{kl}(n, \theta)\}$ validates the representation

$$Y(n, \theta) = \sum_{k,l} b_{kl} W_{kl}(n, \theta) \quad b_{kl} = \langle Y, W_{kl} \rangle \quad (12)$$

Consequently, eqn. 11 takes the form

$$\begin{aligned} \varepsilon &= \pi^{-1} \int_{-\pi/2}^{\pi/2} d\theta \sum_n \left| \sum_{k,l} (b_{kl} - a_k a_l^*) W_{kl}(n, \theta) \right|^2 \\ &= \sum_{k,l,m,p} (b_{kl} - a_k a_l^*) (b_{mp}^* - a_m a_p^*) \langle W_{kl}, W_{mp} \rangle \\ &= \sum_{k,l} |b_{kl} - a_k a_l^*|^2 \end{aligned} \quad (13)$$

whose formal minimisation leads readily to Sussman's eigenvalue problem

$$(1/2)(\mathcal{B} + \bar{\mathcal{B}}) \cdot \mathbf{a} = \lambda \mathbf{a} \quad \lambda = \sum_k |a_k|^2 = \bar{a} \cdot \mathbf{a} \quad (14)$$

where \mathcal{B} denotes the matrix $[b_{kl}]$, \mathcal{B} its transpose conjugate and \mathbf{a} is the eigenvector associated with λ and normalised to ensure consistency with the energy constraint $\lambda = \bar{a} \cdot \mathbf{a}$ in eqn. 14. With the expansion coefficients (a_k) identified as the components of \mathbf{a} , ε in eqn. 13 reduces to

$$\varepsilon_0 = \sum_{k,l} |b_{kl}|^2 - \lambda^2 \geq 0 \quad (15)$$

Clearly, ε_0 attains its minimal value for the largest eigenvalue of $(\mathcal{B} + \bar{\mathcal{B}})/2$.

Conclusion: Sussman's algorithm is indeed applicable to the problem of DTWD synthesis provided that an appropriate

definition is adapted. The least squares synthesis is achieved by identifying the expansion coefficients in eqn. 1 with the energy normalised constituents of the eigenvector (a) corresponding to the largest eigenvalue of $(\mathcal{B} + \bar{\mathcal{B}})/2$. As a by-product, the presented sequence overcomes the rather awkward need to deal separately with odd and even expansion coefficients. In all, perhaps one more reason for preferring the defining of eqn. 7 over eqn. 5.

J. WEXLER
S. RAZ

19th September 1989

Department of Electrical Engineering
Israel Institute of Technology—Technion
Haifa 32000, Israel

References

- 1 CLAASEN, T. A. C. M., and MECKLENBRAUER, W. F. G.: 'The Wigner distribution—a tool for time-frequency signal analysis. Part II: Discrete time signals', *Philips J. Res.*, 1980, 35, pp. 276–300
- 2 SUSSMAN, S. M.: 'Least-square synthesis of radar ambiguity functions', *IRE Trans. Inform. Theory*, 1962, pp. 246–254
- 3 YU, K. S., and CHANG, S.: 'Signal synthesis from Wigner distribution', *Proc. IEEE Int. Conf. Acoust., Speech, Signal Processing*, 1985, USA, pp. 1037–1040
- 4 BOUDREAU-BARTELIS, G. F., and PARKS, T. W.: 'Time-varying filtering and signal estimation using Wigner distribution synthesis techniques', *IEEE Trans. Acoust., Speech, Signal Processing*, 1986, ASSP-34, (3), pp. 442–451
- 5 KUMAR, B. V. K. V., NEUMAN, C. P., and DEVOS, K. J.: 'Discrete Wigner synthesis', *Signal Processing*, North-Holland, 1986, 11, pp. 277–304
- 6 CHEN, D. S. C.: 'A nonaliased discrete time Wigner distribution for time-frequency signal analysis', in *Proc. IEEE Int. Conf. Acoust., Speech, Signal Processing*, 1982, France, pp. 1333–1336
- 7 PEYRIN, F., and FROST, R.: 'A unified definition for the discrete-time, discrete-frequency, and discrete-time/frequency Wigner distributions', *IEEE Trans. Acoust., Speech, Signal Processing*, 1986, ASSP-34, (4), pp. 858–866

ACTIVE MODE-LOCKING OF AN Yb : Er FIBRE LASER

Indexing terms: Optical fibres, Lasers

We report FM mode-locked operation of a single-mode Yb : Er fibre laser at 1.56 μm . To date pulses of 70 ps duration and peak output powers of 90 mW have been achieved.

Introduction: Laser sources producing short pulses in the 1.5 μm wavelength region are of interest for several reasons. This spectral region is important for silica based communications systems and is also of interest for studying nonlinear pulse propagation in the negative group velocity dispersion regime of silica.

We have previously described¹ the AM mode-locking of a bulk Yb : Er glass rod using an acousto-optic modulator. In this letter we describe an Yb : Er fibre laser which has been FM mode-locked using the technique recently used² to mode-lock a Nd-doped fibre laser. Geister and Ulrich have also recently reported³ mode-locking of a Nd fibre laser using an integrated optical modulator. In this letter we give the first report of mode-locked operation on the $4^1_{1,3,2}$ to $4^1_{1,5,2}$ transition at 1.56 μm in an Er-doped fibre laser. This type of laser is of particular interest because the fibre already incorporates those features which are necessary for achieving pulse compression, that is, a Kerr nonlinearity to produce temporally chirped pulses and negative group velocity dispersion to cause the compression.

The fibre used in this experiment and its CW operation has been described elsewhere.⁴ In summary, the fibre (core diameter 4.6 μm , NA = 0.25) is doped with 1.5% Yb and 0.08% Er. Pump light at 1.06 μm is absorbed by the Yb ions. This excitation is efficiently transferred to the Er ions and lasing action occurs on the familiar 1.5 μm transition in the Er.

Experimental: Fig. 1 shows a schematic diagram of the experimental arrangement used. The pump laser was a CW Nd : YAG laser capable of delivering several watts of power.

The pump light was focused into a 60 cm length of fibre using a 10 \times microscope objective (MO). The input mirror (M1) was highly reflecting at 1.56 μm and transmitted $\sim 90\%$ of the pump light. This mirror was butted to the fibre end. Because optical damage to the mirror coating occurred for pump powers of the order of 400–500 mW, the pump power was kept below 300 mW. The other fibre end was terminated in index-matching liquid (IM) to avoid backreflections into the fibre. Such reflections are detrimental to the mode-locked operation² and may even cause unwanted laser oscillations in the fibre. The output light from this end was collimated with another 10 \times microscope objective and was focused through the mode-locker (ML) onto the output coupler (M2) which had a transmission of 4.5% at 1.56 μm .

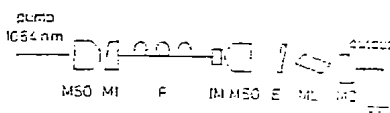


Fig. 1 Experimental arrangement

The mode-locker used was a 3 cm long LiNbO₃ phase modulator with Brewster cut ends in order to give a small loss for a single polarisation state. The crystal was mounted in a resonant LC circuit housing with inductive RF signal coupling. The voltage was applied to the crystal z-axis to take advantage of the largest electro-optic coefficient r_{31} . The circuit could be tuned over several MHz near 100 MHz. Efficient mode-locking was achieved by applying RF powers of 0.5–1.0 W.

The addition of two more cavity elements was found to be important. The first was a 0.25 mm thick uncoated étalon (E) which was used to control the oscillation bandwidth. This helped stabilise the output pulses. The second was a polarisation controller (P).⁵ Initially, this consisted of a 3 cm disc around which the fibre was wound once. By rotating this loop about the fibre axis some control of the polarisation incident on the mode-locker could be achieved. With this polarisation controller the ratio of horizontal to vertical polarisation at the output was limited to 3:4:1. Under CW conditions this

cavity was found to have an incident power threshold of 150 mW. Since the launch efficiency was approximately 50%, the launched power at threshold was ~ 75 mW. At $1.064\text{ }\mu\text{m}$ the absorption coefficient is 3.4 dB/m , so for the 60 cm fibre length used, the absorbed power at threshold was 28 mW.

The mode-locked pulses were observed using a fast GaInAs photodiode in conjunction with a sampling scope. The combined risetime of this system was approximately 60 ps. Fig. 2 shows a picture of a typical sampling scope trace when the mode-locker was turned on. The measured FWHM duration is 90 ps, which implies an actual pulsedwidth of ~ 70 ps. The corresponding bandwidth was found to be 11.5 GHz using a scanning Fabry-Perot interferometer. This gives a time-bandwidth product of 0.8, which is comparable to that expected⁶ for chirped FM mode-locked pulses with a Gaussian shape (0.63). With 300 mW of incident pump power the average output power with this cavity was limited to $100\text{ }\mu\text{W}$, indicating peak output powers of 17 mW.

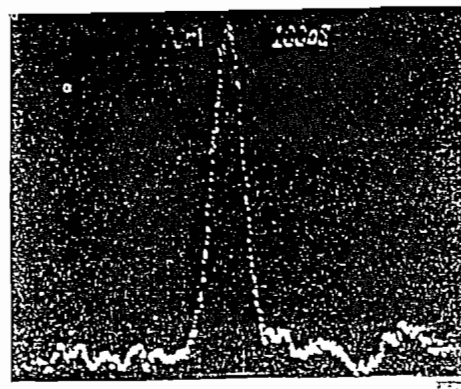


Fig. 2 Typical sampling scope trace showing stable mode-locked pulses
Baseline structure results from detection system used, and is not
optical in origin

Several factors are responsible for the relatively low output powers. Fresnel reflections off various intracavity elements contribute significantly to the cavity loss as does the poor polarisation control. Two improvements were subsequently made which serve to indicate the importance of minimising the cavity losses. The uncoated index matching cell window was replaced by a window AR-coated at $1.56\text{ }\mu\text{m}$. The single polarisation controller disc was replaced by a set of three discs of the diameter (17 mm) appropriate for the given fibre size and the operating wavelength.⁵ This disc combination permitted a polarisation extinction ratio in excess of 100:1. With these simple improvements the CW threshold power was reduced to 100 mW incident (~ 50 mW launched, 19 mW absorbed). With 300 mW incident pump power, the average output power increased to $620\text{ }\mu\text{W}$. The pulse width remained the same as before and consequently the peak output power is approximately 90 mW.

Discussion: The laser we have described has to date produced external peak powers of 90 mW. With the 4.5% output coupling we have used this corresponds to an intracavity peak power of 2.0 W. Using data for undoped silicon glass (nonlinear refractive index $3.2 \times 10^{-16}\text{ cm}^2/\text{W}$) we estimate that the pulses experience single pass frequency chirps of the order of 200 MHz. This chirp is still somewhat smaller than the pulse bandwidth. Moderate increases in the peak power would make the chirp significant compared with the bandwidth. We expect this to result in noticeable changes in the pulse duration as a result of self-phase modulation.

Further work is aimed at increasing the peak power. Some possible approaches which are under investigation are:

- (a) coupling in more pump power by means of a dichroic coupler to avoid mirror damage
- (b) using a shorter pump wavelength to increase the Yb absorption

(c) reducing the cavity losses. One possibility here is the use of a modulator applied externally in direct contact with the fibre.*

Acknowledgments: Partial funding for this work, as well as studentships (A.K., D.P.S., M.W.P.) and a postdoctoral fellowship (P.J.S.) was provided by the SERC under the JOERS initiative. We are grateful to the Optical Fibre Group at Southampton University for supplying the fibre used in these experiments.

D. C. HANNA
A. KAZER
M. W. PHILLIPS
D. P. SHEPHERD
P. J. SUNI

14th November 1988

Department of Physics
University of Southampton
Southampton SO9 SNH, United Kingdom

References

- 1 HANNA, D. C., KAZER, A., and SHEPHERD, D. P.: *Opt. Commun.*, 1987, 63, p. 417
- 2 PHILLIPS, M. W., FERGUSON, A. L. and HANNA, D. C.: submitted to *Optics Letters*
- 3 GEISTER, G., and ULRICH, R.: *Opt. Commun.*, 1988, 68, p. 137
- 4 FERMANN, M. E., HANNA, D. C., SHEPHERD, D. P., SUNI, P. J., and TOWNSEND, J. E.: 'Efficient operation of an Yb-sensitised Er fibre laser at $1.56\text{ }\mu\text{m}$ ', *Electron. Lett.*, 1988, 24, (18), pp. 1135-1136
- 5 LEFEVRE, H. C.: 'Single-mode fibre fractional wave devices and polarisation controllers', *ibid.*, 1980, 16, p. 773
- 6 KUZENGA, D. J., and SIEGMAN, A. E.: *IEEE J. Quantum Electron.*, 1970, QE-6, p. 694

* PATERSON, D. B., GODIL, A. A., KINO, G. S., and KHURI-YAKUB, B. T.: to be published; PHILLIPS, M., FERGUSON, A. L., and KINO, G. S.: in preparation

RELIABILITY COMPARISON OF SHORT-CHANNEL MOSFETs WITH COBALT SALICIDE AND TITANIUM SALICIDE STRUCTURES

Indexing terms: Semiconductor devices and materials, MOS devices, FETs, Reliability

Short-channel LDD MOSFETs are fabricated by a CoSi_2 salicide process with and without ion beam mixing, and a TiSi_2 salicide process with ion beam mixing. The results of hot carrier stress measurements indicate the superior reliability of CoSi_2 MOSFETs fabricated with ion beam mixing.

Introduction: The scaling down of device feature size in VLSI technology has been motivated by the promise of faster operating speeds. However, the RC time delay due to interconnects and contacts does not scale with device size. As devices are scaled down, the delay becomes significant. To reduce the delay, low resistivity materials such as the refractory metal silicides and the near noble and noble metal silicides have been used for contacts and interconnects. Two very promising metal silicides are TiSi_2 and CoSi_2 because of their low resistivities and their ability to form self-aligned silicide (salicide) structures.¹⁻³ In our work, we compare the device reliability of short-channel MOSFETs with CoSi_2 and TiSi_2 salicide contacts.

Salicide processing: Short-channel ($1.0\text{ }\mu\text{m}$), lightly doped drain/source n-channel MOSFETs (LDD NMOSFETs) were fabricated on 12.5 cm p-type (100)Si wafers with resistivities of $14-22\text{ }\Omega\text{-cm}$ through four different processes: (i) a CoSi_2 salicide process with ion beam mixing (CoSi_2 w/); (ii) a CoSi_2 salicide process without ion beam mixing (CoSi_2 w/o); (iii) a TiSi_2 salicide process with ion beam mixing (TiSi_2 w/); and

STUDIES OF EXCITED-STATE ABSORPTION AT $1.5\mu\text{m}$
IN Er^{3+} DOPED SILICA FIBRES

J R Armitage, C G Atkins, R Wyatt, B J Ainslie & S P Craig
British Telecom Research Laboratories
Martlesham Heath
Ipswich IP5 7RE
ENGLAND
+44 473 645364

D P Shepherd
University of Southampton, Physics Department
Highfield
Southampton SO9 5NH
ENGLAND

ABSTRACT

Measurements on Er^{3+} doped silica fibres relating to absorption of laser photons by upper laser level ions will be presented. The results indicate that this effect does not seriously degrade amplifier performance.

STUDIES OF EXCITED-STATE ABSORPTION AT $1.5\mu\text{m}$
IN Er^{3+} DOPED SILICA FIBRES

J R Armitage, C G Atkins, R Wyatt, B J Ainslie & S P Craig

British Telecom Research Laboratories

Martlesham Heath

Ipswich IP5 7RE

ENGLAND

+44 473 645364

D P Shepherd

University of Southampton, Physics Department

Highfield

Southampton SO9 5NH

ENGLAND

SUMMARY

Er^{3+} doped silica fibre lasers and amplifiers operating at around $1.54\mu\text{m}$ are of particular interest in telecommunications as this wavelength coincides with the low-loss transmission window of conventional silica optical fibres. In order to design efficient devices, a detailed understanding of the spectroscopy of Er^{3+} ions in silica is needed. Recent measurements performed on Er^{3+} doped fibres^[1] have indicated that absorption of pump photons by Er^{3+} ions residing in the $1.5\mu\text{m}$ upper laser level is significant, particularly at wavelengths around 800nm. It has also been suggested that absorption of laser photons by ions in this upper laser level may be occurring and degrading device performance. In this paper, gain measurements on Er^{3+} doped fibres will be presented, which indicate that the cross-section for absorption of

laser photons by upper laser level ions is small in comparison with the stimulated emission cross-section.

To quantify the effects of excited state absorption of laser photons, the following experiment was undertaken. An Ar^+ ion laser operating at 528.7nm was used to pump a length of Er^{3+} doped fibre, and two external cavity semiconductor diode lasers, with a combined tuning range of 1.49 to 1.64 μm , were used to probe the transmission of the doped fibre (see Figure 1). Approximately 100mW of 528.7nm radiation was launched into the fibre, this power being sufficient to invert totally the 1.5 μm laser transition. The change in transmission of the fibre between its pumped state (when all the ions are in the upper laser level) and the unpumped state (with all the ions in the ground state) was then measured at a large number of wavelengths across the 1.5 μm band. In a separate experiment, the absorption and fluorescence lineshapes were measured, from which the variation of the absorption and stimulated emission cross-sections with wavelength could be determined. If σ_1 , σ_2 and σ_3 are the cross-sections for absorption by ground state ions, for stimulated emission on the laser transition and for absorption by upper laser level ions respectively (see Figure 2), then the spectral variation of the change in transmission through the doped fibre will be proportional to $\sigma_1 + \sigma_2 - \sigma_3$, whereas the fluorescence and absorption spectra yield the sum $\sigma_1 + \sigma_2$. From the close correspondence between the shapes of these two sets of data (see Figure 3), it can be concluded that the cross-section for excited state absorption of laser photons is insignificant in comparison to σ_1 and σ_2 , and that excited state absorption of lasing photons does not seriously affect amplifier performance.

Further gain measurements will be presented for fibres of different glass composition, together with studies of the fluorescence at 800nm from the $^4I_{9/2}$ level for fibres pumped at wavelengths around $1.5\mu\text{m}$ - a more direct indication of upper laser level absorption lineshape.

REFERENCES

[1] J R Armitage, C G Atkins, R Wyatt, B J Ainslie & S P Craig "Spectroscopic studies of Er³⁺ doped single mode silica fibre" Paper TUM27, CLEO '88

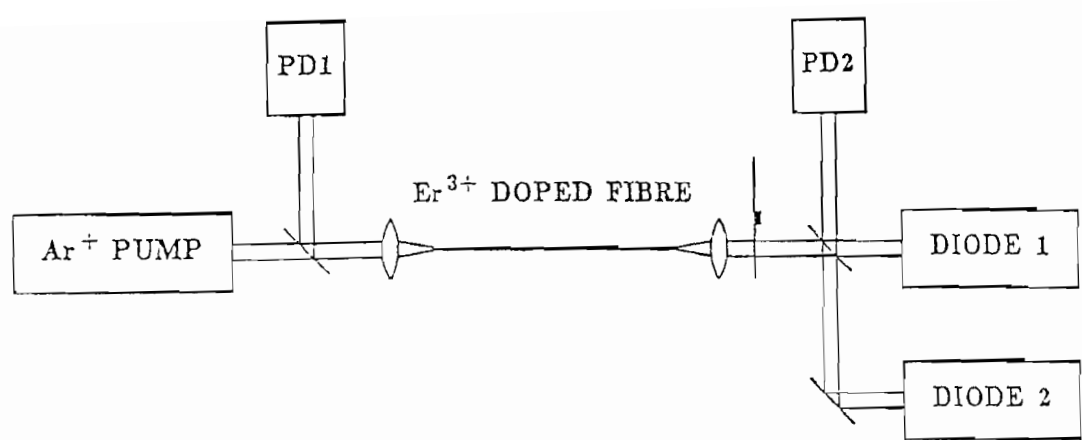


Figure 1

Schematic diagram of experimental apparatus

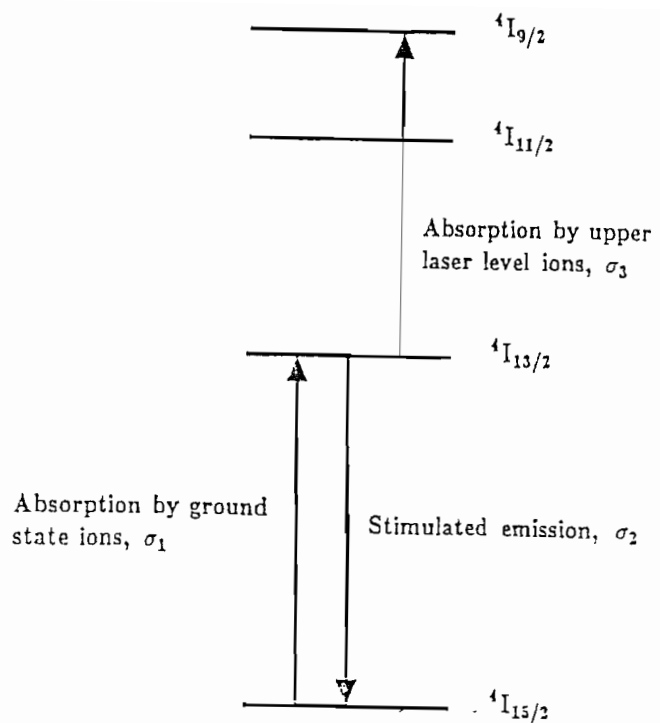


Figure 2

Partial Energy level diagram for Er^{3+} ions in silica

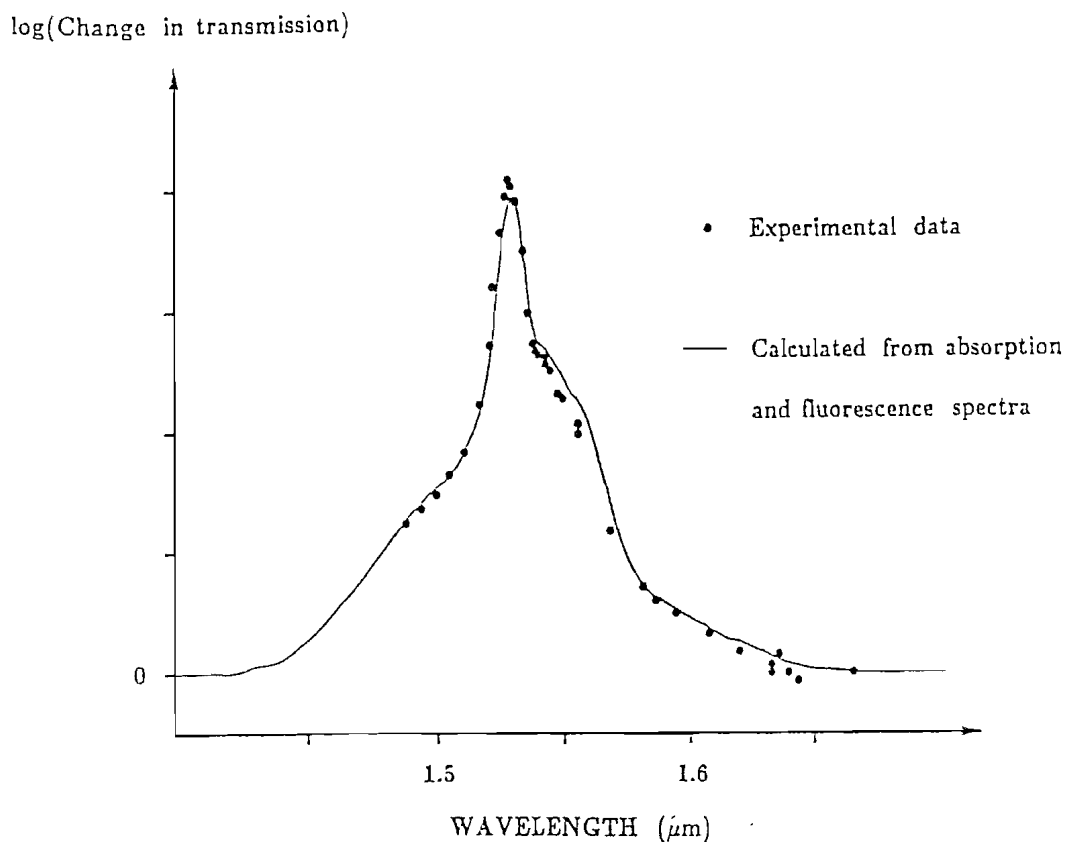


Figure 3

Comparison between experimentally measured change in transmission of the pumped and unpumped fibre as a function of signal wavelength, and calculation based on measured absorption and fluorescence spectra.